DANISH METEOROLOGICAL INSTITUTE

——— SCIENTIFIC REPORT ———

03-03

DMI-HIRLAM parallel tests with upstream and centered difference advection of the moisture variables for a summer and winter period in 2002

Bjarne Amstrup
Niels Woetmann Nielsen
Bent Hansen Sass

COPENHAGEN 2003

ISSN Nr. 0905-3263 (printed)
ISSN Nr. 1399-1949 (online)
ISBN-Nr. 87-7478-474-9

DMI-HIRLAM parallel tests with upstream and centered difference advection of the moisture variables for a summer and winter period in 2002

Bjarne Amstrup, Niels Woetmann Nielsen and Bent Hansen Sass
Danish Meteorological Institute

1. Introduction

Based on some parallel tests during the first quarter of 2002 (Amstrup *et al.*, 2002), a minor upgrade with a large impact of the DMI-HIRLAM operational suite took place on April 17, 2002. The purpose of the upgrade was mainly to eliminate or reduce the long-standing problem of predicting weak to moderate precipitation too frequently by the DMI-HIRLAM operational system. A step towards solving the problem was taken by the upgrade in December 2001. The main contribution to the improved prediction of small precipitation amounts by this upgrade came from a change in the parameterization of shallow convection (Sass, 2001). Further investigations indicated that the overprediction of small precipitation amounts had significant contributions from the smallest resolved scales of the model. In an attempt to further improve the prediction of small precipitation amounts, forecast experiments were therefore done with first order upstream advection of the moisture variables and TKE. This type of advection was tested, because of its smoothing effect on the advected fields (p. 99 in Haltiner, 1971). The promising results of the forecast experiments with upstream advection motivated a preoperational test with this scheme applied for the moisture variables and TKE. The sea surface stress predicted by the DMI-HIRLAM model system is used in a storm surge model with the purpose of predicting the water level of the Danish Waters. For this reason preoperational tests for winter had highest priority, and runs were done for a few winter periods, including the first quarter of 2002. The test results showed a significant reduction in the overprediction of small precipitation amounts and a neutral impact on the prediction of large precipitation amounts (Amstrup *et al.*, 2002). There was little time and computer resources left for extending the preoperational tests to a summer period. The results for the winter periods appeared so promising that it was decided to make the preoperational system operational on 17 April 2002. Verification results for the summer of 2002 showed significant improvement for the lowest precipitation class, as compared with previous summers, but a moderate degradation was noted for the highest precipitation class (Nielsen and Amstrup, 2001a; Nielsen and Amstrup, 2002a; Nielsen and Amstrup, 2001b; Nielsen and Amstrup, 2002b). It was also noted that the operational system failed to predict some heavy precipitation events over Denmark in June. There was little doubt that the underprediction of heavy precipitation was an (unanticipated) effect of upstream advection of the moisture fields. Since good prediction of severe weather has high priority there was a need for finding a solution to 'the overprediction of small precipitation amount'-problem without inventing upstream advection of the moisture fields. The

present report describes important parts of the work done in the search for such a solution. Modifications to the STRACO-scheme have been developed and tested (Sass and Yang, 2002). These modifications are described in some detail in section 3. Extended-period runs as well as case studies with and without the modifications to the STRACO-scheme and including few modifications to other parts of the model system have been made. Case studies have been made for three days in June 2002 (15 June, 18-19 June and 20 June) with heavy precipitation over Denmark. These cases are presented and discussed in section 3.2. This section begins with a presentation of the DMI-HIRLAM model domains followed by a brief summary of the performed experiments. In section 4 standard observation verification results for the extended period runs are presented and discussed. The selected periods are the full month of January 2002 and the period from June 10 2002 to June 21 2002 (the June-period). Finally, section 5 contains discussion and conclusions.

2. Modified convection scheme

The convection scheme used operationally at DMI is named STRACO which stands for "Soft TRAnsition COndensation". It is based on a humidity budget closure (Sass *et al.*, 2002). This implies that the vertically integrated humidity supply in a convective air column during a physics time step can be vertically redistributed due to convection. The moisture supply comes from dynamics and turbulence. Convection may start from any model level provided that an onset of convection is supported in the modeling of the convective cloud ascent. Several convective parts of the atmosphere, separated by stable layers, may be diagnosed in a vertical air column. For shallow convective phenomena there is a regulation of the interaction between turbulence and convection with the effect that the subgrid scale vertical transports for very shallow phenomena are described mainly by the turbulence scheme while transports over deeper layers are taken over by the convection scheme. Convective parts of the atmosphere deeper than 200 hPa in the vertical may use all available moisture from dynamics and turbulence in the vertical redistribution of moisture.

The prognostic model equations involve updates to both specific humidity, cloud condensate and temperature. The effect of 'overshooting eddies' on the convective transports are included. This involves modeling of fluxes across the transition between the convective cloud tops and the stable layer above. Evaporation terms of cloud condensate and precipitation appear in the equations. The precipitation microphysics follow essentially the comprehensive treatment by Sundqvist (Sundqvist, 1993).

Operational experience has revealed some shortcomings of the convection scheme. It has been found that too many convective episodes are generated with weak convective activity. This is reflected in a too high frequency of small precipitation intensities. On the other hand, heavy convective precipitation events are sometimes underestimated. Also convection tends to start too early in the day when describing the diurnal cycle of precipitation.

Modifications to the STRACO scheme have been developed and tested during Autumn and Winter 2001-2002 in order to improve on these shortcomings of the scheme.

The model versions 12a and 12b (dmiconfig numbers 12a and 12b as listed in Appendix A), respectively apply to the updated STRACO scheme. The main features of the modifications

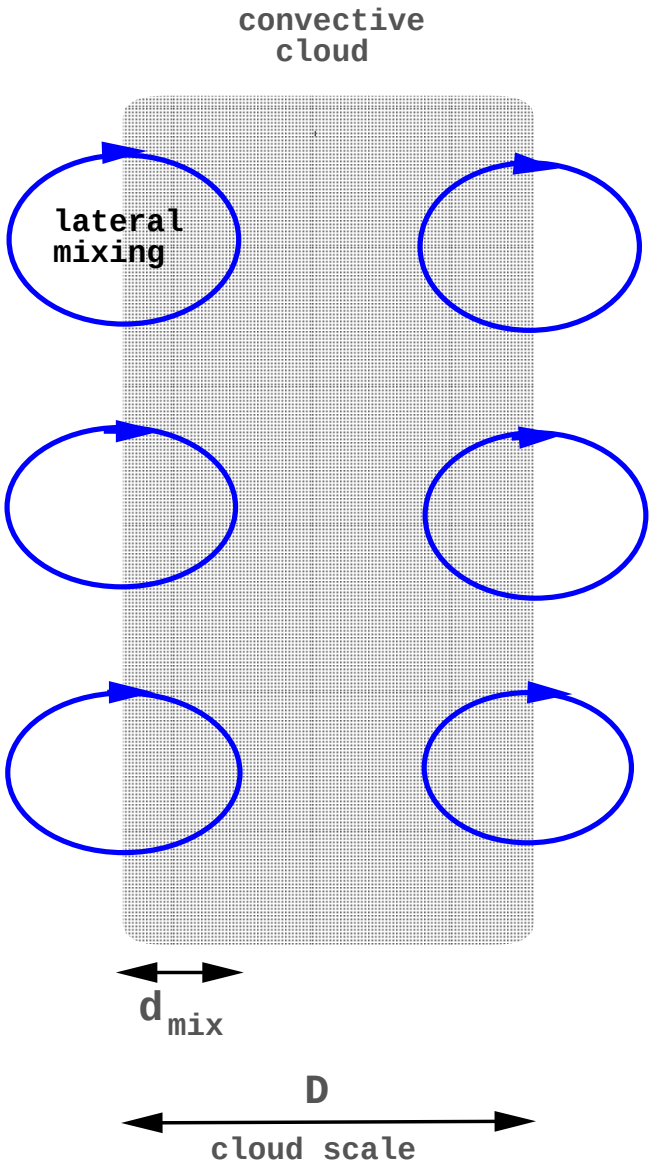

Figure 1: Schematic illustration of the mixing process in a convective cloud.

are briefly outlined below. A detailed description of the new scheme is available (Sass, 2002). The main modification to the scheme is concerned with the modeling of the convective 'cloud parcel ascent' where the formulation of a lateral turbulent mixing process has been included. Previously, the buoyancy computation is essentially governed by the computation of a moist adiabat without considering entrainment effects of environmental air. A realistic treatment of the entrainment effect during the convective cloud ascent appears to be very important in defining the vertical extent of convection. The effect of the mixing, depending on the humidity, temperature and wind shear in the environments has been parameterized in the modified scheme. These effects are particularly strong for convection in relatively dry environmental air. The convective cloud will get cooler, and its moisture content will be reduced (less buoyant convective cloud). As a consequence it is more difficult to start a deep convection process in the model, and convective processes tend to be delayed by typically an hour in the diurnal cycle of precipitation (shown in 1-dimensional column experiments).

Interestingly it turns out that the convection often gets stronger in the new scheme once a

significant synoptic forcing allows the convection scheme to generate deep convective clouds.

The mixing process is shown schematically in Figure 1. A volume fractional entrainment ε_e per unit length of vertical parcel ascent is tentatively described according to the equation below.

$$\varepsilon_e = \left(K_{\varepsilon 0} + \frac{K_{\varepsilon 1}}{Ri_*}\right)\left(\frac{z}{K_{\varepsilon 3} + z}\right)\frac{L_0}{L} \tag{1}$$

In eq. (1) Ri_* is a Richardson number which enables that the effects of wind shear is incorporated. It is argued that increasing wind shear gives rise to more mixing of the convective cloud with the environments.

$$Ri_* = \left(\frac{\theta}{g}\left|\frac{\partial V}{\partial z}\right|^2\right)^{-1}\left(K_{\varepsilon 2} + \left|\frac{\partial \theta}{\partial z}\right|\right) \tag{2}$$

In (1) $K_{\varepsilon 0} = 1.3 \cdot 10^{-4}$, $K_{\varepsilon 1} = 7.5 \cdot 10^{-4}$.

The second brackets of (1) expresses a height dependency of the entrainment process being dimensionless and increases from zero at the surface towards 1 at great heights. $K_{\varepsilon 2} = 1.0 \cdot 10^{-4}\,\mathrm{K\,m^{-1}}$ and $K_{\varepsilon 3} = 500\,\mathrm{m}$.

In (1) the horizontal resolution dependence is described by the last term. The model grid size is L, and L_0 is set to 10 km. If it is maintained that the parameterized convection should describe effects of subgrid scale features being 1-2 orders of magnitude smaller in area extent than the grid square, it is reasonable to assume that the dimension D of the parameterized convective clouds ($D < L$) decreases roughly proportional to the grid size. It is then assumed that the ratio between the surface and the volume of a convective cloud increases as the horizontal dimension of the cloud decreases. For a ball-shaped cloud the ratio goes to infinity and is inversely proportional to the size of the convective cloud. As a consequence one might expect that a dilution process with a characteristic length scale *dmix* (see Figure 1) is becoming more efficient at high model resolution. As a first approximation one might expect that a volumetric dilution becomes inversely proportional to grid size which is expressed by the last term of eq. (1). An important consequence of the resolution dependent dilution is that the vertical extent of parameterized convection will automatically be reduced as the model grid size is reduced. As a consequence, the parameterization of 'deep convection' will automatically tend to be 'switched off' as the horizontal resolution gets increasingly high.

Secondly, modifications to the sub-grid scale condensation (cloud cover parameterization) have been included. A time dependent amplitude of the grid box variation of total specific humidity has been introduced. This modification reduces substantially a tendency of the previous scheme to produce compensating condensation during precipitation release. Also the evaporation of small precipitation intensities has been somewhat increased, based on comparisons of the currently used evaporation formula with other alternative formulations. The reader is referred to Sass (2002) for further details.

Here we focus on the results with use of the "bug"-fixed version presently (as of July 20, 2002) used on the SX-6 machines, namely 'E', 'G', 'N', 'O', 'P' and 'J'

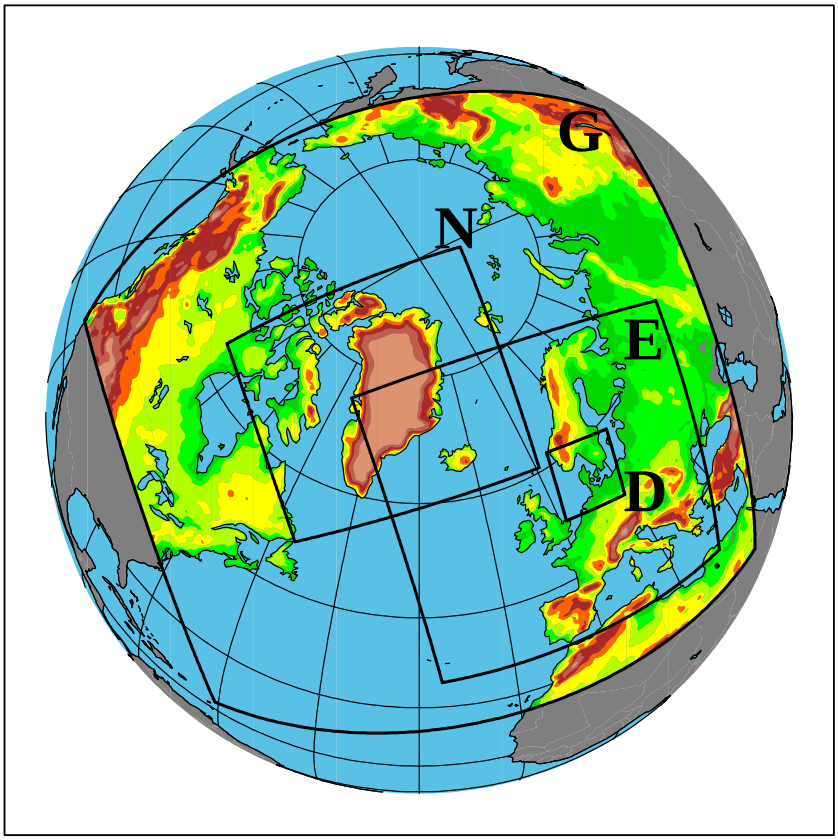

	G	E	D	N
$x_{\text{lon},1}$	$-63.725°$	$-54.275°$	$-36.675°$	$-29.075°$
$y_{\text{lat},1}$	$-37.527°$	$-28.677°$	$-15.177°$	$-5.277°$

Figure 2: Operational DMI-HIRLAM areas and the starting coordinates (south west corner) in the rotated coordinate system.

3. Experiments

3.1. Setups

The operational DMI-HIRLAM model domains are shown in Figure 2. The domains are all on a rotated grid with polar coordinates $(P_{\text{lat}}, P_{\text{lon}}) = (0°, 80°)$. The starting coordinates (south west corner) in the rotated coordinate system are given in the figure as well. Table 12 in Appendix A shows the variables that have changed in the setups for different runs. "G45/D15" is the operational setup (Sass *et al.*, 2002).

Runs in two periods have been made. January is for the whole of January 2002 starting from an operationally archived DMI-HIRLAM-G first guess file valid on 03 UTC January 1. The June period is also in 2002 and the runs start from an operationally archived DMI-HIRLAM-G/DMI-HIRLAM-E first guess file valid on 03 UTC June 10 and runs until 21 UTC June 21, 2002. For the January period ECMWF analyses files for every 6 hours have been used as boundaries for DMI-HIRLAM-G since some FRAME boundaries were missing in

the UNITREE archive and it is not possible to extract these files from the ECMWF mars archive. For the June period, FRAME boundary files have been used for DMI-HIRLAM-G. Accordingly, this period has been run exactly like the operational suite in this respect. However, a variable in the setups—including the operational setup—has the effect that if new FRAME boundary files are available for the 18 UTC runs they will be used for the long 18 UTC runs instead of the 6 hour older FRAME boundary files from 12 UTC. This only influences the long 18 UTC runs and should have only minor effects in the tests and it is the same for all runs.

Beside the updated STRACO version all runs except for G4O/D1O (see Table 12 in Appendix A) have used locally received NOAA16 AMSU-A radiation data (see, e.g., Amstrup, 2001; Schyberg *et al.*, 2003 for further details). In the last column of the table the RTTOV (Radiative Transfer model for TOVS) version number used in the analysis is listed. RTTOV is the radiative forward model used for calculating brightness temperatures corresponding to the level 1c processed observational data for the AMSU-A channels. RTTOV5 is used in the preoperational test setup for including NOAA16 AMSU-A data. RTTOV7 is needed for use of data from the recently launched NOAA17 satellite and has been used in some test runs to check that it works with NOAA16 data until NOAA17 data also become available. The use of NOAA16 data should, however, have only modest influence on the results presented here as illustrated in the differences between G4O/D1O and G4N/D1N (see section 4).

3.2. Case studies

In the considered period three cases were selected for a more detailed study. The cases are: 15 June (C1), 18-19 June (C2) and 20-21 June (C3). The cases are discussed and maps shown in subsections 3.3.1, 3.4.1 and 3.5.1, respectively. Here we give a brief introduction. All three cases give considerable amounts of precipitation in Denmark. Isolated thunderstorms develop in C1, while more widespread thunderstorms develop in C2 and C3. The most severe thunderstorms occurred in C2. The synoptic pattern varies from case to case, although frontal circulations and associated tongues of low-level maxima in equivalent potential temperature (θ_e) are present in all the cases.

In C1 precipitation appears to be mainly concentrated in the warm frontal zone and its northwestward extension into a warm occlusion. Showers and isolated thunderstorms develop at and ahead of the cold front. No cyclogenesis occurs in C1. However, in C2 and C3 rather intense cyclogenesis for the season takes place.

In C2 widespread and locally intense thunderstorm outbreaks occur in a weak surface low that forms below the right entrance region (RER) of an upper-tropospheric jet streak. The surface low gradually dissipates as it moves across Denmark from southwest to northeast. Simultaneously a new surface low intensifies further north below the downstream region of the trough in the exit region of the jet streak. In the dissipating surface low over Denmark the precipitation generally weakens as the system moves eastward. The main precipitation activity gradually shifts to the region of cyclogenesis further north.

In C3 cyclogenesis is in progress over Denmark. The intensifying surface low moves northeastward from Holland to southern Finland. The center of the low passes over the Copenhagen area around 23 UTC on 20 June. The cyclogenesis follows the classical picture. The initial

Table 1: Short description of differences between pairs of experiments. The label in the left column is a combination of the last letter in the two experiment names.

JP	D1J versus D1P	impact of shift from dmiconfig 11 to dmiconfig 12**b**
EG	D1E versus D1G	impact of shift from upstream advection of TKE to centered difference advection of TKE
NP	D1N versus D1P	impact of shift from high to low resolution in the 3D-Var analysis
NE	D1N versus D1E	impact of shift from RTTOV5 to RTTOV7
OE	D1O versus D1E	impact of shift from no use of NOAA16 AMSU-A data to use of these data with use of RTTOV7

surface low forms in the RER of an upper-tropospheric jet streak downstream of an advancing upper-level trough. In the course of development the cyclone moves below the jet axis to the left exit region of a jet streak near the base of the upper-level trough. The cyclone enters its mature stage on the cyclonic shear side of the jet. Note that contrary to C2 no new surface low forms in C3. The precipitation in C3 is mainly concentrated in the warm frontal and bent-back frontal zone. Outbreak of thunderstorms occur here as well as along and ahead of the cold front.

3.3. The weather development over Denmark on 15 June

Figure 3 shows that the weather in Denmark on 15 June was influenced by an eastward moving upper-tropospheric short wave and its associated frontal system. The surface fronts are shown indirectly by 'kinks' in the mean sea level pressure contours. Precipitation mainly occurred in the region of rising motion in the warm air branch of the ageostrophic frontal circulation. Precipitation also tended to occur in regions with strong upper-tropospheric positive absolute vorticity advection downstream of the trough.

Scattered thunderstorms developed over Jutland in connection with the passage of the warm front and its northwestward extension into a warm occlusion. More widespread outbreaks of thunderstorms took place at the cold front as it swept eastward across northern Germany.

3.3.1. Predicted and observed accumulated precipitation 06 to 18 UTC 15 June

The upper rows of Figures 9-11 show the operationally forecasted 12 h (6-18 h) accumulated total, convective and stratiform precipitation, respectively. Figures 12 and 13 show the corresponding observed amounts of total precipitation. The forecasted amounts are about evenly distributed between convective and stratiform precipitation.

The forecasts, and in particular G45, underestimate the amounts of precipitation in the short-wave system. G45 miss almost completely the convective precipitation in northern Germany and at the Baltic Sea coast of Germany and Poland. D15 has generally more convective precipitation than G45, but the predicted amounts are still too small in northern Germany, and the model does not predict the substantial convective precipitation amounts

observed in northern Poland.

Over southern Scandinavia there is generally better agreement between the predicted and observed amounts, although the predicted precipitation extends too far eastward.

3.3.2. Impact studies

Figure 14 shows the 12 hour accumulated precipitation verifying at 18 UTC 15 June for 6 of the experiments D1x listed in Table 3. Note that 5 of the experiments (x=O, E, P, N and G) are done with dmiconfig number 12b and only 1 (D1J) is done with dmiconfig number 11. In the interpretation of Figure 14 reference is made to Table 1. This table defines the meaning of JP, EG, NP, NE and OE. For example is NP a reference to the pair of figures D1N and D1P, and according to Table 1 NP shows the impact of shifting from high to low resolution in the 3D-VAR analysis.

It is clear from Figure 14 that a shift from dmiconfig number 11 to dmiconfig number 12b (involving modifications of STRACO as briefly described in section 2) has a significantly larger impact on the accumulated precipitation than any of the other changes investigated in the experiments shown in Figure 14 (See Appendix A for explanation of dmiconfig numbers). The amounts of precipitation are in general considerably larger in dmiconfig number 12b, although the amounts in D1J have increased compared to the operational run D15 (Figure 9, upper left). The difference between the latter two mainly shows the impact of shifting from upstream advection of specific humidity (q), cloud water (CW) and turbulent kinetic energy (TKE) in D15 to centered difference advection of q and CW in D1J. Note in particular that the band of observed substantial amounts of accumulated precipitation (10-25 mm/12 h) close to the Baltic Sea shore of Germany and Poland is not present in D1J, but appears in all experiments done with dmiconfig number 12b. Observations show that the band is generated by thunderstorms. Figure 14 therefore indicates that the modifications in STRACO leading to dmiconfig number 12b enables the model to generate (convective) precipitation amounts in fair agreement with observations. Convective systems are not in general expected to be predictable beyond 6 hours. For this reason even a 'perfect' model would predict an accumulated precipitation field deviating from the observed field both with respect to amount and location. It is therefore no surprise that the precipitation fields of the runs done with dmiconfig number 12b differ considerably in the details. The limited number of (available) precipitation measurements combined with the small-scale structures of the field makes it impossible to point to one of the forecasts as the best one. From the EG-pair it is clear that there is a better prediction of the precipitation maximum along the upwind side of southern Norway and perhaps some indication of a better location of the Germany-Poland precipitation band in D1G, i.e. in the run with centered difference advection instead of upstream advection of TKE. If one should give a best and worst score to one of the runs in Figure 14 the choice would fall on D1G and D1J, respectively.

3.4. The weather development over Denmark on 18 June

On 18 June the weather in northern Europe was influenced by a slowly eastward moving high amplitude upper-level ridge with a strong jet stream on its upstream side (Figure 4). A

tongue of high θ_e air was present in the lower troposphere on the 'warm' side of the frontal zone upstream of the ridge (Figure 5). Potential instability is likely to be present in this tongue of 'warm' θ_e air, as indicated by the moist static instability $(\theta_e(800) - \theta_e(400))/(p(800) - p(400))$ depicted in Figure 4. Due to the coincidence between the maxima in moist static instability and θ_e (see Figure 4b and Figure 5), the latter figure also shows the northeastward displacement of the tongue of 'warm' θ_e air during the course of the day. Outbreak of thunderstorms occur within the region of maximum low-level θ_e, which is located to the west of the ridge in low-level potential temperature θ, as shown by inter comparison of Figure 4 and Figure 6. The release of potential instability may be triggered by rising motion associated with low-level warm advection around the crest of the θ wave shown in Figure 6. Rising motion forced by upper-level positive vorticity advection (PVA) may also contribute. According to Figure 5 PVA is present above the low-level maximum in θ_e. More substantial upper-level PVA forcing occurs above colder low-level air in the RER of the upper-level jet streak upstream of the ridge (see Figure 5, over the eastern part of the British Channel and England). Relatively weak cyclogenesis occurs in this region. The developing cyclone moves north-northeastward and by midnight 19 June the main precipitation activity has shifted from the low-level maximum in θ_e to the region of cyclogenesis over Scandinavia (near the local maximum in wind speed at 850 hPa in Figure 6).

The environment of the thunderstorms is characterized by weak to moderate vertical wind shear and geostrophic wind veering with height in the lower troposphere. In such an environment thunderstorms may develop into multicell storms, where successive cells are triggered by downdrafts. The new cells may form without larger scale forcing. The mechanism is lifting of air to the level of free convection (LFC) along the outflow boundaries (gust fronts) of the downdrafts from mature and dying cells. In an environment with warm advection (geostrophic wind veering with height) new cells in a multicell storm tends to form to the right of the movement of individual cells (Rotunno and Klemp, 1982).

Observations (SYNOPs, satellite images and lightening stroke detections) indicate that several multicell storms moved across parts of Denmark on tracks from southwest towards northeast (in the wind direction at and above 700 hPa). The first storm moved across the northwestern part of Jutland between 11 and 13 UTC. The next multicell storm arrived at the west coast of Jutland around 16 UTC. As the storms moved across Jutland they joined and formed a south to north oriented squall line, which was in a dissipating stage when it passed the eastern part of the country. It is likely that larger scale lifting connected with the eastward advancing cold front (Figure 6) contributes to the line organization.

3.4.1. Predicted and observed accumulated 12h precipitation 18 UTC 18 UTC 18 June and 06 UTC 19 June

It is a difficult task for numerical weather prediction (NWP) models to treat the type of convection described above properly. One reason is that the horizontal model resolution is too coarse to resolve these systems, which means that they are parameterized fully or partly by the model. Another and related reason is that the forcing of the convection tends to be local, depending on previous convective cell developments.

The results of the parallel experiments described below confirm that the DMI-HIRLAM

system has severe difficulties in case C2.

The operationally forecasted 12 hour (6-18 hour) accumulated precipitation amounts of total, convective and stratiform precipitation are shown in Figures 9-11 (middle row), respectively. The corresponding observed accumulated total precipitation is shown in Figures 12 and 13 (upper right). The predicted precipitation is almost purely convective in both G45 and D15 with the largest amounts in G45. This model also has the precipitation farthest eastward over Denmark in fair agreement with the observations. However, the predicted amounts are far too low. In D15 and in G45 the maximum values over Jutland is below 4 and 8 mm/12 h, respectively, while the observations show values between 40 and 50 mm/12h at several locations. The subsequent 12 h forecasts (not shown) also predicted far too low precipitation amounts and missed some spots with high amounts of precipitation.

3.4.2. Impact studies

Figures 15 to 17 show the 12 hour accumulated total, convective and stratiform precipitation, respectively, verifying at 18 UTC 18 June. Both the predicted and observed precipitation over Denmark is mainly convective. The picture is generally similar to that shown for 15 June, with D1J clearly having the worst score. It is interesting to note that the differences in the predicted amounts of stratiform precipitation (Figure 17) between the runs are small compared to the differences in the predicted amounts of convective precipitation (Figure 16). The banded structure in the predicted fields (not so clear in D1J) is not so easy to identify in the observed field, probably because of a too low spatial density of the observations. Anyway, the measured lightening detection pattern (Nielsen and Rasmussen, 2002) shows a banded structure similar to the predicted accumulated precipitation patterns. Satellite images (Nielsen and Rasmussen, 2002) together with DMI-HIRLAM analyses (Figures 4-6) indicate that the banded structure is generated by convective precipitation systems traveling with the wind in the middle troposphere. Each band is generated by one or more systems that develop successively on the equatorward side of an eastward moving upper-tropospheric jet. The minimum in the predicted precipitation between the North Sea band(s) and the bands over northern Germany coincides with an area without lightening detections (Nielsen and Rasmussen, 2002). It represents a break in time between outbreaks of thunderstorm systems. The limited predictability of the convective systems is believed to contribute significantly to the scatter in details (i.e. amounts and location of extremes) between the predicted fields generated by dmiconfig number 12b runs. This, combined with insufficient precipitation measurements, makes it difficult to select a best forecast. The important message is that all the runs with dmiconfig number 12b are able to generate large convective precipitation amounts in fair agreement with the observed amounts (above 40 mm/12 h at several locations in Jutland). All of the models failed to predict the isolated area of precipitation over northern Poland and underestimate the amounts at the Norwegian Skagerak coast.

Figure 18 shows the predicted accumulated (total) precipitation over the next 12 hours (verifying at 06 UTC 19 June).

3.5. The weather development over Denmark on 20 June

The broad features of the weather development in Northern Europe on 20 June is depicted in Figure 7 and Figure 8. By 06 UTC a surface low has formed over Belgium below the right entrance region of a jet streak downstream of an upper-tropospheric trough. In Figure 7 the trough is seen as a grey-shaded, cusp formed local minimum in the 300 hPa wind speed. During the day the surface low intensifies and moves northeastward. By 00 UTC on 21 June the surface low is over southern Sweden and directly beneath the jet core at 300 hPa. It has deepened more than 8 hPa within the preceding 18 hours. On Midsummer Day it continued to intensify and arrived to southern Finland with gale force surface winds. Like in case C1 and C2 a major part of the precipitation was generated in the frontal zone. In Figure 8 the closely packed isotherms of θ_e show the location of the frontal zone at 850 hPa. Note how the cyclogenesis has intensified the cold and warm frontal zones by 00 UTC 21 June. Note also the rapid eastward advance of the cold front relative to the more slowly northward moving warm front.

Thunderstorms were reported, mainly in regions with potentially unstable air. The latter regions tend to coincide with maxima in low-level θ_e as shown in Figure 8. In this figure yellow to red colors show the moist static instability $((\theta_e(850) - \theta_e(400))/(p(850) - p(400)))$ which can be considered as a bulk measure of potential instability.

3.5.1. Predicted and observed accumulated 12h precipitation 18 UTC 20 June

The predicted and observed precipitation for the 12 h period up to 18 UTC June 20 is shown in Figures 9-11 (bottom row) and Figures 12 and 13 (bottom left), respectively. As in cases C1 and C2 the predicted amounts are split into total, convective and stratiform precipitation. The precipitation fields in G45 and D15 are more similar than in the two other cases. Over Southern Scandinavia the predicted amounts also agree fairly well with the observations. However, the models fail to predict the substantial amounts of (convective) precipitation over northern Poland and predict too small amounts of (convective) precipitation over Northern Germany.

The three cases studied in details indicate that the operational system has severe problems in predicting convective precipitation. In all three cases the models either failed to predict precipitation generated by convective systems or seriously underestimated the amounts. The studies also indicate that this problem gets worse as the horizontal model resolution is increased. There is reason to suspect that the upstream advection scheme applied to the moisture variables and to the turbulent kinetic energy smoothes the smallest scales represented by the model too strongly. The smoothing tends to reduce the moisture convergence. The latter is feeding the convection in the model, and a reduction in moisture convergence therefore has the effect of reducing the generation of convective precipitation in the models.

The obs-verification results presented in section 4.2 (below) indicate that the suppression of convective precipitation with upstream advection of the moisture variables is related to a stabilization of the troposphere with increasing forecast lead time.

4. Verification results

4.1. Precipitation verification

Besides the subjective verification of the precipitation results in the three cases presented above, a standard verification of precipitation in terms of contingency tables for the two considered periods has been done. The periods are: The June2002-period (from 0610 to 0621) and the full month of January 2002. The verification is done on the national scale against the Danish SYNOP station list and on the European scale against the EWGLAM (European Working Group on Limited Area Model) station list. The Danish SYNOP station list includes the following stations (when available): 6030, 6041, 6052, 6058, 6060, 6070, 6079, 6080, 6081, 6104, 6110, 6111, 6119, 6120, 6156, 6160, 6170, 6180, 6181, 6190.

The numbers in the contingency tables are obtained by counting the number of observed and predicted precipitation amounts in each of five classes. The five precipitation classes are (precipitation amounts in mm): $P1 < 0.2$, $0.2 \leq P2 < 1.0$, $1.0 \leq P3 < 5$, $5 \leq P4 < 10$ and $P5 \geq 10$. P is either F (forecast) or O (observation) in the given tables. The "sum" rows and columns are the sums of the numbers in the given observation classes or forecast classes, respectively. Note that the observed values are uncorrected values. Thus, small observed precipitation values are most likely underestimated (see e.g. Vejen, 2002).

Tables 2–5 for the June2002-period and Tables 8 and 9 for January 2002 show contingency tables of accumulated precipitation over 12 hours based on the national station list. The tables show the results of 8 experiments selected from the list in Table 12 (including the operational runs G45 and D15). Contingency tables based on the EWGLAM station list are shown in Tables 6 and 7 and Tables 10 and 11 for the June2002-period and January 2002, respectively.

Note that the experiments, except for the operational runs, are complementary in the June and January periods. This means that the scores for June not necessarily are representative for January and vice versa.

Tables 2, 3, 6, 8 and 10 show results for 12 hour accumulated precipitation starting at 6 hour forecast length, and Tables 4, 5, 7, 9 and 11 show the corresponding results for 12 hour accumulated precipitation starting at 18 hour forecast length.

The discussion of the contingency tables can be shortened (and simplified) by noting that the contingency tables based on the national and European station lists show similar results both for the accumulation of precipitation starting at 6 and 18 hour forecast length. This means that the discussion can be limited to model version, model resolution (G4* versus D1*) and period. It ought to be added that the scores based on the EWGLAM list and for the accumulation starting at 6 hour forecast length are generally higher than the scores based on the national station list and for accumulation starting at 18 hour forecast length.

The contingency tables clearly show that G4A/D1A have the best overall scores in both the summer and winter period. For the June2002-period G4A/D1A are not included in the contingency tables based on the EWGLAM station list, but there is no reason to believe that the result would be different. The better scores for G4A/D1A is due to a significant improvement in the prediction of class O1 and a smaller degradation in the prediction of the high precipitation classes (O3-O5) linked to much higher numbers in the upper right corner of the tables.

Table 2: Contingency tables for 12 hour precipitation (6-18 h DMI-HIRLAM-G forecasts) in the period 20020610 through 20020621. F stands for forecast and O for observation. The number is the class number (see text). %FO is the percentage of the forecasted values in the same class as the observation class. Danish SYNOP stations.

G4G 0206						
obs→ / ↓for	O1	O2	O3	O4	O5	sum
F1	**142**	12	12	4	0	170
F2	47	**8**	14	3	6	78
F3	21	15	**37**	12	7	92
F4	1	5	13	**13**	8	40
F5	0	1	6	3	**10**	20
sum	211	41	82	35	31	400
%FO	67	20	45	37	32	53

G4E 0206						
obs→ / ↓for	O1	O2	O3	O4	O5	sum
F1	**154**	11	11	4	**1**	181
F2	38	**10**	15	4	5	72
F3	17	14	**32**	12	8	83
F4	2	6	19	**12**	7	46
F5	0	0	5	3	**10**	18
sum	211	41	82	35	31	400
%FO	73	24	39	34	32	55

G4A 0206						
obs→ / ↓for	O1	O2	O3	O4	O5	sum
F1	**193**	20	21	4	**5**	243
F2	14	**12**	30	7	6	69
F3	3	8	**20**	16	8	55
F4	1	1	8	**6**	8	24
F5	0	0	3	2	**4**	9
sum	211	41	82	35	31	400
%FO	91	29	24	17	13	59

G4Q 0206						
obs→ / ↓for	O1	O2	O3	O4	O5	sum
F1	**166**	14	8	1	**1**	190
F2	30	**13**	23	7	5	78
F3	14	12	**27**	8	10	71
F4	1	2	14	**16**	8	41
F5	0	0	10	3	**7**	20
sum	211	41	82	35	31	400
%FO	79	32	33	46	23	57

G4O 0206						
obs→ / ↓for	O1	O2	O3	O4	O5	sum
F1	**138**	10	9	4	0	161
F2	55	**7**	17	2	4	85
F3	17	21	**39**	18	8	103
F4	0	3	10	**5**	8	26
F5	**1**	0	7	6	**11**	25
sum	211	41	82	35	31	400
%FO	65	17	48	14	35	50

G4P 0206						
obs→ / ↓for	O1	O2	O3	O4	O5	sum
F1	**161**	16	10	4	0	191
F2	39	**9**	20	2	6	76
F3	10	12	**29**	13	9	73
F4	1	4	19	**13**	8	45
F5	0	0	4	3	**8**	15
sum	211	41	82	35	31	400
%FO	76	22	35	37	26	55

G4N 0206						
obs→ / ↓for	O1	O2	O3	O4	O5	sum
F1	**161**	16	10	4	0	191
F2	39	**9**	20	2	6	76
F3	10	12	**29**	13	9	73
F4	1	4	19	**13**	8	45
F5	0	0	4	3	**8**	15
sum	211	41	82	35	31	400
%FO	76	22	35	37	26	55

G45 0206						
obs→ / ↓for	O1	O2	O3	O4	O5	sum
F1	**161**	11	9	3	0	184
F2	43	**13**	32	4	9	101
F3	7	17	**33**	21	8	86
F4	0	0	6	**5**	8	19
F5	0	0	2	2	**6**	10
sum	211	41	82	35	31	400
%FO	76	32	40	14	19	55

Table 3: Contingency tables for 12 hour precipitation (6-18 h DMI-HIRLAM-E forecasts) in the period 20020610 through 20020621. F stands for forecast and O for observation. The number is the class number (see text). %FO is the percentage of the forecasted values in the same class as the observation class. Danish SYNOP station list.

D1G 0206						
obs→ / ↓for	O1	O2	O3	O4	O5	sum
F1	**122**	7	8	1	**1**	139
F2	64	**8**	16	2	2	92
F3	22	24	**35**	12	2	95
F4	3	0	13	**10**	10	36
F5	0	2	10	10	**16**	38
sum	211	41	82	35	31	400
%FO	58	20	43	29	52	48

D1E 0206						
obs→ / ↓for	O1	O2	O3	O4	O5	sum
F1	**130**	9	9	1	**1**	150
F2	61	**11**	15	1	3	91
F3	18	17	**35**	11	3	84
F4	2	1	11	**9**	10	33
F5	0	3	12	13	**14**	42
sum	211	41	82	35	31	400
%FO	62	27	43	26	45	50

D1A 0206						
obs→ / ↓for	O1	O2	O3	O4	O5	sum
F1	**191**	17	14	6	**5**	233
F2	18	**14**	23	4	4	63
F3	2	10	**34**	13	6	65
F4	0	0	6	**12**	9	27
F5	0	0	5	0	**7**	12
sum	211	41	82	35	31	400
%FO	91	34	41	34	23	65

D1Q 0206						
obs→ / ↓for	O1	O2	O3	O4	O5	sum
F1	**141**	6	13	1	**1**	162
F2	52	**13**	15	3	1	84
F3	15	17	**41**	11	3	87
F4	0	4	7	**12**	7	30
F5	**3**	1	6	8	**19**	37
sum	211	41	82	35	31	400
%FO	67	32	50	34	61	56

D1O 0206						
obs→ / ↓for	O1	O2	O3	O4	O5	sum
F1	**114**	4	7	0	0	125
F2	58	**10**	13	2	4	87
F3	35	20	**38**	15	5	113
F4	3	5	15	**10**	10	43
F5	**1**	2	9	8	**12**	32
sum	211	41	82	35	31	400
%FO	54	24	46	29	39	46

D1P 0206						
obs→ / ↓for	O1	O2	O3	O4	O5	sum
F1	**151**	13	7	0	**1**	172
F2	45	**9**	22	3	1	80
F3	14	14	**38**	15	7	88
F4	1	3	8	**7**	7	26
F5	0	2	7	10	**15**	34
sum	211	41	82	35	31	400
%FO	72	22	46	20	48	55

D1N 0206						
obs→ / ↓for	O1	O2	O3	O4	O5	sum
F1	**145**	8	10	0	0	163
F2	48	**12**	21	1	3	85
F3	16	19	**35**	19	4	93
F4	2	0	8	**7**	12	29
F5	0	2	8	8	**12**	30
sum	211	41	82	35	31	400
%FO	69	29	43	20	39	53

D15 0206						
obs→ / ↓for	O1	O2	O3	O4	O5	sum
F1	**153**	9	7	0	**2**	171
F2	51	**14**	24	4	1	94
F3	7	18	**40**	23	15	103
F4	0	0	7	**4**	5	16
F5	0	0	4	4	**8**	16
sum	211	41	82	35	31	400
%FO	73	34	49	11	26	55

Table 4: Contingency tables for 12 hour precipitation (18-30 h DMI-HIRLAM-G forecasts) in the period 20020610 through 20020621. F stands for forecast and O for observation. The number is the class number (see text). %FO is the percentage of the forecasted values in the same class as the observation class. Danish SYNOP station list.

G4G 0206						
obs→ / ↓for	O1	O2	O3	O4	O5	sum
F1	**123**	7	10	3	**1**	144
F2	67	**18**	18	7	7	117
F3	31	13	**27**	12	7	90
F4	1	6	13	**6**	12	38
F5	**1**	0	3	4	**3**	11
sum	223	44	71	32	30	400
%FO	55	41	38	19	10	44

G4E 0206						
obs→ / ↓for	O1	O2	O3	O4	O5	sum
F1	**137**	10	9	2	0	158
F2	53	**15**	17	9	2	96
F3	32	12	**27**	11	11	93
F4	1	5	9	**7**	11	33
F5	0	2	9	3	**6**	20
sum	223	44	71	32	30	400
%FO	61	34	38	22	20	48

G4A 0206						
obs→ / ↓for	O1	O2	O3	O4	O5	sum
F1	**194**	24	25	8	**6**	257
F2	23	**6**	22	4	5	60
F3	5	12	**17**	15	13	62
F4	1	2	5	**5**	6	19
F5	0	0	2	0	**0**	2
sum	223	44	71	32	30	400
%FO	87	14	24	16	0	56

G4Q 0206						
obs→ / ↓for	O1	O2	O3	O4	O5	sum
F1	**138**	17	12	4	**5**	176
F2	56	**11**	19	5	3	94
F3	26	13	**31**	18	19	107
F4	2	3	6	**3**	3	17
F5	**1**	0	3	2	**0**	6
sum	223	44	71	32	30	400
%FO	62	25	44	9	0	46

G4O 0206						
obs→ / ↓for	O1	O2	O3	O4	O5	sum
F1	**127**	8	11	2	**2**	150
F2	67	**17**	23	8	3	118
F3	28	16	**27**	10	13	94
F4	1	3	9	**12**	10	35
F5	0	0	1	0	**2**	3
sum	223	44	71	32	30	400
%FO	57	39	38	38	7	46

G4P 0206						
obs→ / ↓for	O1	O2	O3	O4	O5	sum
F1	**126**	17	10	3	**1**	157
F2	64	**12**	18	7	4	105
F3	29	7	**28**	14	13	91
F4	4	4	9	**7**	10	34
F5	0	4	6	1	**2**	13
sum	223	44	71	32	30	400
%FO	57	27	39	22	7	44

G4N 0206						
obs→ / ↓for	O1	O2	O3	O4	O5	sum
F1	**126**	17	10	3	**1**	157
F2	64	**12**	18	7	4	105
F3	29	7	**28**	14	13	91
F4	4	4	9	**7**	10	34
F5	0	4	6	1	**2**	13
sum	223	44	71	32	30	400
%FO	57	27	39	22	7	44

G45 0206						
obs→ / ↓for	O1	O2	O3	O4	O5	sum
F1	**149**	12	3	0	**1**	165
F2	60	**21**	33	9	3	126
F3	14	11	**32**	19	14	90
F4	0	0	2	**2**	11	15
F5	0	0	1	2	**1**	4
sum	223	44	71	32	30	400
%FO	67	48	45	6	3	51

Table 5: Contingency tables for 12 hour precipitation (18-30 h DMI-HIRLAM-E forecasts) in the period 20020610 through 20020621. F stands for forecast and O for observation. The number is the class number (see text). %FO is the percentage of the forecasted values in the same class as the observation class. Danish SYNOP station list.

D1G 0206						
obs→ / ↓for	O1	O2	O3	O4	O5	sum
F1	**112**	9	11	0	**1**	133
F2	75	**13**	13	4	2	107
F3	33	13	**32**	14	8	100
F4	3	9	13	**9**	7	41
F5	0	0	2	5	**12**	19
sum	223	44	71	32	30	400
%FO	50	30	45	28	40	45

D1E 0206						
obs→ / ↓for	O1	O2	O3	O4	O5	sum
F1	**110**	7	9	0	0	126
F2	76	**12**	14	1	2	105
F3	32	15	**36**	18	8	109
F4	3	8	9	**8**	9	37
F5	**2**	2	3	5	**11**	23
sum	223	44	71	32	30	400
%FO	49	27	51	25	37	44

D1A 0206						
obs→ / ↓for	O1	O2	O3	O4	O5	sum
F1	**182**	18	23	10	**7**	240
F2	36	**14**	19	6	6	81
F3	5	8	**25**	12	11	61
F4	0	4	4	**4**	6	18
F5	0	0	0	0	**0**	0
sum	223	44	71	32	30	400
%FO	82	32	35	13	0	56

D1Q 0206						
obs→ / ↓for	O1	O2	O3	O4	O5	sum
F1	**114**	10	12	0	0	136
F2	74	**13**	15	3	4	109
F3	29	12	**29**	17	6	93
F4	4	7	11	**5**	7	34
F5	**2**	2	4	7	**13**	28
sum	223	44	71	32	30	400
%FO	51	30	41	16	43	44

D1O 0206						
obs→ / ↓for	O1	O2	O3	O4	O5	sum
F1	**118**	6	8	1	**1**	134
F2	67	**13**	11	3	1	95
F3	37	21	**33**	16	7	114
F4	0	4	12	**5**	9	30
F5	**1**	0	7	7	**12**	27
sum	223	44	71	32	30	400
%FO	53	30	46	16	40	45

D1P 0206						
obs→ / ↓for	O1	O2	O3	O4	O5	sum
F1	**131**	9	9	0	**1**	150
F2	54	**12**	22	7	1	96
F3	35	16	**25**	14	6	96
F4	3	6	13	**7**	11	40
F5	0	1	2	4	**11**	18
sum	223	44	71	32	30	400
%FO	59	27	35	22	37	47

D1N 0206						
obs→ / ↓for	O1	O2	O3	O4	O5	sum
F1	**124**	8	11	0	**1**	144
F2	67	**9**	18	3	0	97
F3	30	21	**30**	17	10	108
F4	2	5	9	**7**	5	28
F5	0	1	3	5	**14**	23
sum	223	44	71	32	30	400
%FO	56	20	42	22	47	46

D15 0206						
obs→ / ↓for	O1	O2	O3	O4	O5	sum
F1	**148**	10	7	4	**5**	174
F2	59	**17**	23	4	0	103
F3	15	13	**36**	19	10	93
F4	1	4	4	**1**	10	20
F5	0	0	1	4	**5**	10
sum	223	44	71	32	30	400
%FO	66	39	51	3	17	52

Table 6: Contingency tables for 12 hour precipitation (6-18 h forecasts) in the period 20020610 through 20020621. F stands for forecast and O for observation. The number is the class number (see text). %FO is the percentage of the forecasted values in the same class as the observation class. EWGLAM station list.

G4G 0206						
obs→ / ↓for	O1	O2	O3	O4	O5	sum
F1	**4517**	194	102	21	**19**	4853
F2	625	**160**	149	36	23	993
F3	284	171	**257**	95	53	860
F4	29	22	76	**41**	29	197
F5	**7**	4	16	19	**42**	88
sum	5462	551	600	212	166	6991
%FO	83	29	43	19	25	72

G4E 0206						
obs→ / ↓for	O1	O2	O3	O4	O5	sum
F1	**4520**	193	110	21	**23**	4867
F2	613	**161**	137	33	21	965
F3	296	175	**261**	94	52	878
F4	29	18	75	**44**	32	198
F5	**4**	4	17	20	**38**	83
sum	5462	551	600	212	166	6991
%FO	83	29	44	21	23	72

G4N 0206						
obs→ / ↓for	O1	O2	O3	O4	O5	sum
F1	**4596**	200	115	24	**22**	4957
F2	579	**163**	163	35	22	962
F3	262	170	**234**	96	56	818
F4	20	15	72	**38**	30	175
F5	**5**	3	16	19	**36**	79
sum	5462	551	600	212	166	6991
%FO	84	30	39	18	22	72

G45 0206						
obs→ / ↓for	O1	O2	O3	O4	O5	sum
F1	**4702**	233	161	37	**32**	5165
F2	589	**215**	218	54	25	1101
F3	153	98	**173**	87	60	571
F4	17	5	39	**26**	22	109
F5	**1**	0	9	8	**27**	45
sum	5462	551	600	212	166	6991
%FO	86	39	29	12	16	74

D1G 0206						
obs→ / ↓for	O1	O2	O3	O4	O5	sum
F1	**4188**	150	85	18	**20**	4461
F2	727	**145**	113	24	15	1024
F3	457	210	**270**	81	42	1060
F4	58	32	96	**58**	42	286
F5	**32**	14	36	31	**47**	160
sum	5462	551	600	212	166	6991
%FO	77	26	45	27	28	67

D1E 0206						
obs→ / ↓for	O1	O2	O3	O4	O5	sum
F1	**4199**	143	86	20	**19**	4467
F2	719	**154**	114	18	13	1018
F3	438	204	**252**	93	43	1030
F4	71	41	108	**46**	36	302
F5	**35**	9	40	35	**55**	174
sum	5462	551	600	212	166	6991
%FO	77	28	42	22	33	67

D1N 0206						
obs→ / ↓for	O1	O2	O3	O4	O5	sum
F1	**4274**	140	82	21	**15**	4532
F2	647	**154**	127	22	18	968
F3	441	221	**259**	83	47	1051
F4	69	30	108	**65**	37	309
F5	**31**	6	24	21	**49**	131
sum	5462	551	600	212	166	6991
%FO	78	28	43	31	30	69

D15 0206						
obs→ / ↓for	O1	O2	O3	O4	O5	sum
F1	**4675**	209	134	27	**27**	5072
F2	611	**219**	199	50	36	1115
F3	160	108	**200**	86	55	609
F4	13	14	56	**37**	24	144
F5	**3**	1	11	12	**24**	51
sum	5462	551	600	212	166	6991
%FO	86	40	33	17	14	74

Table 7: Contingency tables for 12 hour precipitation (18-30 h forecasts) in the period 20020610 through 20020621. F stands for forecast and O for observation. The number is the class number (see text). %FO is the percentage of the forecasted values in the same class as the observation class. EWGLAM station list.

G4G 0206							G4E 0206						
obs→ / ↓for	O1	O2	O3	O4	O5	sum	obs→ / ↓for	O1	O2	O3	O4	O5	sum
F1	**4482**	168	110	26	**21**	4807	F1	**4497**	167	116	27	**24**	4831
F2	650	**142**	123	34	23	972	F2	622	**148**	121	29	18	938
F3	343	194	**241**	93	44	915	F3	356	186	**234**	89	46	911
F4	40	25	75	**36**	32	208	F4	44	26	70	**42**	32	214
F5	**17**	7	15	15	**37**	91	F5	**13**	9	23	17	**37**	99
sum	5532	536	564	204	157	6993	sum	5532	536	564	204	157	6993
%FO	81	26	43	18	24	71	%FO	81	28	41	21	24	71

G4N 0206							G45 0206						
obs→ / ↓for	O1	O2	O3	O4	O5	sum	obs→ / ↓for	O1	O2	O3	O4	O5	sum
F1	**4529**	180	110	24	**20**	4863	F1	**4761**	232	146	29	**25**	5193
F2	607	**141**	139	32	22	941	F2	588	**193**	206	71	29	1087
F3	345	184	**238**	82	42	891	F3	170	104	**173**	74	68	589
F4	42	21	54	**47**	37	201	F4	10	7	33	**23**	23	96
F5	**9**	10	23	19	**36**	97	F5	**3**	0	6	7	**12**	28
sum	5532	536	564	204	157	6993	sum	5532	536	564	204	157	6993
%FO	82	26	42	23	23	71	%FO	86	36	31	11	8	74

D1G 0206							D1E 0206						
obs→ / ↓for	O1	O2	O3	O4	O5	sum	obs→ / ↓for	O1	O2	O3	O4	O5	sum
F1	**4179**	131	95	21	**19**	4445	F1	**4210**	153	90	13	**20**	4486
F2	754	**138**	106	24	14	1036	F2	730	**126**	96	36	14	1002
F3	498	198	**245**	84	47	1072	F3	484	189	**274**	85	46	1078
F4	63	54	84	**56**	32	289	F4	85	53	70	**41**	31	280
F5	**38**	15	34	19	**45**	151	F5	**23**	15	34	29	**46**	147
sum	5532	536	564	204	157	6993	sum	5532	536	564	204	157	6993
%FO	76	26	43	27	29	67	%FO	76	24	49	20	29	67

D1N 0206							D15 0206						
obs→ / ↓for	O1	O2	O3	O4	O5	sum	obs→ / ↓for	O1	O2	O3	O4	O5	sum
F1	**4233**	130	91	17	**22**	4493	F1	**4700**	192	137	34	**34**	5097
F2	702	**140**	103	22	11	978	F2	639	**212**	188	49	23	1111
F3	489	207	**262**	96	43	1097	F3	174	119	**186**	88	57	624
F4	67	43	81	**50**	38	279	F4	16	11	47	**25**	29	128
F5	**41**	16	27	19	**43**	146	F5	**3**	2	6	8	**14**	33
sum	5532	536	564	204	157	6993	sum	5532	536	564	204	157	6993
%FO	77	26	46	25	27	68	%FO	85	40	33	12	9	73

Table 8: Contingency tables for 12 hour precipitation (6-18 h forecasts) in January 2002. F stands for forecast and O for observation. The number is the class number (see text). %FO is the percentage of the forecasted values in the same class as the observation class. Danish station list. The number in the parenthesis in the head of the subtables is the corresponding number for the "resultatkontrakt".

G4A 0201 (75.0 %)						
obs→ / ↓for	O1	O2	O3	O4	O5	sum
F1	**425**	40	3	1	0	469
F2	163	**86**	71	9	0	329
F3	12	31	**102**	41	8	194
F4	2	2	18	**32**	7	61
F5	0	0	0	3	**3**	6
sum	602	159	194	86	18	1059
%FO	71	54	53	37	17	61

D1A 0201 (77.8 %)						
obs→ / ↓for	O1	O2	O3	O4	O5	sum
F1	**454**	46	5	0	0	505
F2	128	**67**	43	4	0	242
F3	20	44	**129**	43	4	240
F4	0	2	17	**37**	10	66
F5	0	0	0	2	**4**	6
sum	602	159	194	86	18	1059
%FO	75	42	66	43	22	65

G4D 0201 (68.8 %)						
obs→ / ↓for	O1	O2	O3	O4	O5	sum
F1	**355**	34	9	0	0	398
F2	233	**95**	75	12	0	415
F3	13	28	**95**	42	5	183
F4	1	2	15	**29**	11	58
F5	0	0	0	3	**2**	5
sum	602	159	194	86	18	1059
%FO	59	60	49	34	11	54

D1D 0201 (73.6 %)						
obs→ / ↓for	O1	O2	O3	O4	O5	sum
F1	**410**	36	4	0	0	450
F2	172	**73**	50	3	0	298
F3	19	47	**122**	43	5	236
F4	1	3	18	**37**	11	70
F5	0	0	0	3	**2**	5
sum	602	159	194	86	18	1059
%FO	68	46	63	43	11	61

G4Z 0201 (68.8 %)						
obs→ / ↓for	O1	O2	O3	O4	O5	sum
F1	**326**	17	0	0	0	343
F2	236	**77**	37	0	0	350
F3	39	63	**131**	45	4	282
F4	1	2	26	**31**	6	66
F5	0	0	0	10	**8**	18
sum	602	159	194	86	18	1059
%FO	54	48	68	36	44	54

D1Z 0201 (68.9 %)						
obs→ / ↓for	O1	O2	O3	O4	O5	sum
F1	**280**	12	0	0	0	292
F2	268	**65**	22	0	0	355
F3	52	79	**144**	38	2	315
F4	2	3	27	**43**	14	89
F5	0	0	1	5	**2**	8
sum	602	159	194	86	18	1059
%FO	47	41	74	50	11	50

G45 0201 (62.2 %)						
obs→ / ↓for	O1	O2	O3	O4	O5	sum
F1	**243**	6	0	0	0	249
F2	303	**82**	19	0	0	404
F3	53	67	**137**	41	3	301
F4	3	4	36	**35**	7	85
F5	0	0	2	10	**8**	20
sum	602	159	194	86	18	1059
%FO	40	52	71	41	44	48

D15 0201 (62.7 %)						
obs→ / ↓for	O1	O2	O3	O4	O5	sum
F1	**243**	4	0	0	0	247
F2	298	**63**	13	0	0	374
F3	60	85	**149**	27	4	325
F4	1	7	32	**55**	13	108
F5	0	0	0	4	**1**	5
sum	602	159	194	86	18	1059
%FO	40	40	77	64	6	48

Table 9: Contingency tables for 12 hour precipitation (18-30 h forecasts) in January 2002 F stands for forecast and O for observation. The number is the class number (see text). %FO is the percentage of the forecasted values in the same class as the observation class. Danish station list. The number in the parenthesis in the head of the subtables is the corresponding number for the "resultatkontrakt".

G4A 0201 (68.0 %)						
obs→ / ↓for	O1	O2	O3	O4	O5	sum
F1	**355**	23	11	2	0	391
F2	190	**68**	32	2	0	292
F3	42	57	**123**	53	9	284
F4	2	7	26	**27**	6	68
F5	**1**	0	0	2	**3**	6
sum	590	155	192	86	18	1041
%FO	60	44	64	31	17	55

D1A 0201 (73.3 %)						
obs→ / ↓for	O1	O2	O3	O4	O5	sum
F1	**429**	27	11	2	0	469
F2	128	**67**	32	3	0	230
F3	27	54	**116**	41	5	243
F4	5	5	30	**38**	11	89
F5	0	2	3	2	**2**	9
sum	589	155	192	86	18	1040
%FO	73	43	60	44	11	63

G4D 0201 (62.5 %)						
obs→ / ↓for	O1	O2	O3	O4	O5	sum
F1	**286**	14	6	2	0	308
F2	273	**75**	33	3	0	384
F3	26	58	**124**	49	8	265
F4	5	8	26	**27**	3	69
F5	0	0	3	5	**7**	15
sum	590	155	192	86	18	1041
%FO	48	48	65	31	39	50

D1D 0201 (69.7 %)						
obs→ / ↓for	O1	O2	O3	O4	O5	sum
F1	**384**	18	7	2	0	411
F2	168	**64**	27	3	0	262
F3	33	65	**127**	48	6	279
F4	5	6	26	**32**	7	76
F5	0	2	5	1	**5**	13
sum	590	155	192	86	18	1041
%FO	65	41	66	37	28	59

G4Z 0201 (60.6 %)						
obs→ / ↓for	O1	O2	O3	O4	O5	sum
F1	**261**	18	8	0	0	287
F2	258	**51**	26	5	0	340
F3	69	82	**126**	47	4	328
F4	2	4	30	**29**	6	71
F5	0	0	2	5	**8**	15
sum	590	155	192	86	18	1041
%FO	44	33	66	34	44	46

D1Z 0201 (64.6 %)						
obs→ / ↓for	O1	O2	O3	O4	O5	sum
F1	**267**	10	8	1	0	286
F2	276	**55**	17	3	0	351
F3	46	88	**145**	44	3	326
F4	1	2	22	**36**	9	70
F5	0	0	0	2	**6**	8
sum	590	155	192	86	18	1041
%FO	45	35	76	42	33	49

G45 0201 (55.0 %)						
obs→ / ↓for	O1	O2	O3	O4	O5	sum
F1	**198**	7	0	0	0	205
F2	333	**66**	39	2	0	440
F3	58	76	**119**	42	6	301
F4	1	6	33	**40**	4	84
F5	0	0	1	2	**8**	11
sum	590	155	192	86	18	1041
%FO	34	43	62	47	44	41

D15 0201 (55.2 %)						
obs→ / ↓for	O1	O2	O3	O4	O5	sum
F1	**180**	6	0	0	0	186
F2	343	**56**	23	2	0	424
F3	66	90	**143**	49	4	352
F4	1	3	26	**33**	8	71
F5	0	0	0	2	**6**	8
sum	590	155	192	86	18	1041
%FO	31	36	74	38	33	40

Table 10: Contingency tables for 12 hour precipitation (6-18 h forecasts) in January 2002. F stands for forecast and O for observation. The number is the class number (see text). %FO is the percentage of the forecasted values in the same class as the observation class. EWGLAM station list.

G4A 0201							D1A 0201						
obs→ / ↓for	O1	O2	O3	O4	O5	sum	obs→ / ↓for	O1	O2	O3	O4	O5	sum
F1	**9393**	489	198	28	**6**	10114	F1	**10223**	568	229	37	**21**	11078
F2	3085	**1066**	688	90	22	4951	F2	2231	**987**	605	69	11	3903
F3	530	526	**1046**	350	93	2545	F3	547	525	**1074**	317	77	2540
F4	21	28	148	**176**	117	490	F4	32	29	164	**218**	101	544
F5	**8**	1	13	29	**48**	99	F5	**4**	1	21	32	**76**	134
sum	13037	2110	2093	673	286	18199	sum	13037	2110	2093	673	286	18199
%FO	72	51	50	26	17	64	%FO	78	47	51	32	27	69

G4D 0201							D1D 0201						
obs→ / ↓for	O1	O2	O3	O4	O5	sum	obs→ / ↓for	O1	O2	O3	O4	O5	sum
F1	**8627**	409	160	23	**3**	9222	F1	**9351**	462	157	35	**19**	10024
F2	3748	**1162**	770	95	26	5801	F2	2947	**1031**	637	69	10	4694
F3	630	506	**1015**	357	107	2615	F3	704	581	**1110**	330	88	2813
F4	26	33	134	**167**	112	472	F4	31	34	166	**204**	108	543
F5	**6**	0	14	31	**38**	89	F5	**4**	2	23	35	**61**	125
sum	13037	2110	2093	673	286	18199	sum	13037	2110	2093	673	286	18199
%FO	66	55	48	25	13	60	%FO	72	49	53	30	21	65

G4Z 0201							D1Z 0201						
obs→ / ↓for	O1	O2	O3	O4	O5	sum	obs→ / ↓for	O1	O2	O3	O4	O5	sum
F1	**8033**	258	69	20	**3**	8383	F1	**7662**	269	97	28	**16**	8072
F2	3967	**926**	414	43	10	5360	F2	4253	**875**	382	43	7	5560
F3	977	878	**1344**	284	83	3566	F3	1051	908	**1318**	271	66	3614
F4	48	43	224	**265**	91	671	F4	54	53	258	**278**	101	744
F5	**12**	5	42	61	**99**	219	F5	**17**	5	38	53	**96**	209
sum	13037	2110	2093	673	286	18199	sum	13037	2110	2093	673	286	18199
%FO	62	44	64	39	35	59	%FO	59	41	63	41	34	56

G45 0201							D15 0201						
obs→ / ↓for	O1	O2	O3	O4	O5	sum	obs→ / ↓for	O1	O2	O3	O4	O5	sum
F1	**7048**	169	40	7	**2**	7266	F1	**6849**	200	84	21	**18**	7172
F2	4804	**949**	375	43	9	6180	F2	4804	**825**	301	38	2	5970
F3	1121	916	**1370**	275	67	3749	F3	1306	1007	**1374**	268	57	4012
F4	56	68	262	**275**	106	767	F4	64	73	295	**283**	127	842
F5	**8**	8	46	73	**102**	237	F5	**14**	5	39	63	**82**	203
sum	13037	2110	2093	673	286	18199	sum	13037	2110	2093	673	286	18199
%FO	54	45	65	41	36	54	%FO	53	39	66	42	29	52

Table 11: Contingency tables for 12 hour precipitation (18-30 h forecasts) in January 2002 F stands for forecast and O for observation. The number is the class number (see text). %FO is the percentage of the forecasted values in the same class as the observation class. EWGLAM station list.

G4A 0201							D1A 0201						
obs→ / ↓ for	O1	O2	O3	O4	O5	sum	obs→ / ↓ for	O1	O2	O3	O4	O5	sum
F1	**8842**	419	167	25	**7**	9460	F1	**9975**	579	244	43	**20**	10861
F2	3219	**986**	614	86	23	4928	F2	2145	**835**	546	77	17	3620
F3	727	636	**1127**	371	97	2958	F3	670	634	**1087**	331	79	2801
F4	37	39	122	**142**	106	446	F4	39	32	155	**175**	108	509
F5	**9**	5	18	29	**48**	109	F5	**5**	5	16	27	**57**	110
sum	12834	2085	2048	653	281	17901	sum	12834	2085	2048	653	281	17901
%FO	69	47	55	22	17	62	%FO	78	40	53	27	20	68

G4D 0201							D1D 0201						
obs→ / ↓ for	O1	O2	O3	O4	O5	sum	obs→ / ↓ for	O1	O2	O3	O4	O5	sum
F1	**8215**	360	141	21	**6**	8743	F1	**9204**	455	187	34	**18**	9898
F2	3806	**1053**	664	93	22	5638	F2	2720	**884**	521	74	15	4214
F3	764	622	**1096**	363	115	2960	F3	858	693	**1157**	343	84	3135
F4	45	43	128	**156**	100	472	F4	45	48	156	**174**	115	538
F5	**4**	7	19	20	**38**	88	F5	**7**	5	27	28	**49**	116
sum	12834	2085	2048	653	281	17901	sum	12834	2085	2048	653	281	17901
%FO	64	51	54	24	14	59	%FO	72	42	56	27	17	64

G4Z 0201							D1Z 0201						
obs→ / ↓ for	O1	O2	O3	O4	O5	sum	obs→ / ↓ for	O1	O2	O3	O4	O5	sum
F1	**7465**	268	88	20	**3**	7844	F1	**7353**	309	139	35	**19**	7855
F2	4168	**838**	394	52	22	5474	F2	4266	**806**	385	56	10	5523
F3	1123	895	**1291**	320	74	3703	F3	1127	902	**1256**	288	59	3632
F4	63	71	235	**202**	94	665	F4	76	56	243	**211**	101	687
F5	**15**	13	40	59	**88**	215	F5	**12**	12	25	63	**92**	204
sum	12834	2085	2048	653	281	17901	sum	12834	2085	2048	653	281	17901
%FO	58	40	63	31	31	55	%FO	57	39	61	32	33	54

G45 0201							D15 0201						
obs→ / ↓ for	O1	O2	O3	O4	O5	sum	obs→ / ↓ for	O1	O2	O3	O4	O5	sum
F1	**6524**	167	49	9	**2**	6751	F1	**6715**	239	93	24	**15**	7086
F2	4891	**870**	336	46	11	6154	F2	4676	**805**	341	44	8	5874
F3	1334	965	**1365**	298	76	4038	F3	1355	958	**1322**	299	75	4009
F4	76	70	241	**227**	99	713	F4	80	75	264	**223**	115	757
F5	**9**	13	57	73	**93**	245	F5	**8**	8	28	63	**68**	175
sum	12834	2085	2048	653	281	17901	sum	12834	2085	2048	653	281	17901
%FO	51	42	67	35	33	51	%FO	52	39	65	34	24	51

The worst scores for the summer period are shared by several model versions, without any clear candidate.

For January 2002 G45/D15 (the operational DMI-HIRLAM versions) have the worst scores, but note that the inter comparison is against model versions (G4D/D1D and G4Z/D1Z) that are complementary to those for the June2002-period. Furthermore, the inter comparison is not clean since the operational models made use of a coupling to ECMWF that differed significantly from that utilized by the other runs. Note also that G4Z/D1Z have a significantly better prediction of the precipitation classes O3-O5 and a worse prediction of classes O1 and O2 than G4D/D1D and G4A/D1A.

4.2. Observation verification

Figures 21-25 show conventional observation verification (obs-verification) results with use of the standard EWGLAM station list and a list of Danish SYNOP stations for the June period. It is clear from these figures that the differences are very small among the experiments using dmiconfig 12b (E, G, N, P, and O). Compared to this cluster G4J/D1J (using dmiconfig 11) has slightly better score in many of the shown parameters. The scores for the OE-pair indicate that there is a neutral to weak positive impact of shifting from no use (G4O/D1O) to use (G4E/D1E) of NOAA16 data. The scores for the NE-pair shows a neutral or for some upper level parameters a weak positive impact of shifting from use of RTTOV5 (G4N/D1N) to RTTOV7 (G4E/D1E). This result indicates that the use of RTTOV7 is definitely no worse than use of RTTOV5 in this period. It should, however, be kept in mind that there are other differences in the 3D-Var code than the RTTOV version difference. Figures 26-28 show the results for the January period for three test-runs (A, D, and Z) and the operational models (G45/D15). It is clear form these figures that the operational versions generally have the best scores. Too much emphasis should not be put into this result because (as mentioned previously) a comparison with the operational models is unfair since the coupling to ECMWF boundaries are very different in the test runs.

No conclusion about the relative performance of the test models can be based on these results since the model with the best scores differ for different variables. A far more clear picture is seen in the results for the obs-verification of the vertical structures shown in figures 29-33. It is clear form these figures that G4Z/D1Z have a much better vertical structure than both G4A/D1A and G4D/D1D. Model versions A and D both use upstream advection of q, CW and TKE and differs only by the dmiconfig number, (11 and 12b, respectively). The significant improvement of the vertical structure for G4Z/D1Z is therefore mainly due to the shift from upstream to centered difference advection of q and CW. Stated in another way: the use of the upstream advection scheme has a bad influence on the vertical structure both in the old dmiconfig 11 and in the new dmiconfig 12. The same tendencies can be seen in a comparison between the operational runs and the hirtst runs done in very near real time in parallel with the new configuration. For the short June period the vertical structure differences are similar (figures not shown).

5. Conclusion

It has been shown in the present report that utilization of an upstream advection scheme for specific humidity (q) and specific cloud water (CW) results in an unrealistic reduction in predicted amounts of precipitation. A splitting of the precipitation into stratiform and convective precipitation showed that the reduction in predicted precipitation mainly occurred in the convective part. This is in agreement with the finding that the problem with too low predicted precipitation amounts was considerably higher in the summer period.

Vertical temperature profiles (e.g., Figure 31) clearly showed that the troposphere above the planetary boundary layer (the free atmosphere) became increasingly more stable with larger forecast lead times in the experiments using upstream advection of q and CW instead of centered difference advection. The largest stabilization occurred during the first 12 hours of the forecasts. It was further shown that the impact of a shift from upstream to centered difference advection of turbulent kinetic energy (TKE) was marginal. It is believed that the much stronger negative impact of upstream advection in summer is due to the fact that the free atmosphere tends to be less stably stratified in this season than in winter. Consequently, both the probability of convection and the probability of suppressing convection by the stabilizing effect of the upstream advection of q and CW is higher in summer.

For January 2002 the root mean square (rms) error scores of temperature and geopotential height at standard pressure levels were also considerably better with centered difference advection of q and CW (G4Z/D1Z) than with upstream advection of these parameters (G4A/D1A and G4D/D1D). The difference in rms error scores between the two experiments with upstream advection (G4A/D1A and G4D/D1D) was much smaller than the corresponding differences to G4Z/D1Z, and probably because of the significant impact of the upstream advection no clear improvement was seen by shifting from dmiconfig 11 to dmiconfig 12b (see Appendix A for explanation of the dmiconfig numbers). Anyway, the shift from dmiconfig 11 to dmiconfig 12b with centered difference advection of q and CW (experiments D1J and D1P, respectively) showed improved results with dmiconfig 12b. This was particularly clear when comparing predicted accumulated precipitation fields for three cases in the June2002-period. In one of these cases (18 June), which was dominated by convective multicell systems, the improvement was substantial and occurred mainly in the predicted convective precipitation.

The case studies done in the June2002-period, and the 18 June case in particular, left the impression that a significant part of the scatter in the details of the predicted accumulated precipitation fields could be ascribed to the low-predictability nature of convective precipitation systems. If this turns out to be true; the "poor-man" mini-ensemble for the 18 June case (Figure 15), consisting of the experiments D1* (*=O, E, P, N and G) gives an impression of the statistical uncertainty of the predicted accumulated precipitation. According to Table 2 the perturbations in the mini-ensemble consists of a shift from upstream advection to centered difference advection of TKE, a shift from high to low resolution in the 3D-Var analysis, a shift from RTTOV5 to RTTOV7 and a shift from no use of NOAA16 AMSU-A data to use of these data by means of RTTOV7.

Appendix A. Details concerning experiments

Table 12: Experimental setups. See text for explanation.

model	3D-Var	hm.exe	# CPU	version	N_{upstream}	period	RTTOV
G45/D15	low	32 bit	3/11	11	56 (q,CW,TKE)	—	5
G4Z	—	32 bit	4	12	32 (TKE)	June	5
G4Z/D1Z	low	64 bit	4	12**b**	32 (TKE)	January	5
G4D/D1D	low	64 bit	4	**11**	**56** (q,CW,TKE)	January	5
G4A/D1A	low	64 bit	4	12**b**	**56** (q,CW,TKE)	January	5
G4A/D1A	low	64 bit	1	12**a**	**56** (q,CW,TKE)	June	5
G4X/D1X	low	32 bit	4	12	32 (TKE)	June	5
G4Y/D1Y	high	32 bit	4	12	32 (TKE)	June	5
G4H/D1H	high	64 bit	4	12	32 (TKE)	June	5
G4I/D1I	low	64 bit	4	12	32 (TKE)	June	5
G4J/D1J	low	64 bit	1	**11**	32 (TKE)	June	5
G4K/D1K	low	64 bit	**1**	12	32 (TKE)	June	5
G4L/D1L	high	64 bit	**1**	12	32 (TKE)	June	5
G4M/D1M	high	64 bit	**1**	12**a**	32 (TKE)	June	7
G4Q/D1Q	high	64 bit	**1**	12**a**	**0** (none)	June	5
G4E/D1E	high	64 bit	4	12**b**	32 (TKE)	June	7
G4G/D1G	high	64 bit	4	12**b**	**0** (none)	June	7
G4N/D1N	high	64 bit	4	12**b**	32 (TKE)	June	5
G4P/D1P	low	64 bit	4	12**b**	32 (TKE)	June	5
G4O/D1O	high	64 bit	4	12**b**	32 (TKE)	June	—

The operational DMI-HIRLAM model domains are shown in Figure 2. The domains are all on a rotated grid with polar coordinates $(P_{\text{lat}}, P_{\text{lon}}) = (0°, 80°)$. The starting coordinates (south west corner) in the rotated coordinate system are given in the figure as well. Table 12 shows the variables that have changed in the setups for different runs. "G45/D15" is the operational setup (Sass *et al.*, 2002). The first column is the model and G4x is for DMI-HIRLAM-G and D1x is for DMI-HIRLAM-E. The second column shows whether a "low"-resolution (0.45°) or "high"-resolution 3D-Var (0.15°) has been used for the DMI-HIRLAM-E analyses. The third column shows whether a 32 bit or a 64 bit version of the forecast model (named hm.exe) has been used in the given experiment. The fourth column shows the number of CPU's used in the runs and the fifth column shows which version (dmiconfig number) of the DMI-HIRLAM model has been used. dmiconfig number 11 is the operational version and 12 is the test version

as of summer 2002. The 64 bit without the extra **a** or **b** in the dmiconfig version number have a modified straco021.f version (with zrest and zqcd1 initialized to zero). The 64 bit version with 12**a** in the dmiconfig number indicates a further modification ("BHS"-revision to the other revision) of the straco021.f subroutine. The 64 bit version with 12**b** has the reproducibility problem bug-fixed and yet another small revision of the STRACO scheme by including extra namelist variables and revised initial settings of 4 of the namelist variables. The previous and the new values are given as follows:

variable	new	old
`cpcr`	25000	10000
`cenfac0`	1.3×10^{-4}	2.5×10^{-4}
`cenfac1`	7.5×10^{-4}	1.0×10^{-3}
`coefent`	0.15	0.30

Two parameters (`cenfac0` and `cenfac1`) used to describe lateral entrainment for the convective cloud have been reduced. Also the cloud top entrainment parameter (`coefent`) has been decreased. Finally, a vertical scale parameter (`cpcr`) defining interaction between updates due to turbulence and convection has been increased. These tunings were established from experimentation in the HIRLAM project collaboration during summer 2002.

The variable `$w->{hlm}->{euler}->{nupsadv}` given in column 6 is set as a sum of indices ($u \sim 1$, $v \sim 2$, $T \sim 4$, $q \sim 8$, CW ~ 16 and TKE ~ 32) given to the variables for which the upstream scheme should be used. As an example 56(=8+16+32) is used for runs in which the upstream scheme is used for q, CW and TKE. The value 32 is used for runs in which the upstream scheme is used only for TKE. The second last column shows the period for which the run has been made. January is for the whole of January 2002 starting from an operationally archived DMI-HIRLAM-G first guess file valid on 03 UTC January 1. The June period is also in 2002 and the runs start from an operationally archived DMI-HIRLAM-G/DMI-HIRLAM-E first guess file valid on 03 UTC June 10 and runs until 21 UTC June 21, 2002. For the January period ECMWF analyses files for every 6 hours have been used as boundaries for DMI-HIRLAM-G since some FRAME boundaries were missing in the UNITREE archive and it is not possible to extract these files from the ECMWF mars archive. For the June period, FRAME boundary files have been used for DMI-HIRLAM-G. Accordingly, this period has been run exactly like the operational suite in this respect. However, a variable in the setups—including the operational setup—has the effect that if new FRAME boundary files are available for the 18 UTC runs they will be used for the long 18 UTC runs instead of the 6 hour older FRAME boundary files from 12 UTC. This only influences the long 18 UTC runs and should have only minor effects in the tests and it is the same for all runs.

References

Amstrup, Bjarne. 2001. *Impact of ATOVS AMSU-A radiance data in the DMI-HIRLAM 3D-Var analysis and forecasting system.* DMI Scientific Report 01-06. Danish Meteorological Institute.

Amstrup, Bjarne, Jørgensen, Jess U. and Sass, Bent Hansen. 2002. *DMI-HIRLAM parallel tests during first quarter of 2002*. DMI Intern Report 02-06. Danish Meteorological Institute.

Haltiner, George J. 1971. *Numerical Weather Prediction*. J. Wiley & Sons. ISBN: 0-471-34580-6.

Nielsen, Niels W. and Amstrup, Bjarne. 2001a. *DMI-HIRLAM Verification/Benchmarking Report for the second quarter of 2001*. DMI Intern Rapport 01-09. Danish Meteorological Institute.

Nielsen, Niels W. and Amstrup, Bjarne. 2001b. *DMI-HIRLAM Verification/Benchmarking Report for the third quarter of 2001*. DMI Intern Rapport 01-14. Danish Meteorological Institute.

Nielsen, Niels W. and Amstrup, Bjarne. 2002a. *DMI-HIRLAM Verification/Benchmarking Report for the second quarter of 2002*. DMI Intern Rapport 02-08. Danish Meteorological Institute.

Nielsen, Niels W. and Amstrup, Bjarne. 2002b. *DMI-HIRLAM Verification/Benchmarking Report for the third quarter of 2002*. DMI Intern Rapport 02-12. Danish Meteorological Institute.

Nielsen, Niels Woetmann and Rasmussen, Leif. 2002. Uvejret den 18. juni 2002. *Vejret*, **92+93**, 1–23.

Rotunno, R. and Klemp, J. B. 1982. The influence of the shear-induced pressure gradient on thunderstorm motion. *Mon. Weather Rev.*, **110**, 136–151.

Sass, B. H. 2002. *A research version of the STRACO cloud scheme*. DMI Technical Report 02-10. Danish Meteorological Institute.

Sass, B. H. and Yang, Xiaohua. 2002. Recent tests of proposed revisions to the STRACO cloud scheme. *Hirlam Newsletter*, **41**, 167–174.

Sass, Bent Hansen. 2001. Modelling of the time evolution of low tropospheric clouds capped by a stable layer. *HIRLAM Technical Report*, **50**.

Sass, Bent Hansen, Nielsen, Niels Woetmann, Jørgensen, Jess U., Amstrup, Bjarne, Kmit, Maryanne and Mogensen, Kristian S. 2002. *The Operational DMI-HIRLAM System - 2002 version*. DMI Technical Report 02-5. Danish Meteorological Institute.

Schyberg, Harald, Landelius, Tomas, Thorsteinsson, Sigurdur, Tveter, Frank Thomas, Vignes, Ole, Amstrup, Bjarne, Gustafsson, Nils, Järvinen, Heikki and Lindskog, Magnus. 2003. Assimilation of ATOVS data in the HIRLAM 3D-Var System. *HIRLAM Technical Report*, **to be published**.

Sundqvist, H. 1993. Inclusion of ice phase of hydrometers in cloud parameterization for mesoscale and large-scale models. *Beitr. Phys. Atmosph.*, **66**, 137–147.

Vejen, Flemming. 2002. *Korrektion for fejlkilder på måling af nedbør. Korrektionsprocenter ved udvalgte stationer i 2001.* DMI Technical Report 02-08. Danish Meteorological Institute.

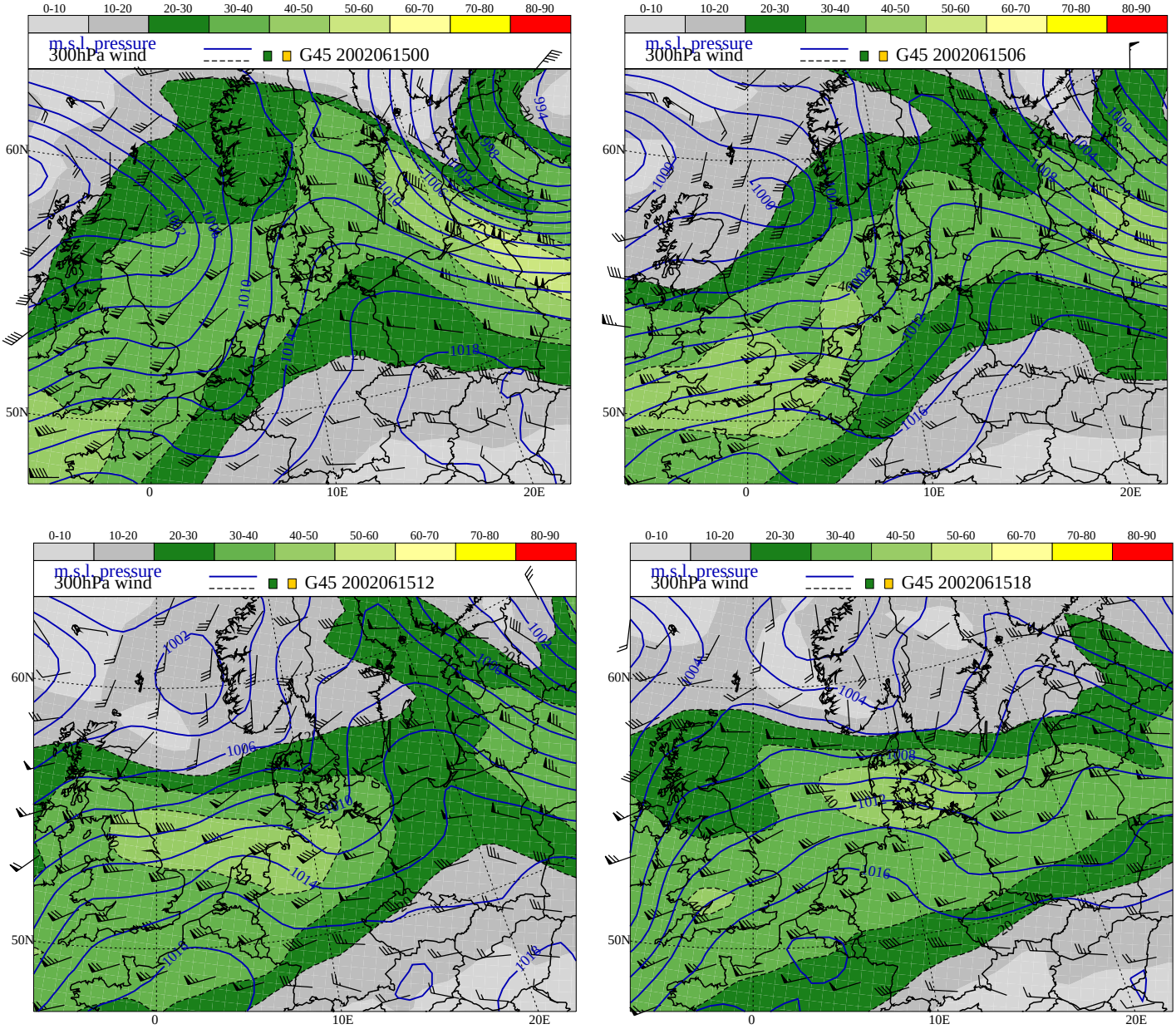

Figure 3: Operational DMI-HIRLAM-G 'analyses' of mslp and wind at 300 hPa valid at **a)** 00 UTC (upper left), **b)** 06 UTC (upper right), **c)** 12 UTC (lower left), and **d)** 18 UTC (lower right) 15 June 2002. Contour interval for mslp is 2 hPa. Contour interval for wind speed is 10 $\mathrm{m\,s^{-1}}$, minimum contour is 20 $\mathrm{m\,s^{-1}}$. Wind arrows are WMO standard.

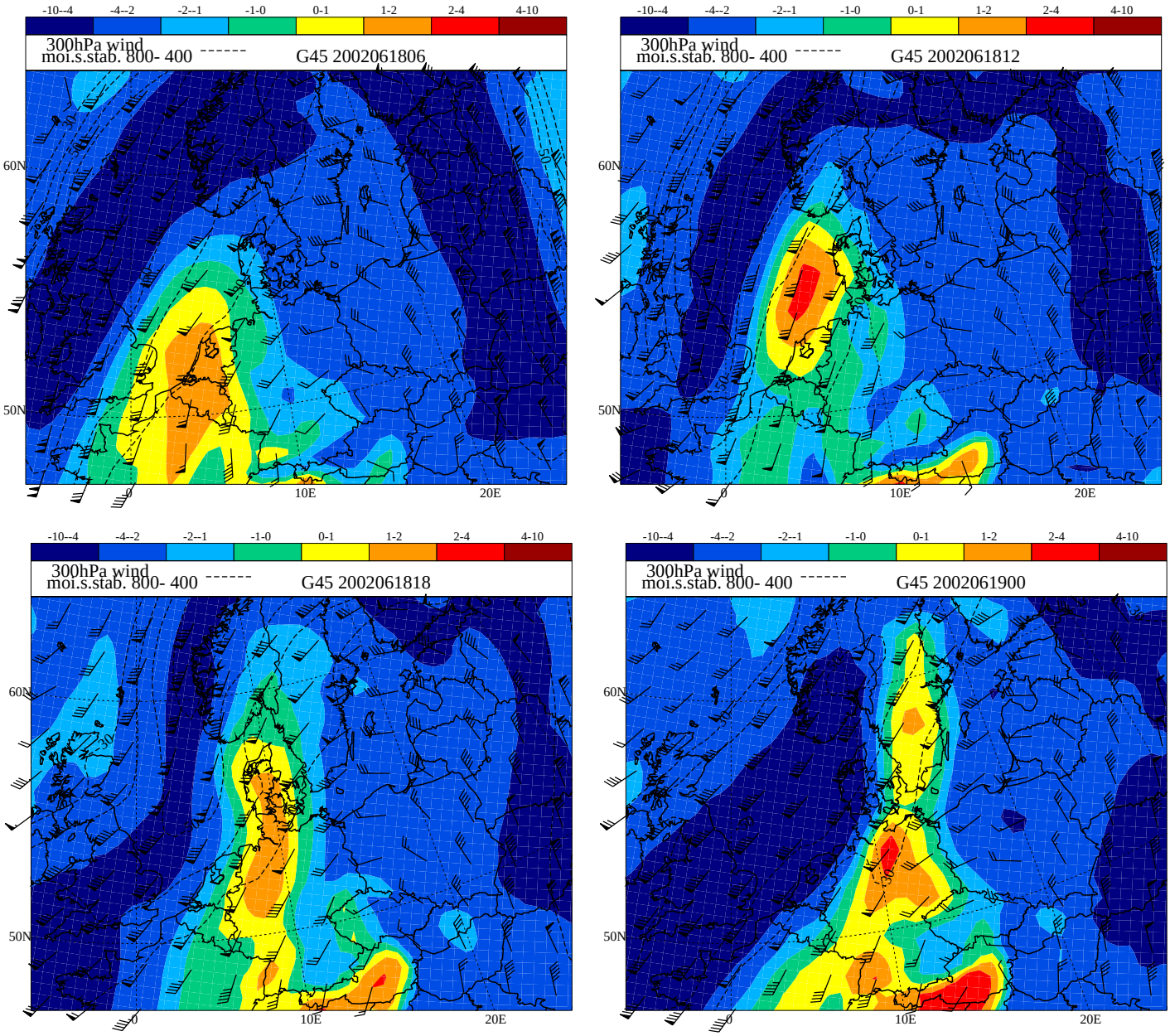

Figure 4: Operational DMI-HIRLAM-G 'analyses' of 'bulk moist static instability' $(\theta_e(800) - \theta_e(400))/(p(800) - p(400))$ and wind at 300 hPa valid at **a)** 06 UTC 18 June 2002 (upper left), **b)** 12 UTC 18 June 2002 (upper right), **c)** 18 UTC 18 June 2002 (lower left), and **d)** 00 UTC 19 June 2002 (lower right). Contour interval for 'bulk moist static instability' is 2×10^{-4}K Pa^{-1}, negative and positive values are blue to green and yellow to red, respectively. Contour interval for wind speed is 10 m s^{-1}, minimum contour is 30 m s^{-1}. Wind arrows are WMO standard.

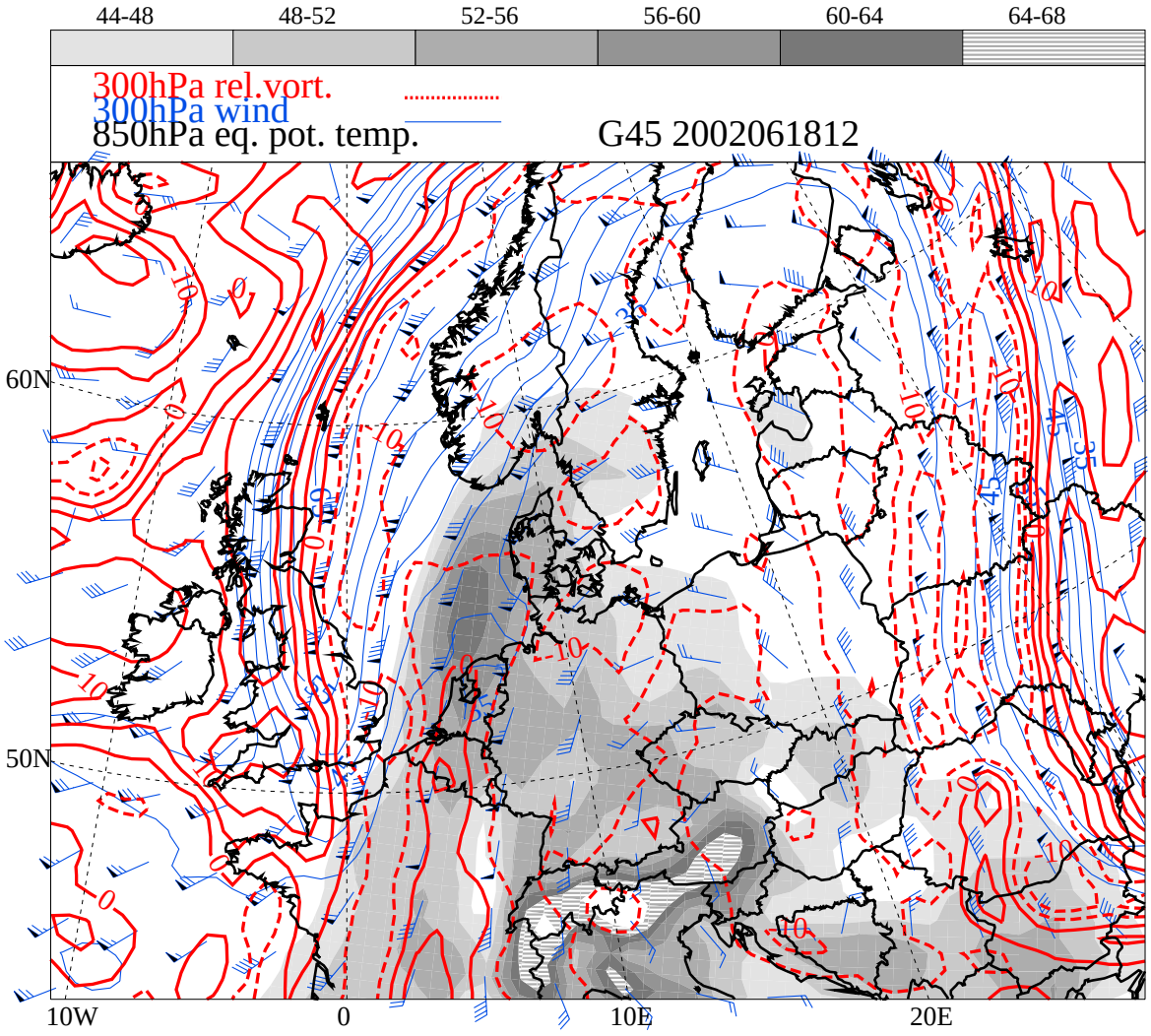

Figure 5: Operational DMI-HIRLAM-G 'analysis' valid at 12 UTC 18 June 2002 of relative vorticity and wind at 300 hPa and eq. pot. temperature at 850 hPa. Contour interval for wind speed is $5\,\mathrm{m\,s^{-1}}$, minimum contour is $35\,\mathrm{m\,s^{-1}}$. Wind arrows are WMO standard. Contour interval for relative vorticity is $5 \times 10^{-5}\mathrm{s^{-1}}$.

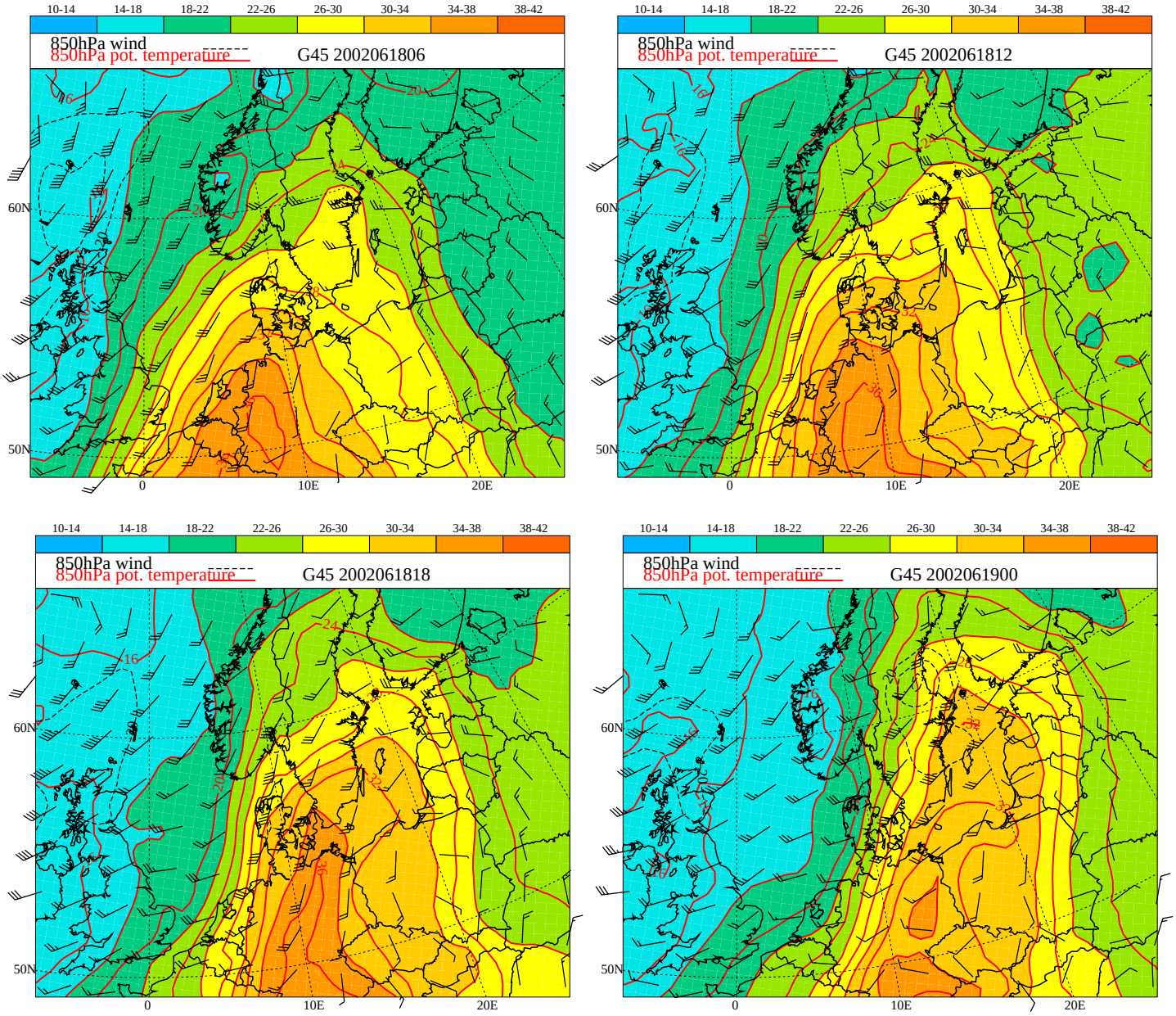

Figure 6: Operational DMI-HIRLAM-G 'analyses' of potential temperature (θ) and wind at 850 hPa valid at **a)** 06 UTC 18 June 2002 (upper left), **b)** 12 UTC 18 June 2002 (upper right), **c)** 18 UTC 18 June 2002 (lower left), and **d)** 00 UTC 19 June 2002 (lower right). Contour interval for θ is 2 K and for wind speed 5 m s^{-1}, minimum contour is 20 m s^{-1}. Wind arrows are WMO standard.

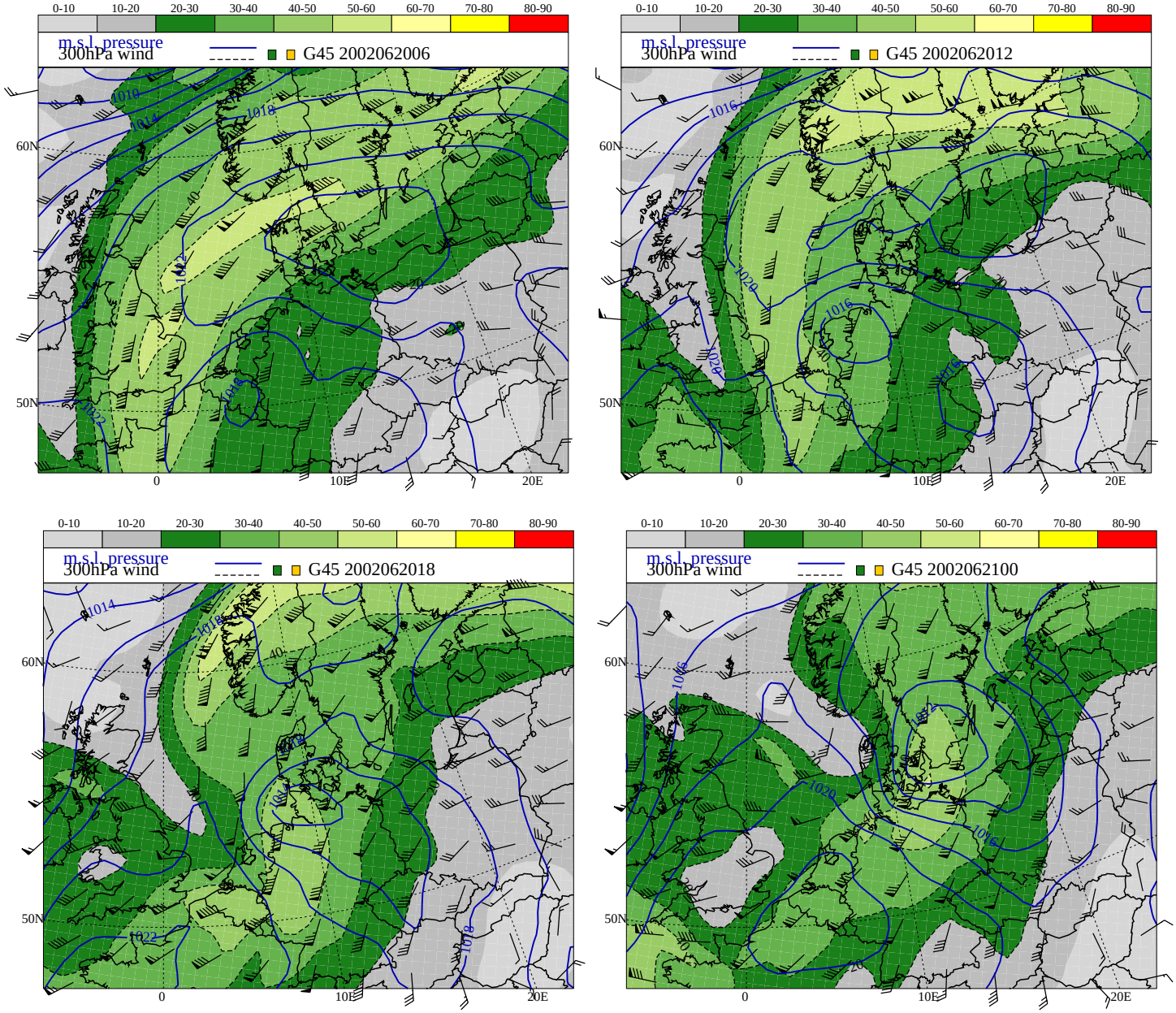

Figure 7: Operational DMI-HIRLAM-G 'analyses' of mslp and wind at 300 hPa valid at **a)** 06 UTC 20 June 2002 (upper left), **b)** 12 UTC 20 June 2002 (upper right), **c)** 18 UTC 20 June 2002 (lower left), and **d)** 00 UTC 21 June 2002 (lower right). Contour interval for mslp is 2 hPa. Contour interval for wind speed is 10 m s^{-1}, minimum contour is 20 m s^{-1}.

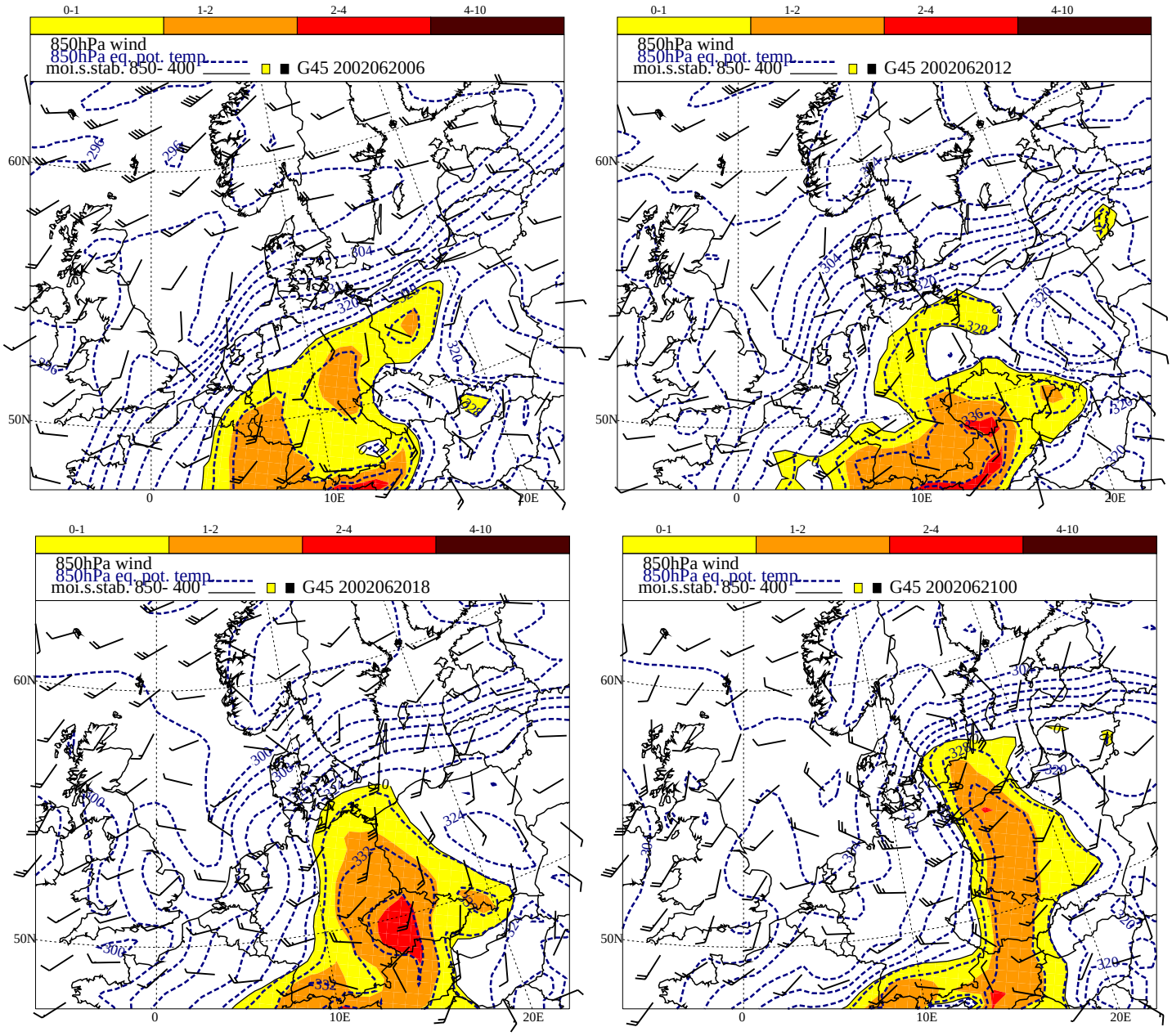

Figure 8: Operational DMI-HIRLAM-G 'analyses' of 850 hPa equivalent potential temperature (θ_e), 'bulk moist static instability' $(\theta_e(850) - \theta_e(400))/(p(850) - p(400))$, and wind at 850 hPa valid at **a)** 06 UTC 20 June 2002 (upper left), **b)** 12 UTC 20 June 2002 (upper right), **c)** 18 UTC 20 June 2002 (lower left), and **d)** 00 UTC 21 June 2002 (lower right). The unit for 'bulk moist static instability' is $10^{-4}\mathrm{K\,Pa^{-1}}$ and only positive values are indicated. The contour interval for θ_e is 2 K. Wind arrows are WMO standard.

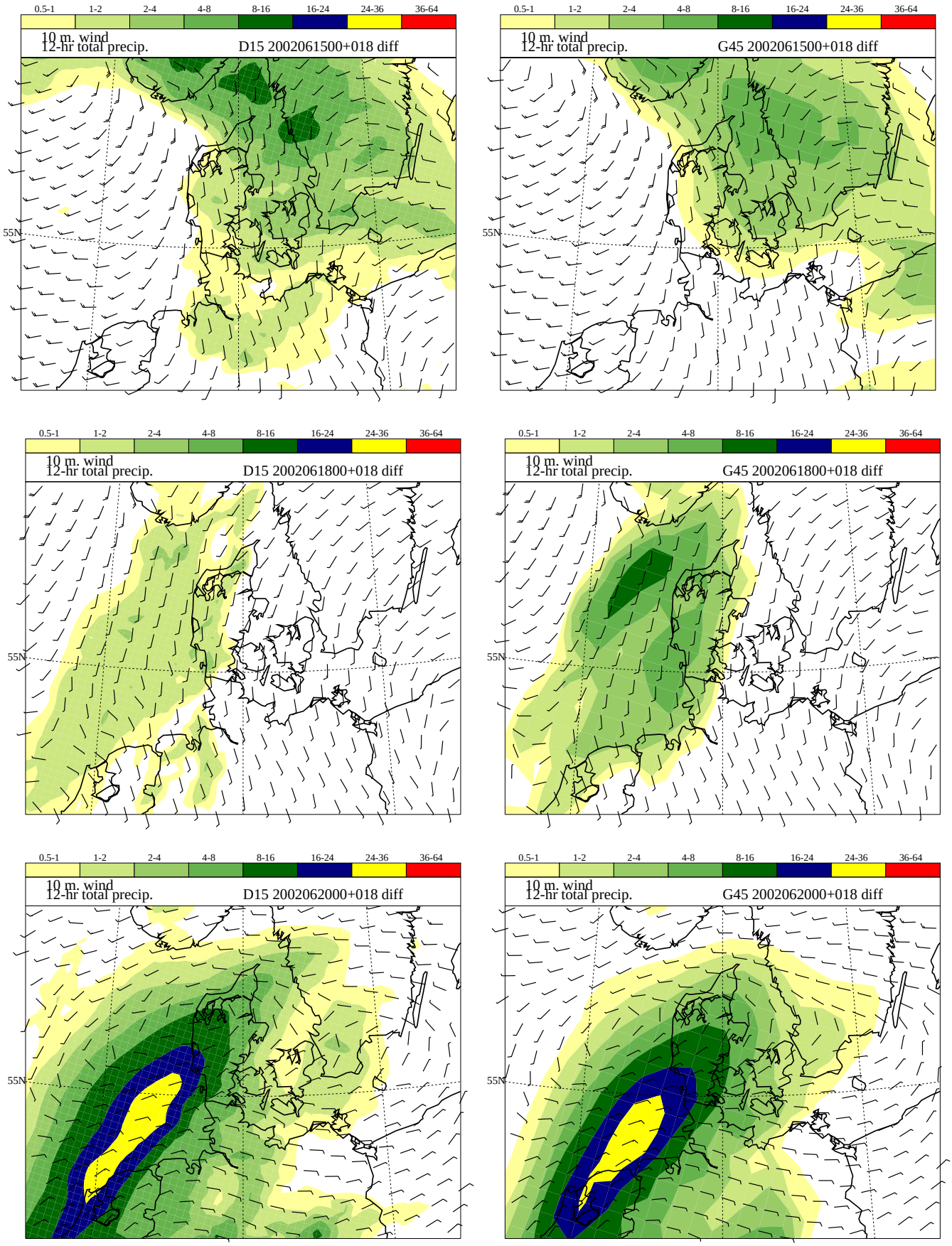

Figure 9: Operational DMI-HIRLAM-E (left) and DMI-HIRLAM-G (right) forecasted (6 h-18 h forecasts) 12 h accumulated precipitation valid on 18 UTC June 15 (upper), June 18 (middle) and June 20 (lower).

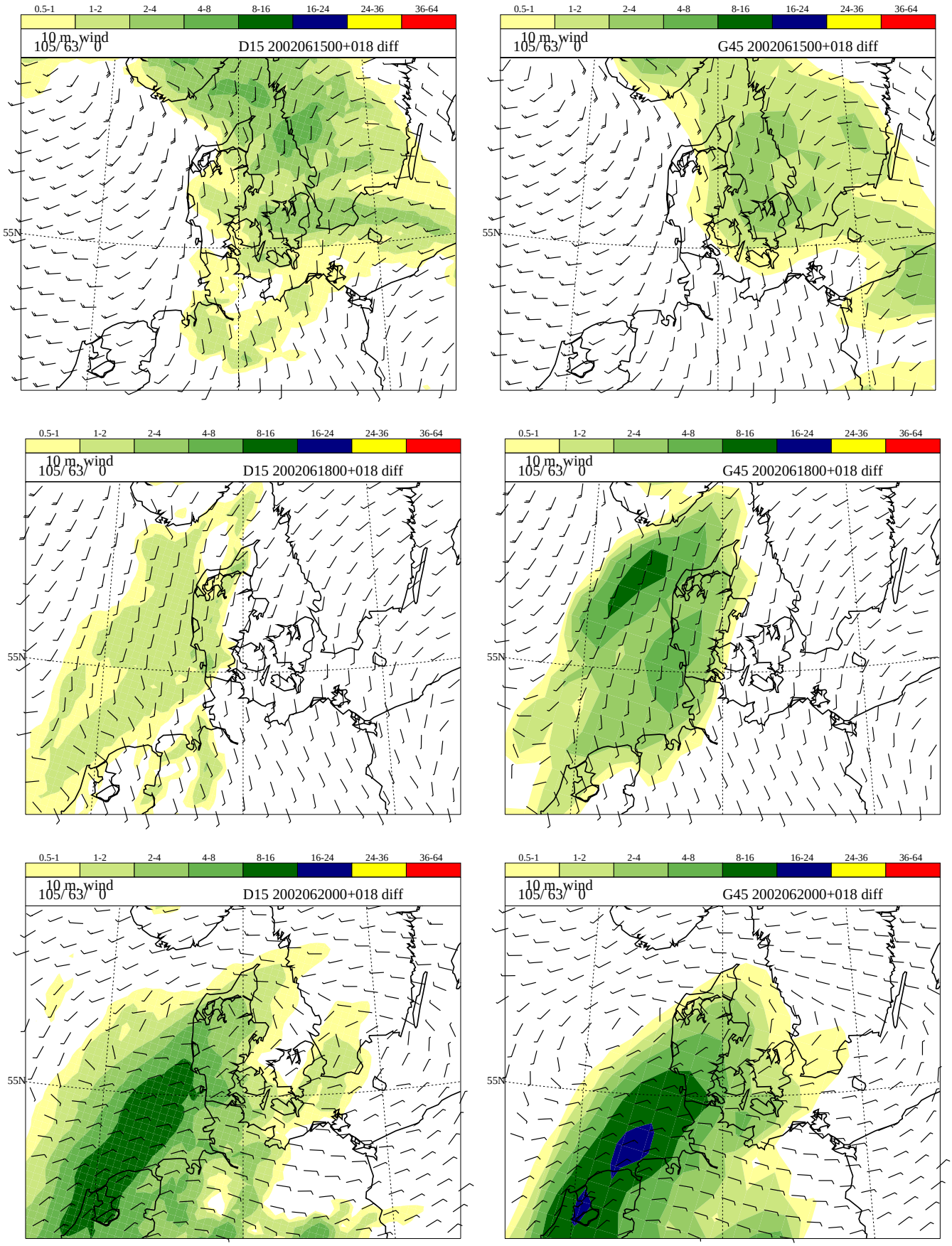

Figure 10: Operational DMI-HIRLAM-E (left) and DMI-HIRLAM-G (right) forecasted (6 h-18 h forecasts) 12 h accumulated convective precipitation valid on 18 UTC June 15 (upper), June 18 (middle) and June 20 (lower).

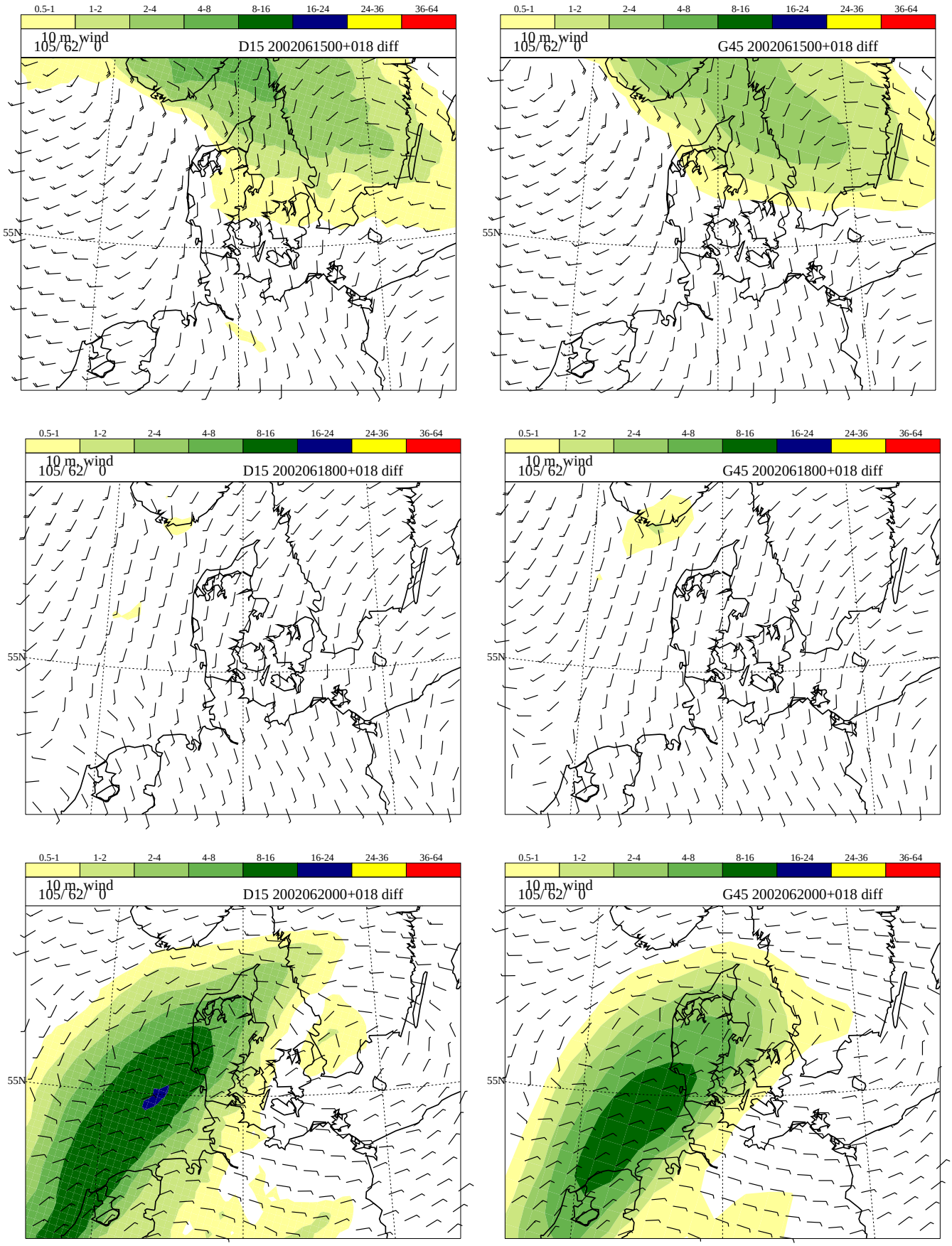

Figure 11: Operational DMI-HIRLAM-E (left) and DMI-HIRLAM-G (right) forecasted (6 h-18 h forecasts) 12 h accumulated stratiform precipitation valid on 18 UTC June 15 (upper), June 18 (middle) and June 20 (lower).

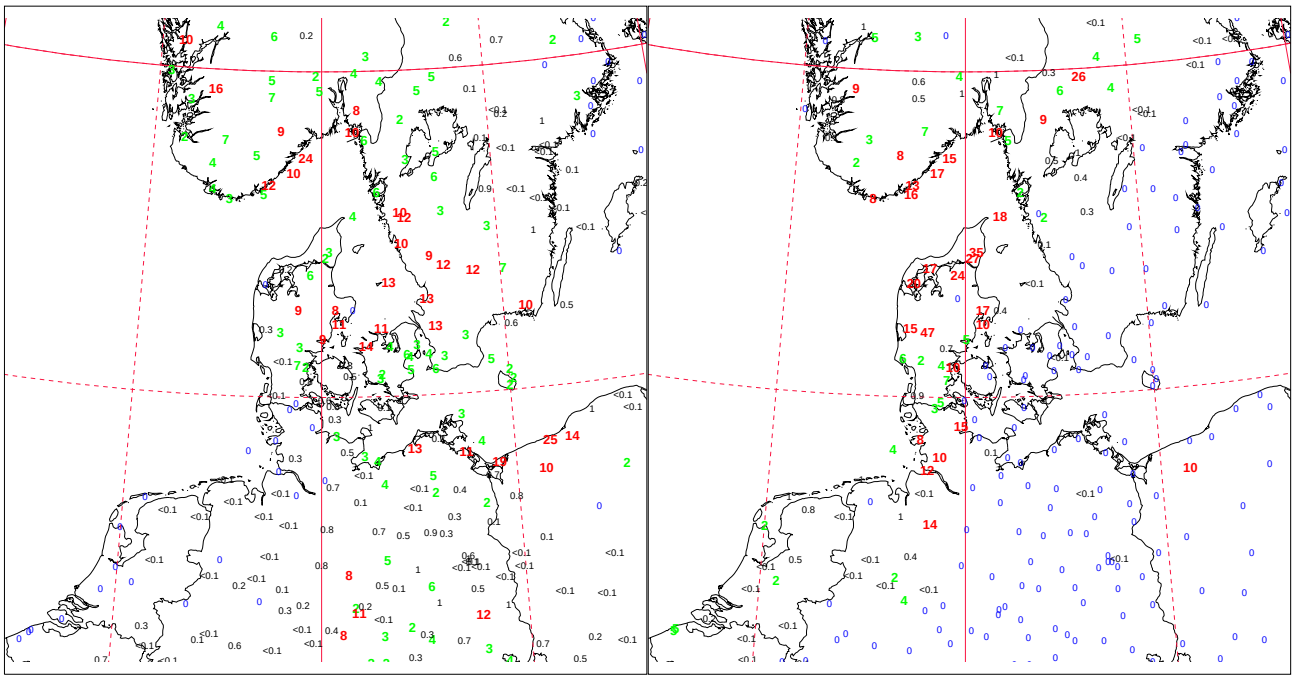

15. juni 2002, 18:00 UTC

18. juni 2002, 18:00 UTC

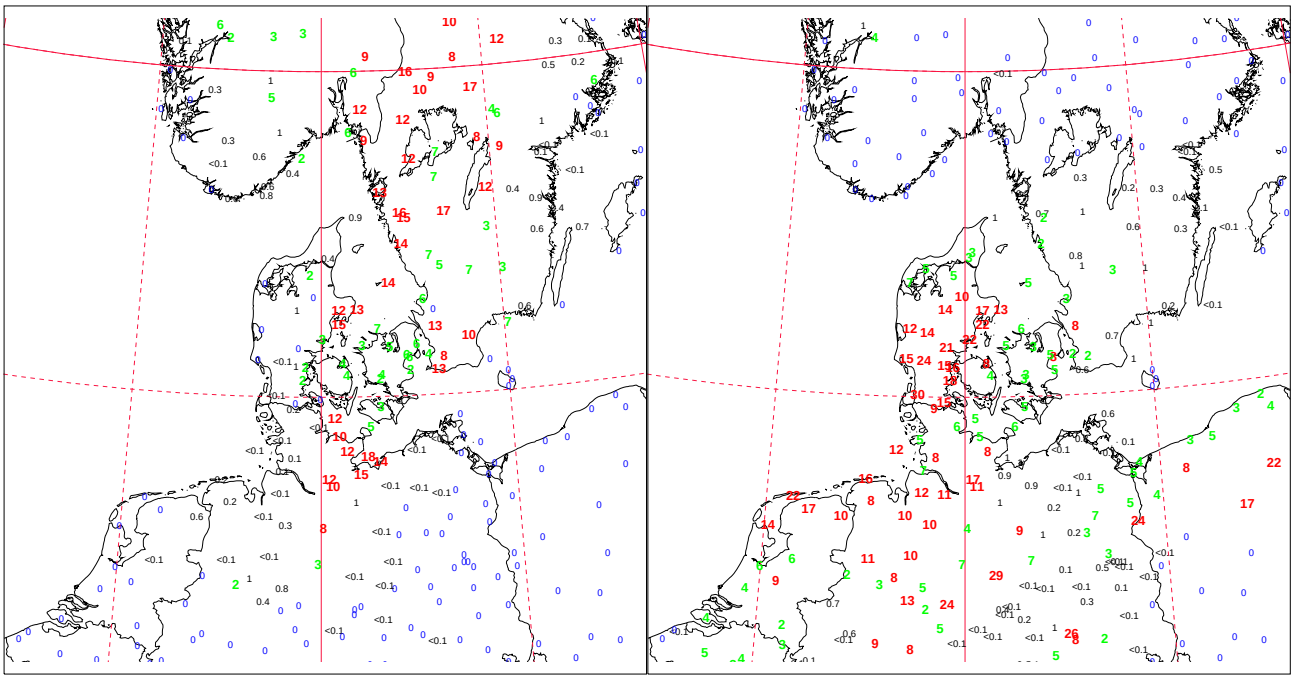

19. juni 2002, 06:00 UTC

20. juni 2002, 18:00 UTC

Figure 12: Observed 12 h accumulated precipitation on 18 UTC June 15 (upper left), 18 UTC June 18 (upper right), 06 UTC June 19 (lower left) and 18 UTC June 20 (lower right). Values larger than or equal to 8 mm has a bold, red and larger font. Values between more than 1 mm and less than 8 mm has a bold, green and larger font. Zero values has a blue font.

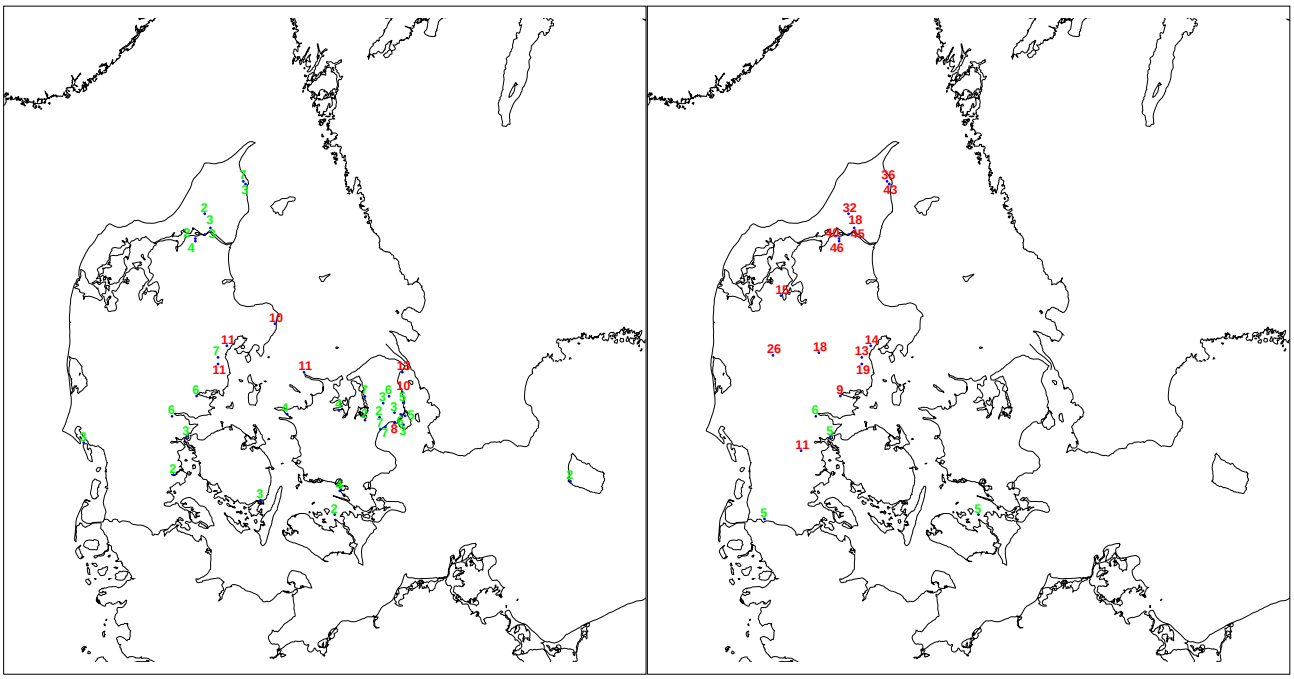

15. juni 2002, 18:00 UTC

18. juni 2002, 18:00 UTC

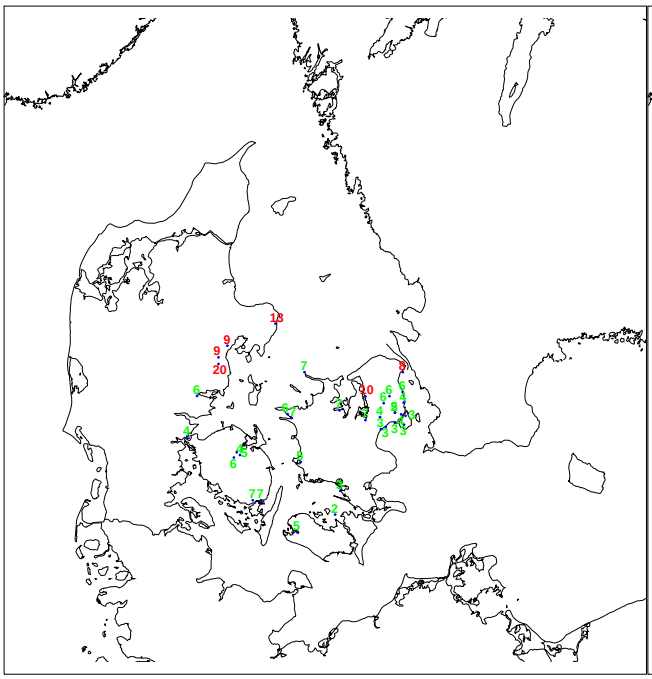

19. juni 2002, 06:00 UTC

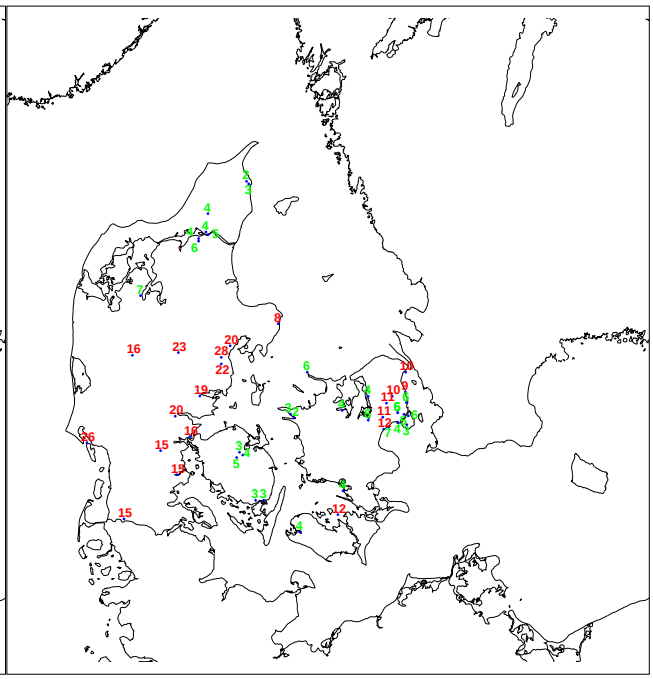

20. juni 2002, 18:00 UTC

Figure 13: "Observed" 12 h accumulated precipitation on 18 UTC June 15 (upper left), 18 UTC June 18 (upper right), 06 UTC June 19 (lower left) and 18 UTC June 20 (lower right) from SVK stations. Only values larger than or equal 2 mm are shown.

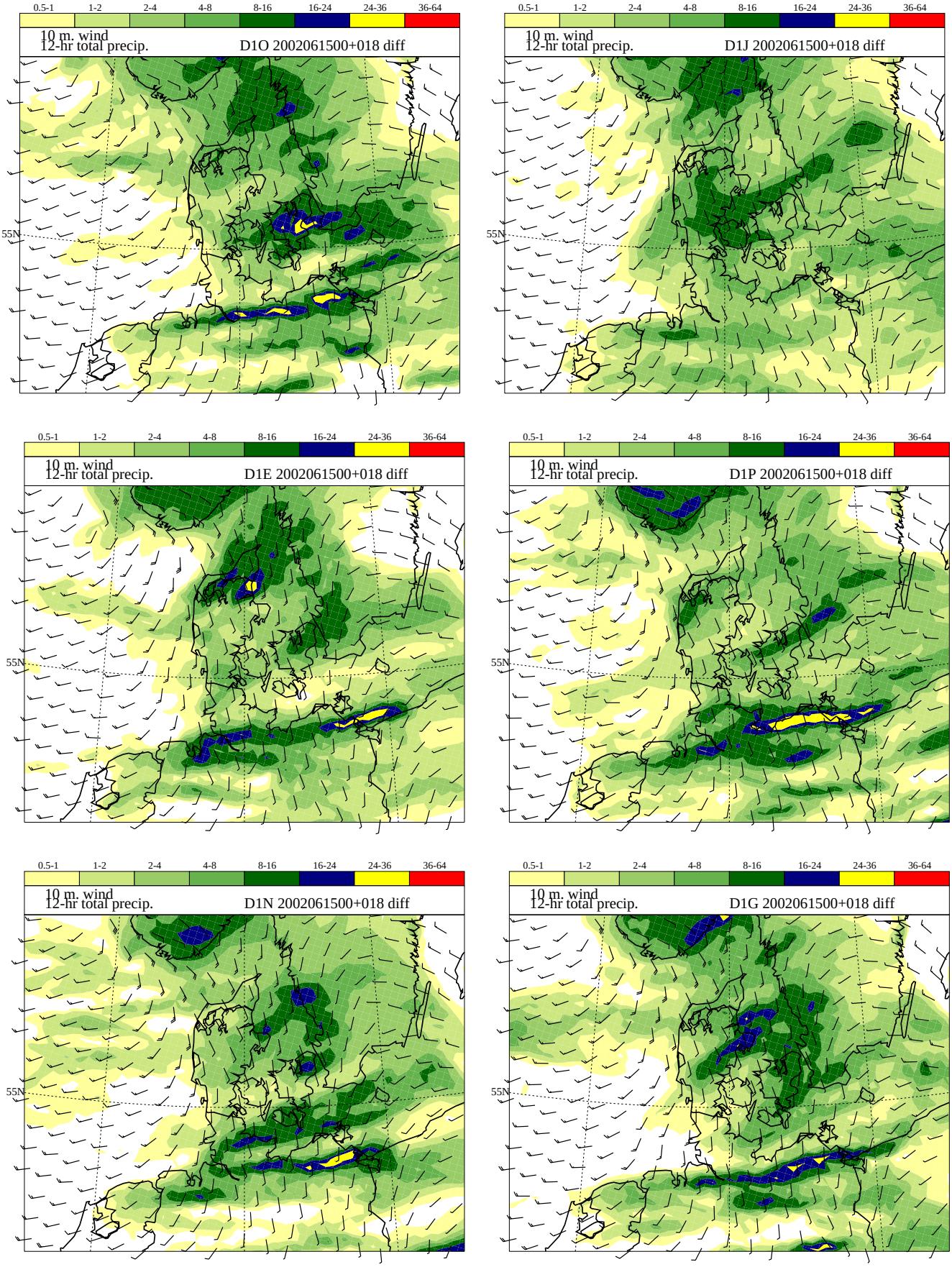

Figure 14: Forecasted (6 h-18 h forecasts) 12 h accumulated precipitation valid on 18 UTC June 15. DMI-HIRLAM-E models. See Table 12 for further details on differences.

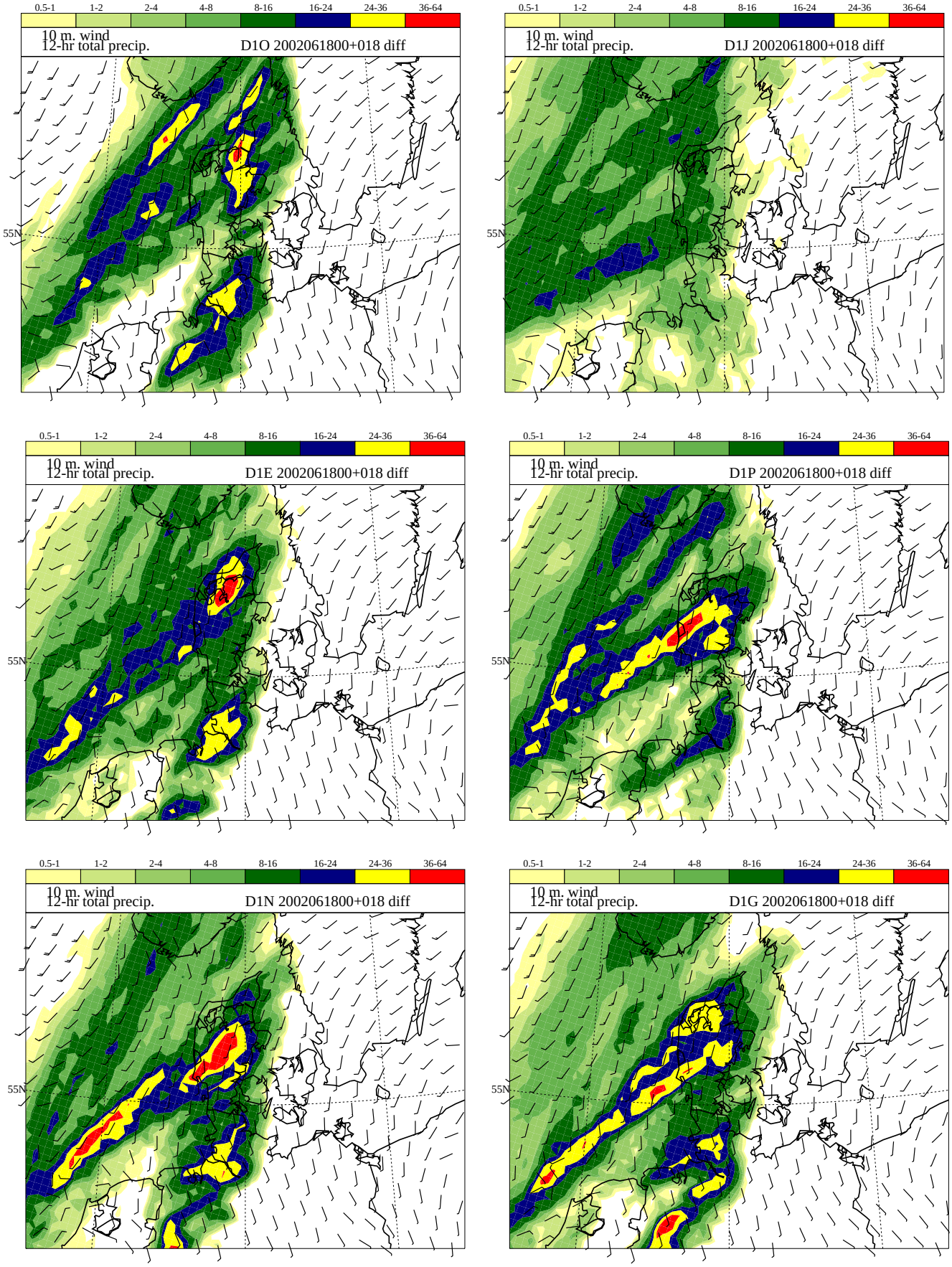

Figure 15: Forecasted (6 h-18 h forecasts) 12 h accumulated precipitation valid on 18 UTC June 18. DMI-HIRLAM-E models. See Table 12 for further details on differences.

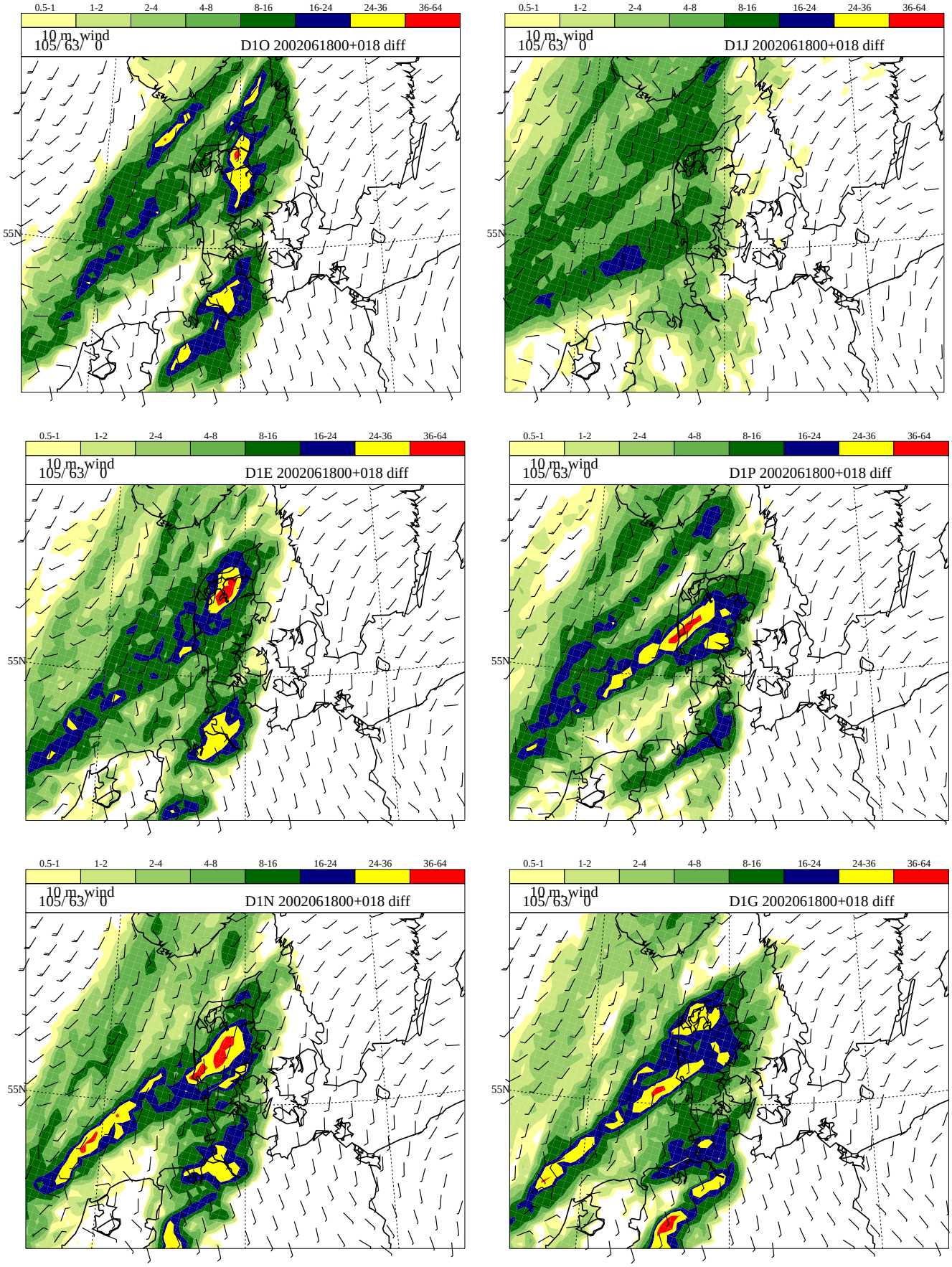

Figure 16: Forecasted (6 h-18 h forecasts) 12 h accumulated convective precipitation valid on 18 UTC June 18. DMI-HIRLAM-E models. See Table 12 for further details on differences.

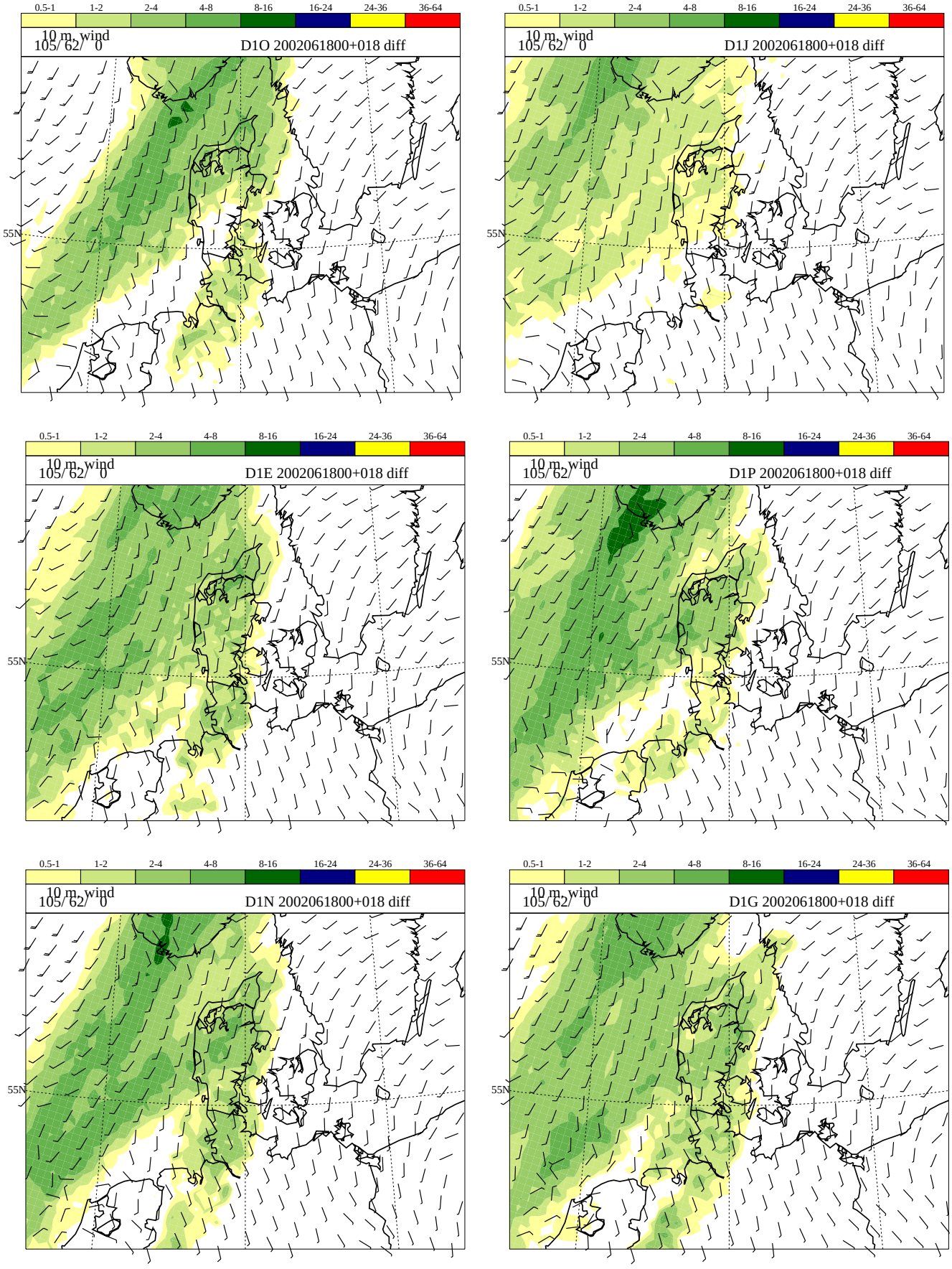

Figure 17: Forecasted (6 h-18 h forecasts) 12 h accumulated stratiform precipitation valid on 18 UTC June 18. DMI-HIRLAM-E models. See Table 12 for further details on differences.

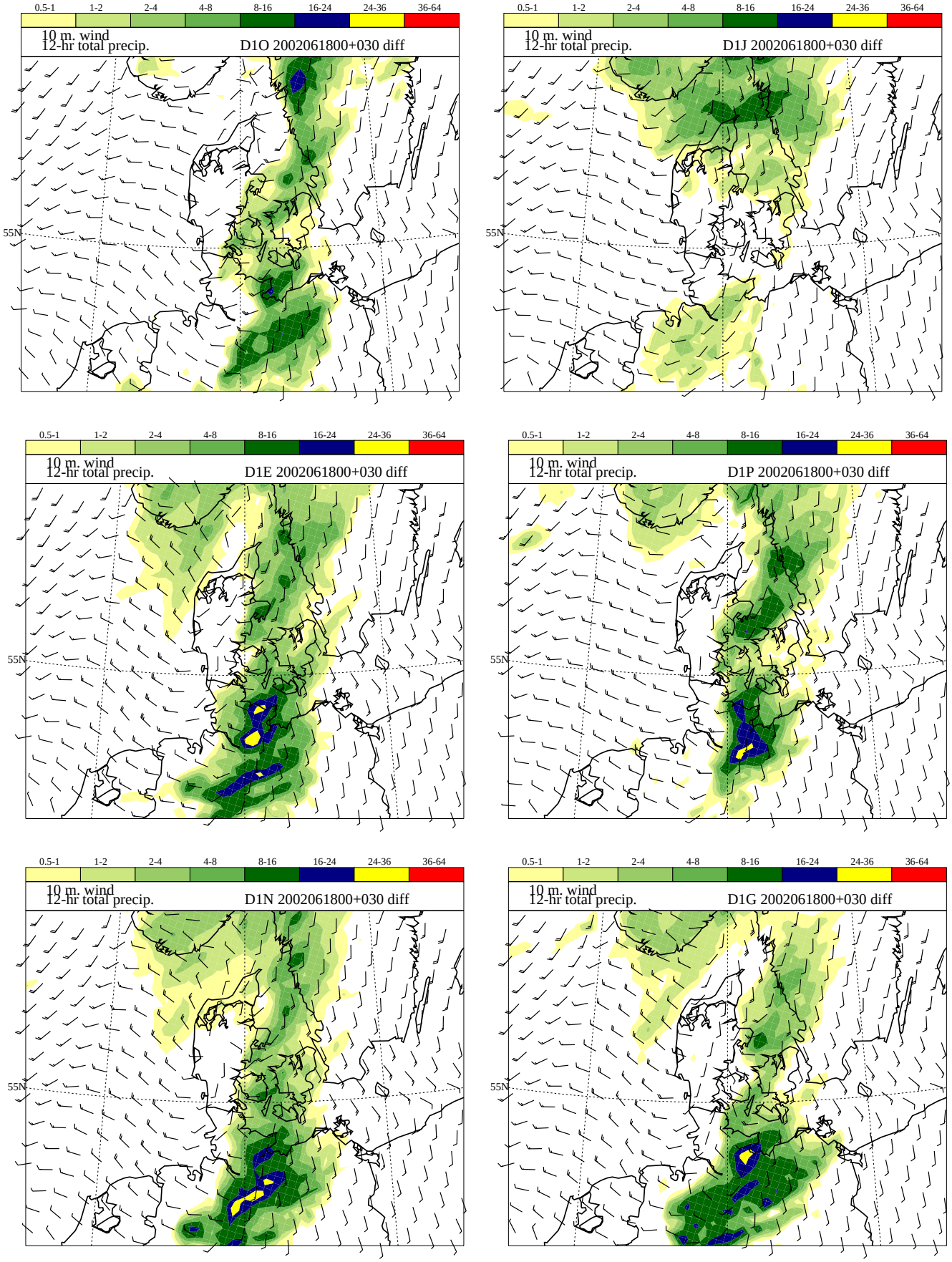

Figure 18: Forecasted (18 h-30 h forecasts) 12 h accumulated precipitation valid on 06 UTC June 19. DMI-HIRLAM-E models. See Table 12 for further details on differences.

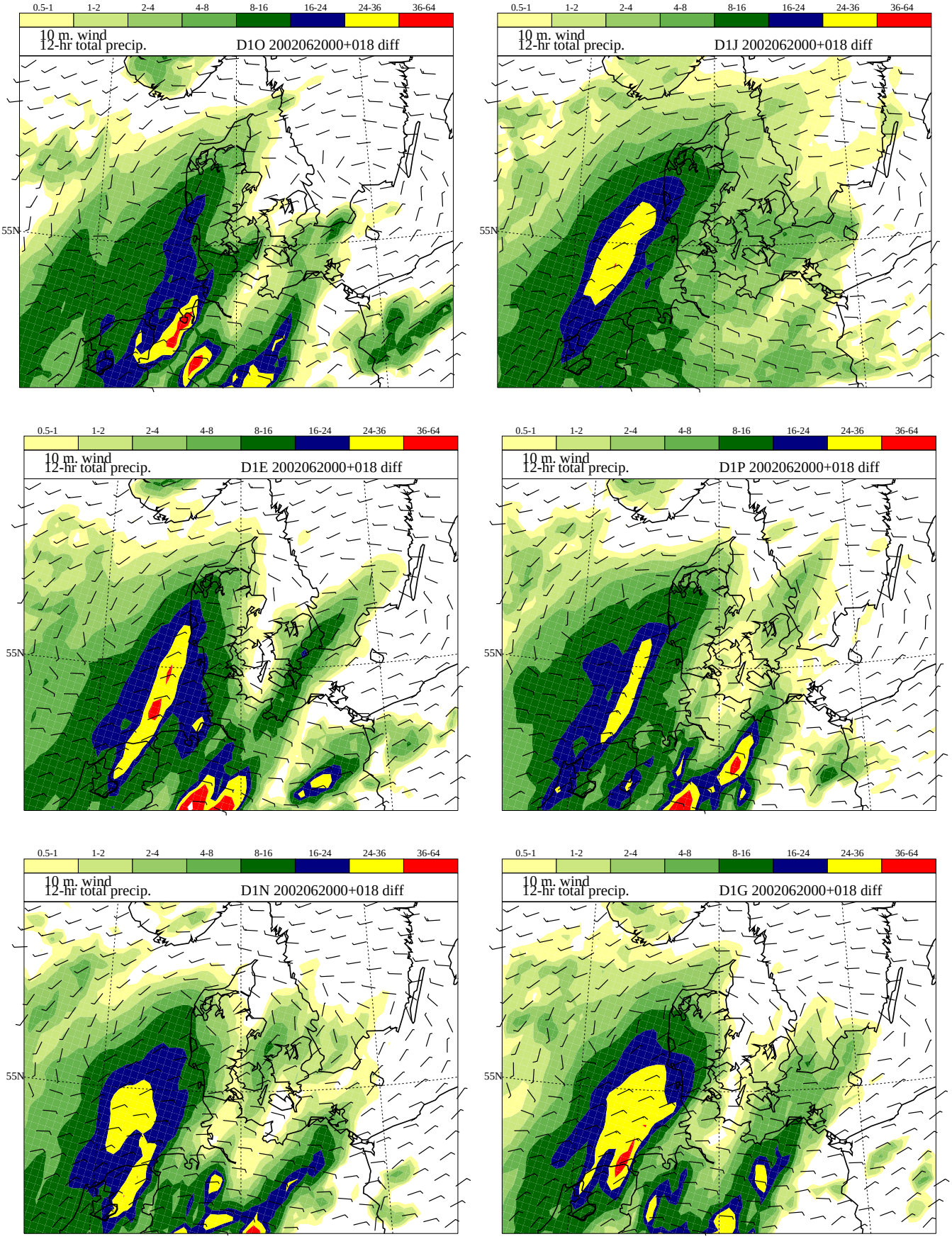

Figure 19: Forecasted (6 h-18 h forecasts) 12 h accumulated precipitation valid on 18 UTC June 20. DMI-HIRLAM-E models. See Table 12 for further details on differences.

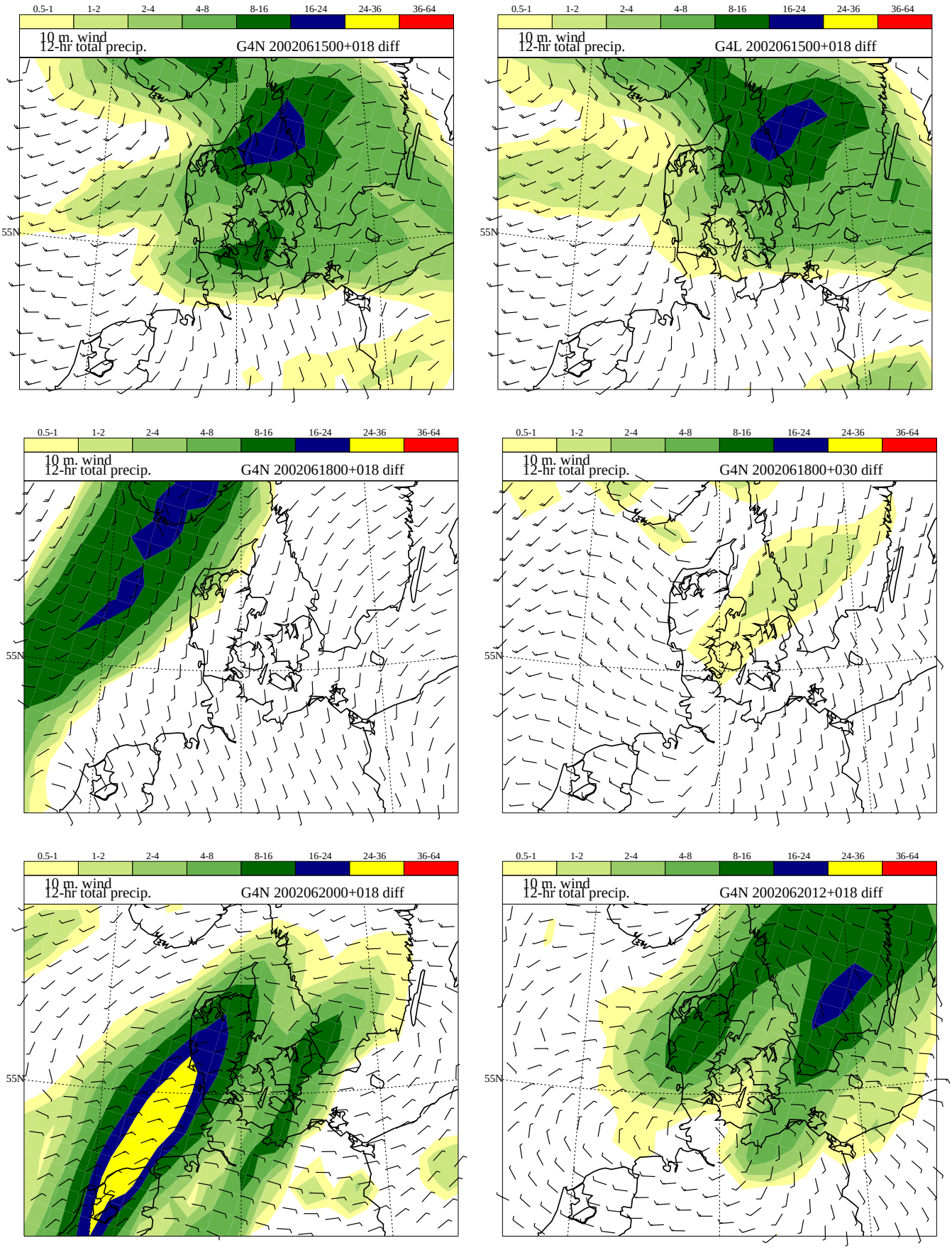

Figure 20: Forecasted (6 h-18 h/18 h-30 h forecasts) 12 h accumulated precipitation valid on dates noted in the sub-figures. DMI-HIRLAM-G model. See Table 12 for further details on differences.

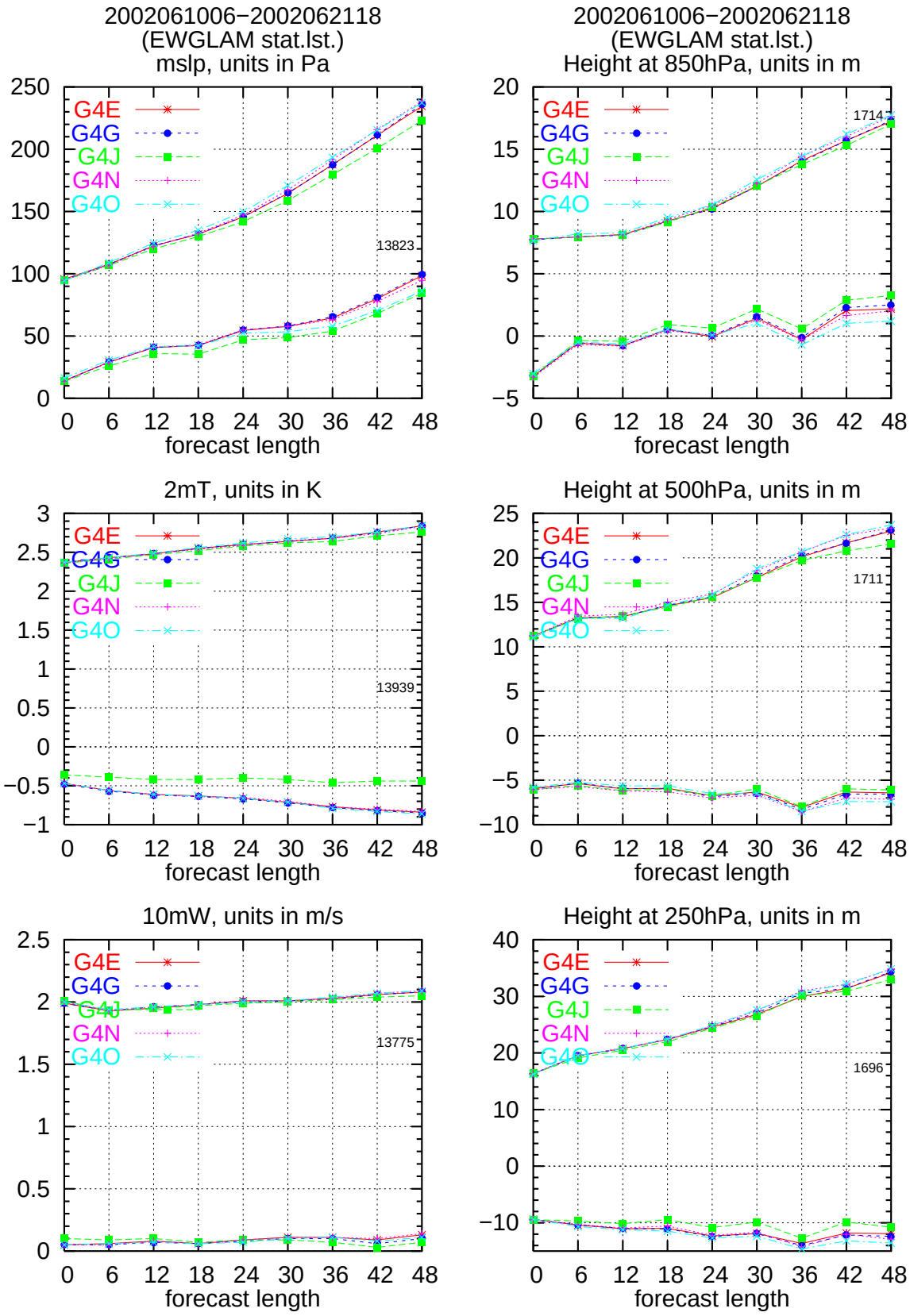

Figure 21: Obs-verification (bias and rms, EWGLAM station list) results of surface parameters and geopotential height for pressure levels specified in the plot. See Table 12 for further details concerning given DMI-HIRLAM-G model run. (The numbers in small print in the plots indicate the number of observations used in the verification).

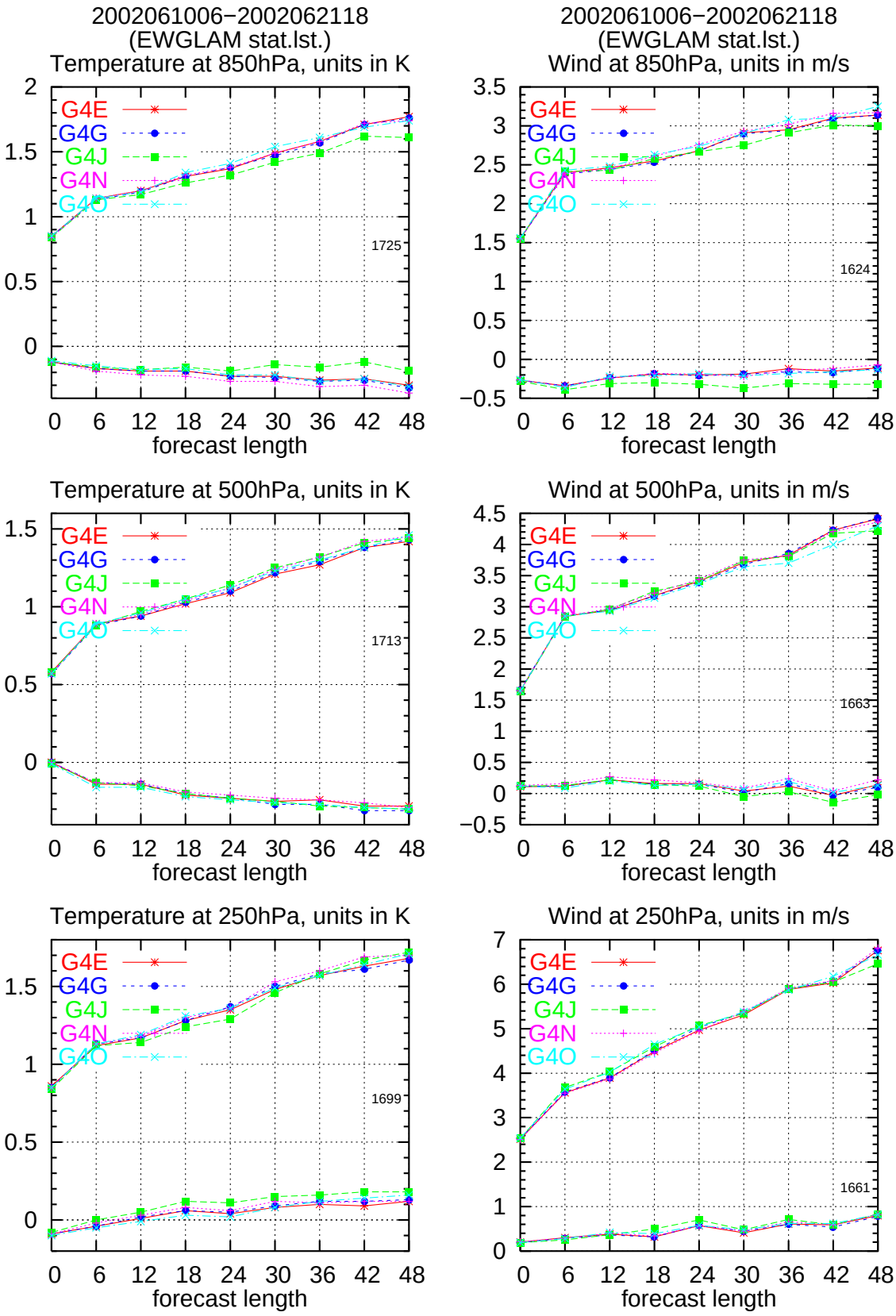

Figure 22: Obs-verification (bias and rms, EWGLAM station list) results of temperature and wind for pressure levels specified in the plot. See Table 12 for further details concerning given DMI-HIRLAM-G model run. (The numbers in small print in the plots indicate the number of observations used in the verification).

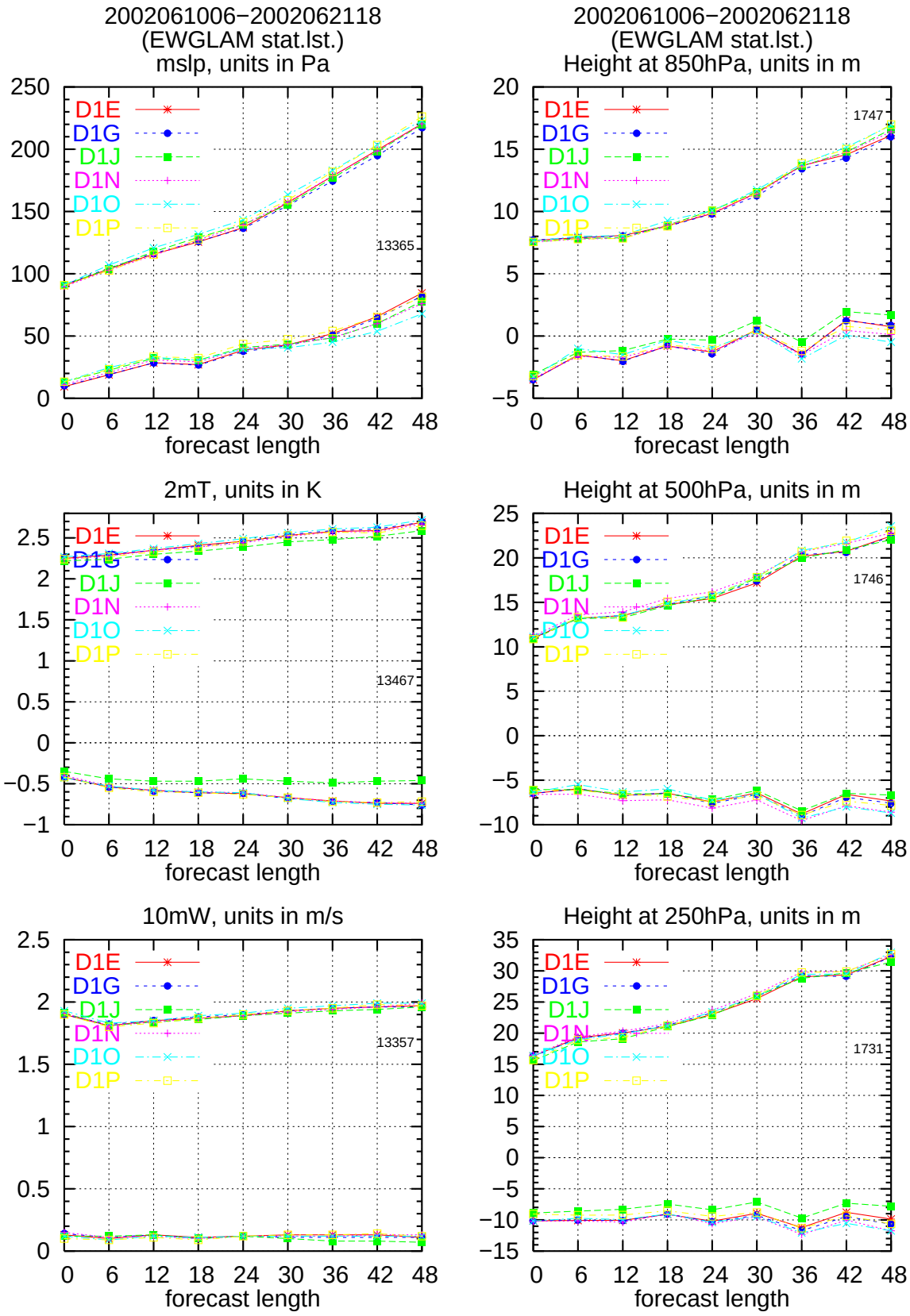

Figure 23: Obs-verification (bias and rms, EWGLAM station list) results of surface parameters and geopotential height for pressure levels specified in the plot. See Table 12 for further details concerning given DMI-HIRLAM-E model run. (The numbers in small print in the plots indicate the number of observations used in the verification).

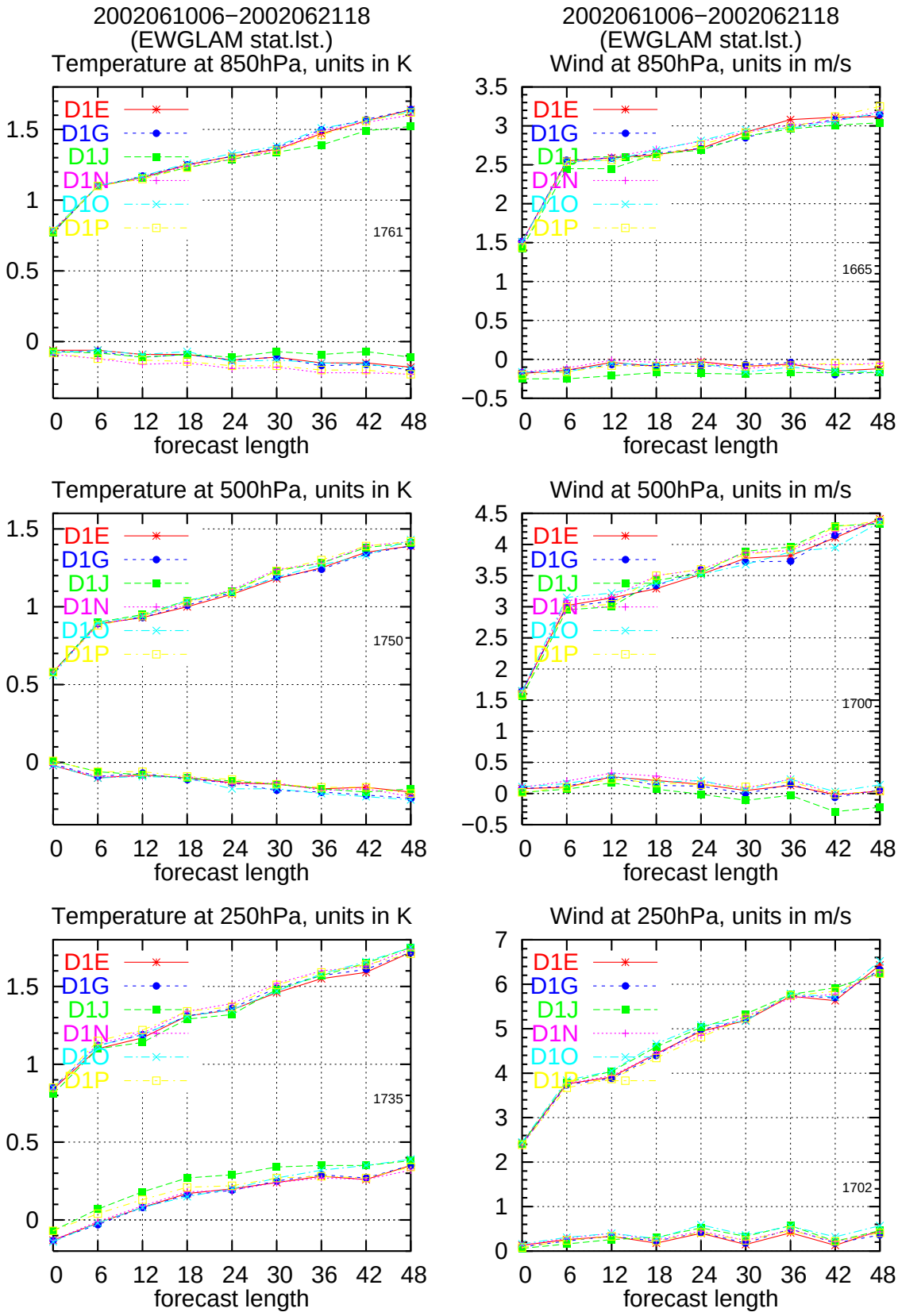

Figure 24: Obs-verification (bias and rms, EWGLAM station list) results of temperature and wind for pressure levels specified in the plot. See Table 12 for further details concerning given DMI-HIRLAM-E model run. (The numbers in small print in the plots indicate the number of observations used in the verification).

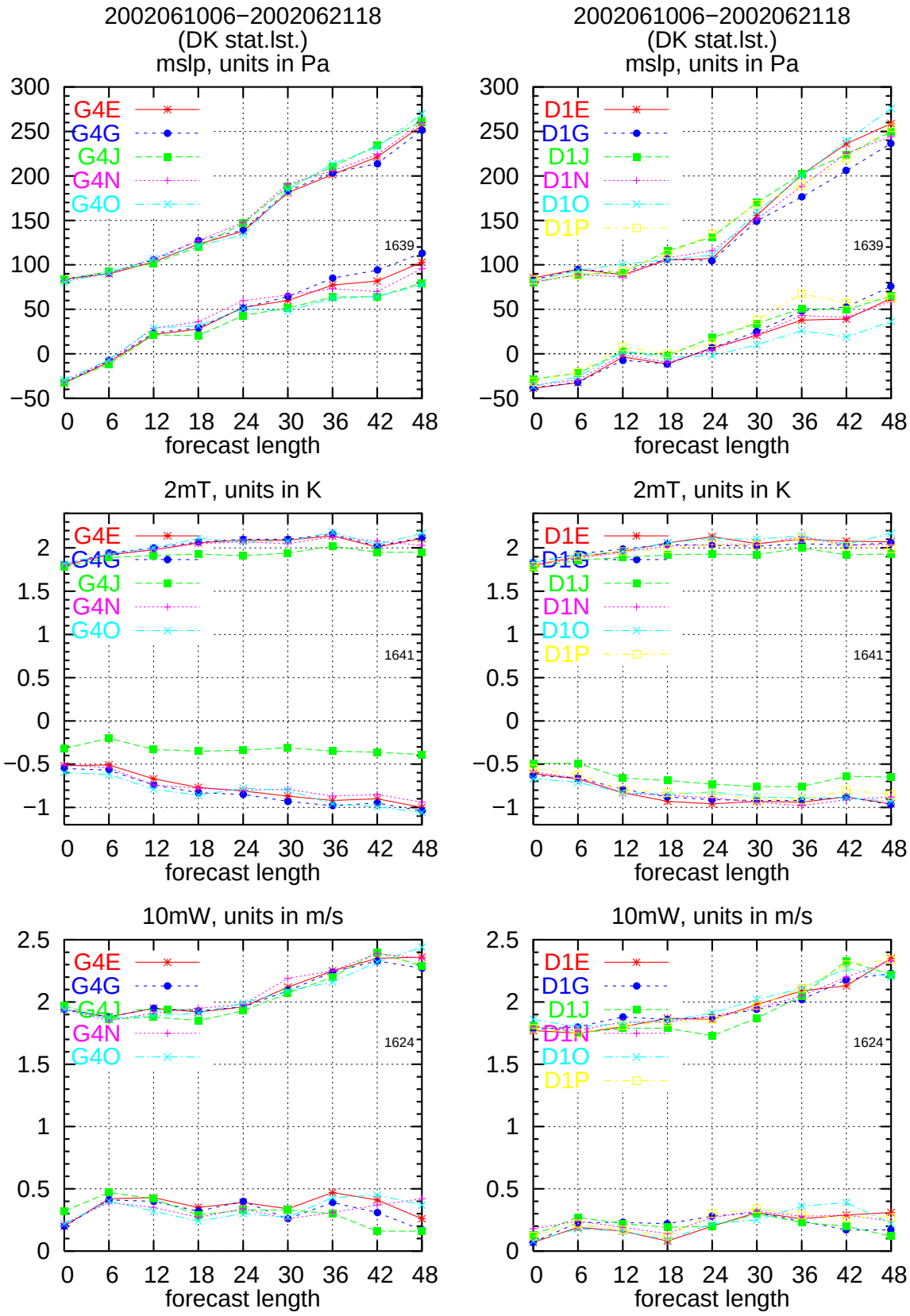

Figure 25: Obs-verification (bias and rms, Danish station list) results of surface parameters specified in the plot. See Table 12 for further details concerning given DMI-HIRLAM-E model run. (The numbers in small print in the plots indicate the number of observations used in the verification).

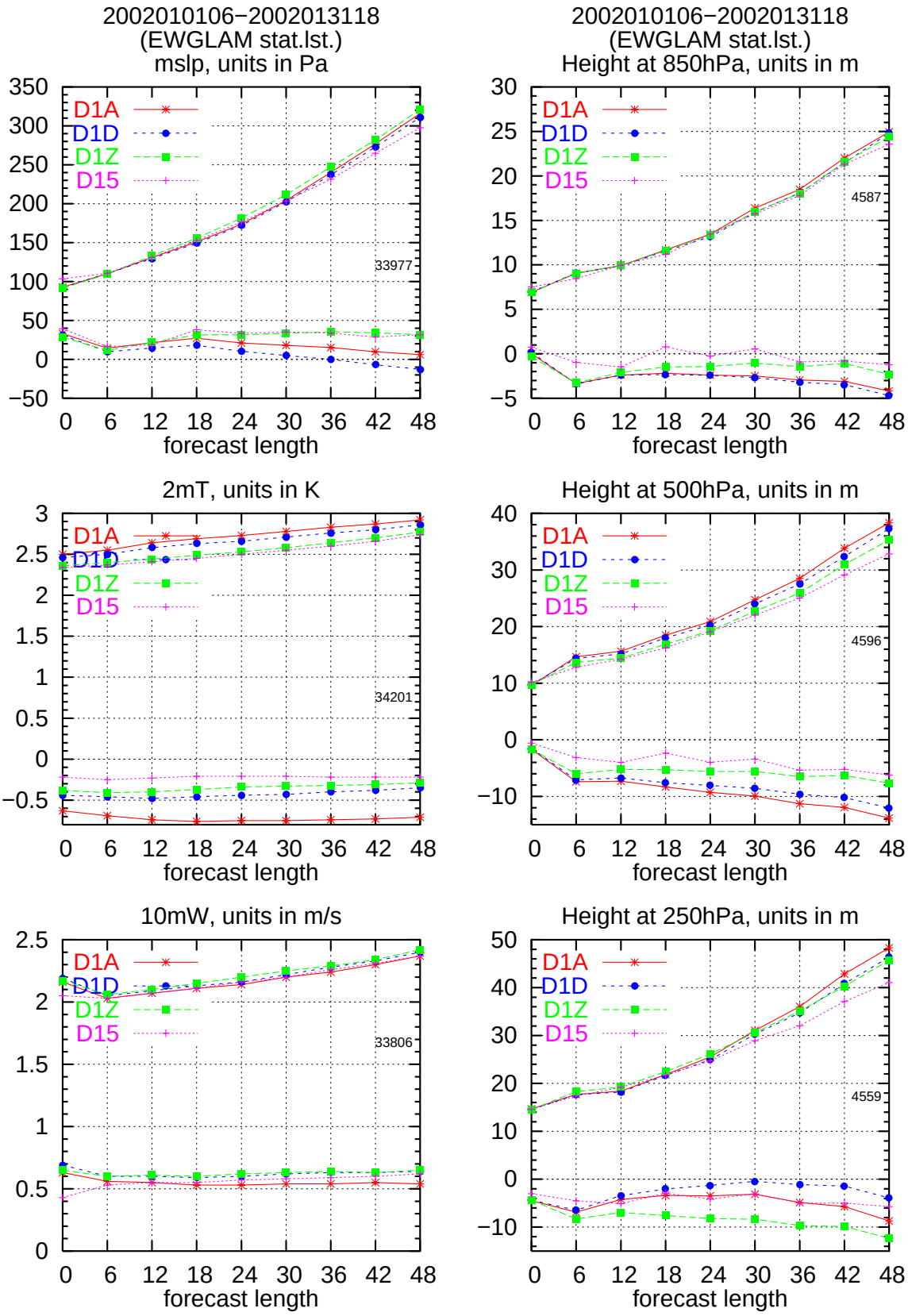

Figure 26: Obs-verification (bias and rms, EWGLAM station list) results of surface parameters and geopotential height for pressure levels specified in the plot. See Table 12 for further details concerning given DMI-HIRLAM-E model run. (The numbers in small print in the plots indicate the number of observations used in the verification).

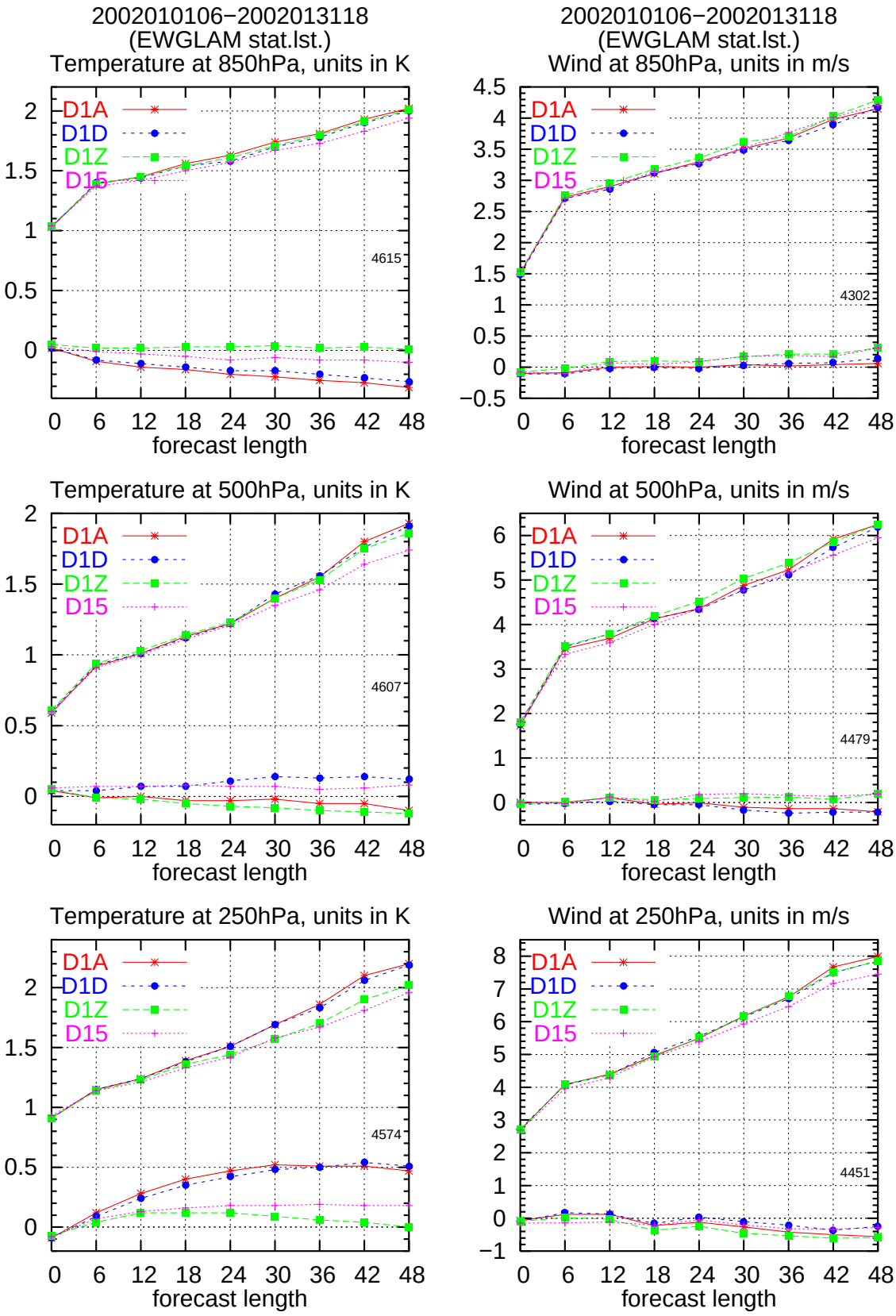

Figure 27: Obs-verification (bias and rms, EWGLAM station list) results of temperature and wind for pressure levels specified in the plot. See Table 12 for further details concerning given DMI-HIRLAM-E model run. (The numbers in small print in the plots indicate the number of observations used in the verification).

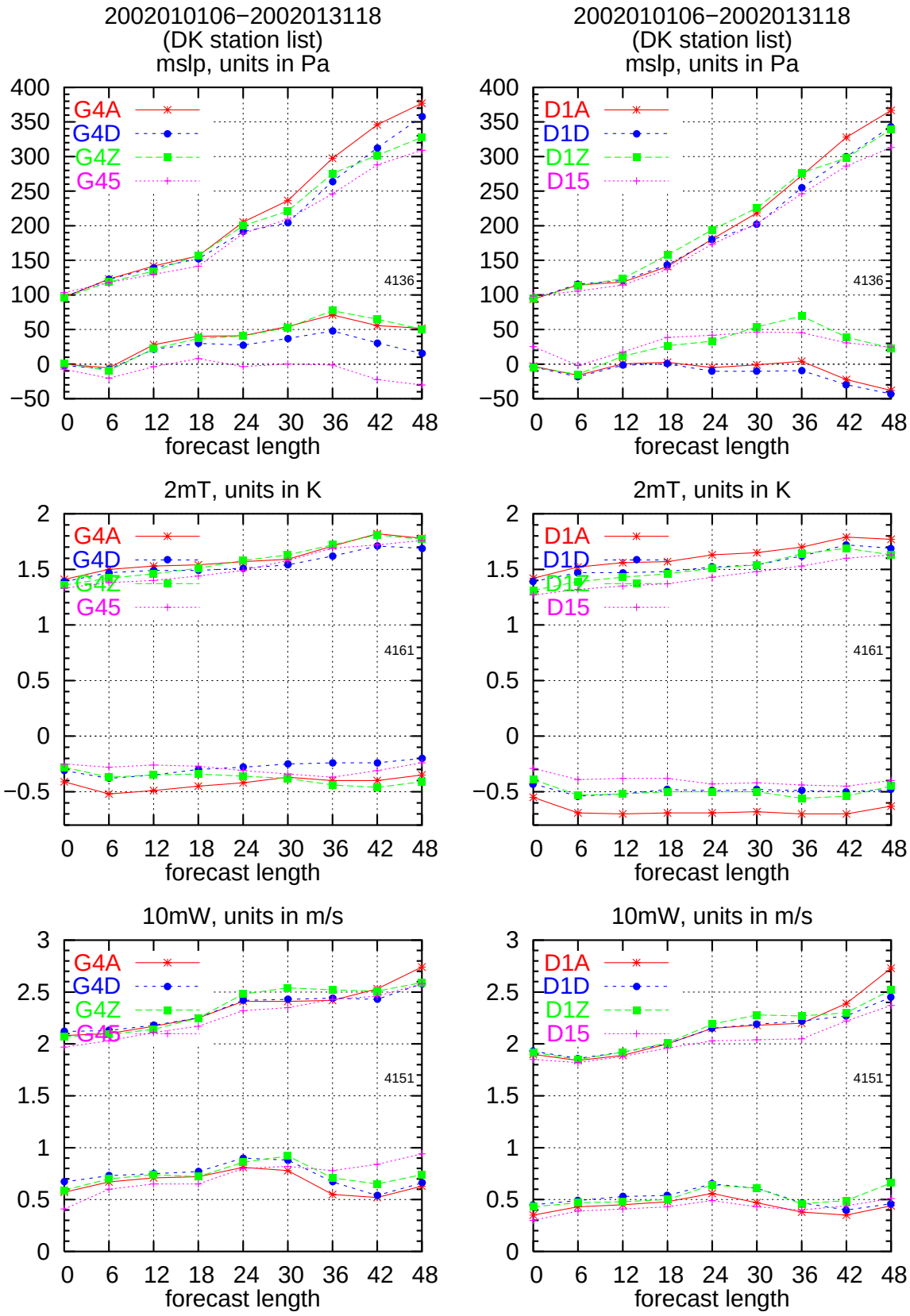

Figure 28: Obs-verification (bias and rms, Danish station list) results of surface parameters specified in the plot. See Table 12 for further details concerning given DMI-HIRLAM-E model run.

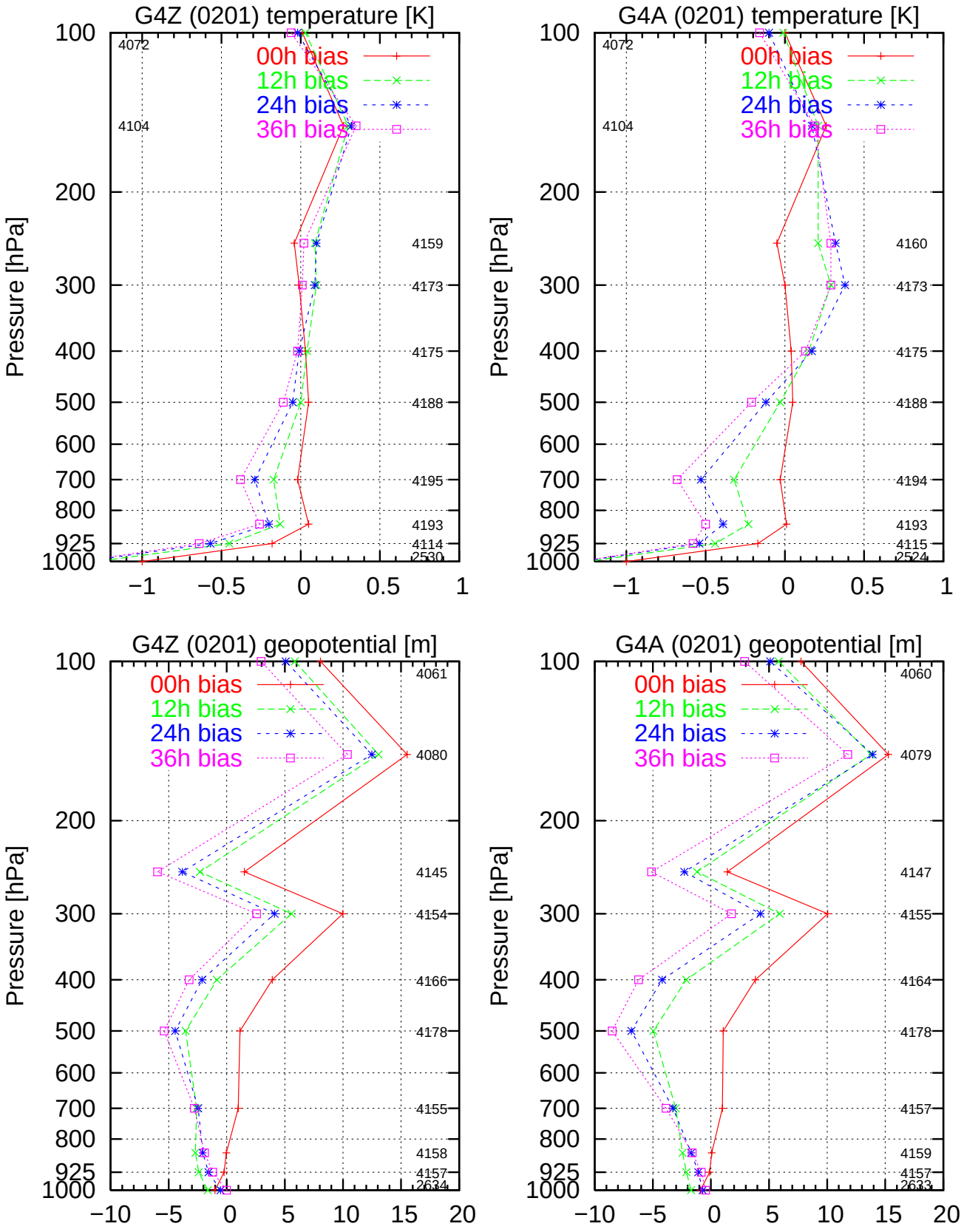

Figure 29: Bias scores at analysis time and for the 12, 24 and 36 hour forecasts of G4Z (left) and G4A (right) as a function of pressure in January 2002. Top row is for temperature and bottom row is geopotential. (The numbers in small print in the plots indicate the number of observations used).

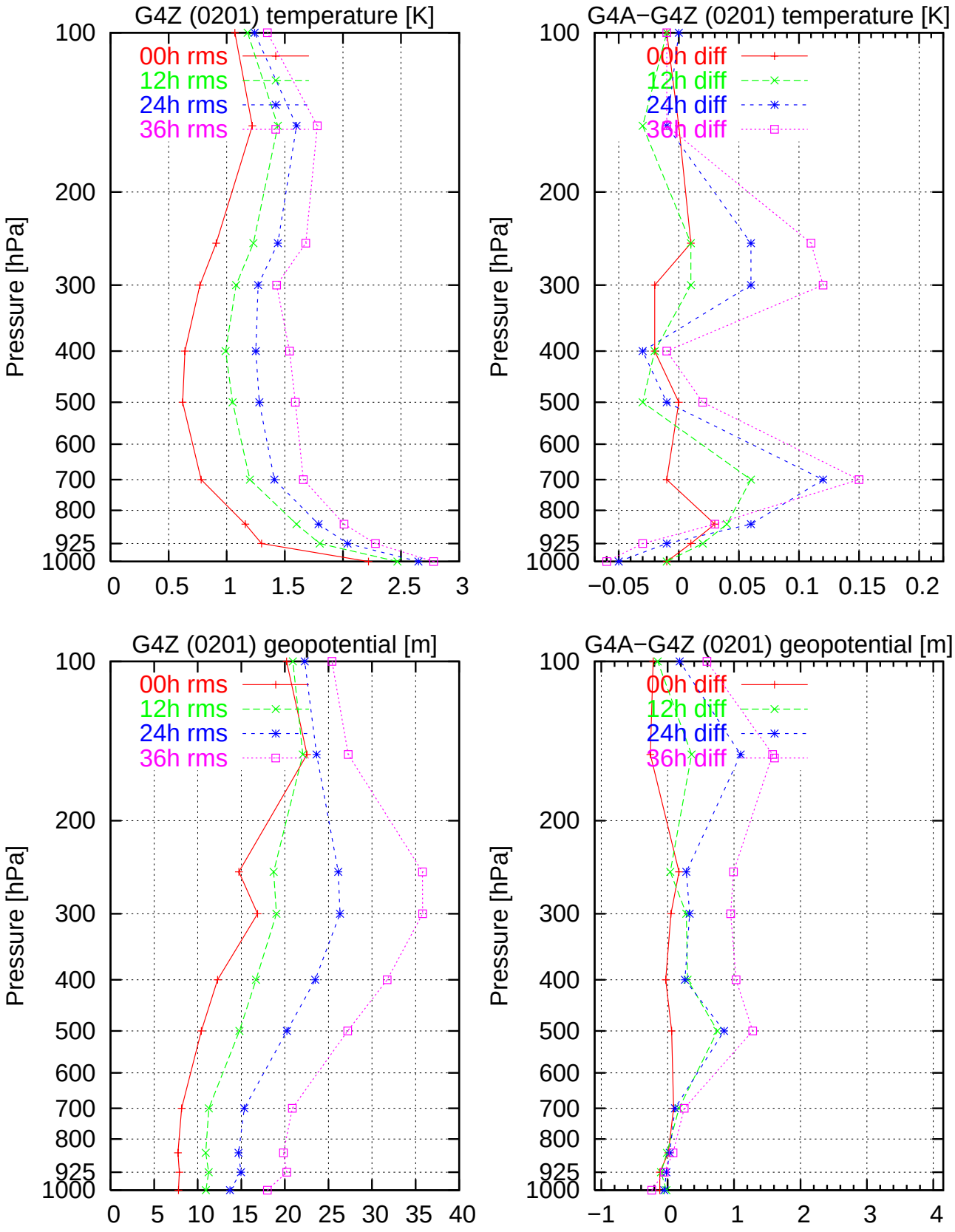

Figure 30: Rms scores for G4Z (left) and differences in rms scores between G4A and G4Z (right) at analysis time and for the 12, 24 and 36 hour forecasts as a function of pressure in January 2002. Top row is for temperature and bottom row is geopotential. Positive values in the difference plots where G4Z has better rms scores.

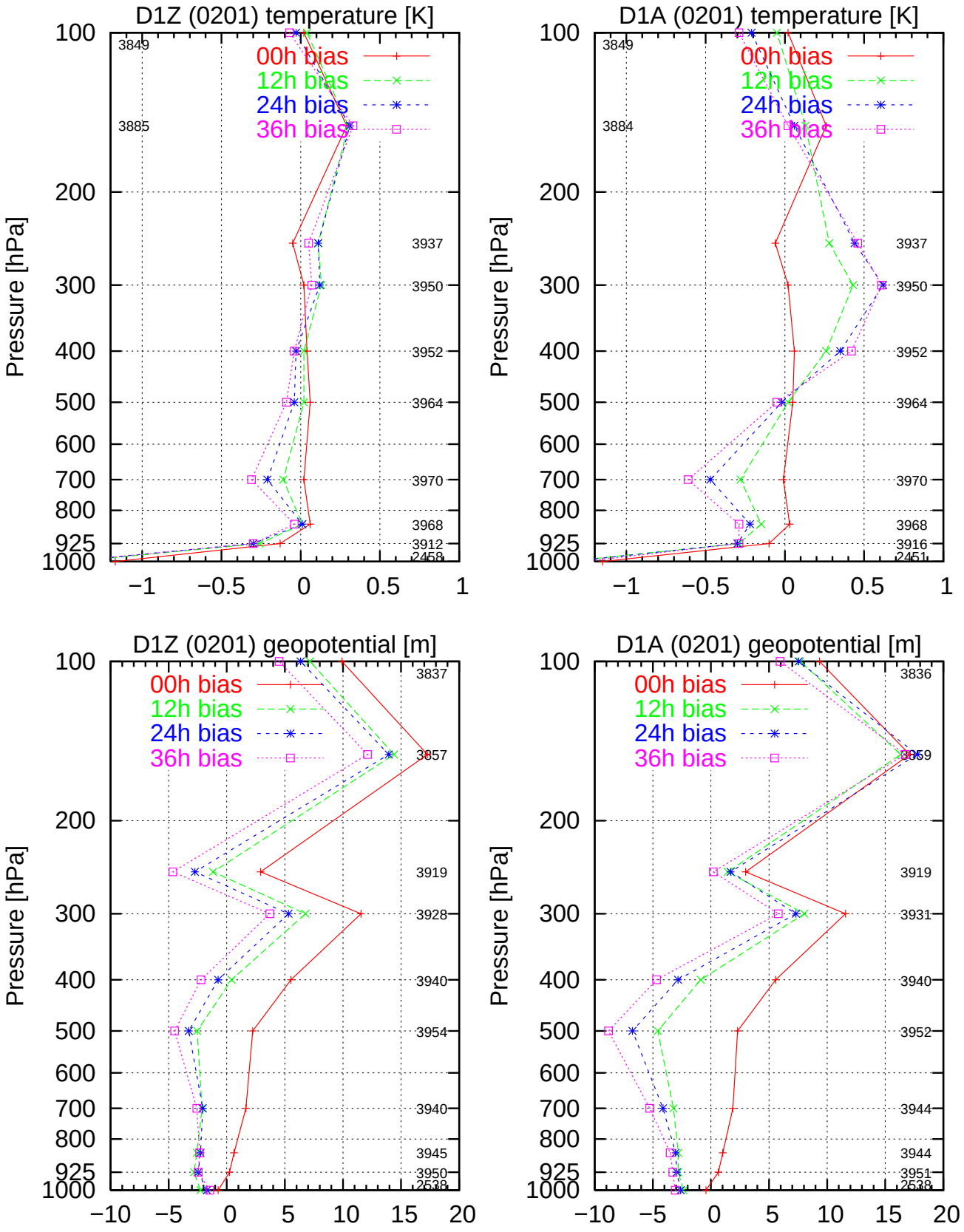

Figure 31: Bias scores at analysis time and for the 12, 24 and 36 hour forecasts of D1Z (left) and D1A (right) as a function of pressure in January 2002. Top row is for temperature and bottom row is geopotential. (The numbers in small print in the plots indicate the number of observations used).

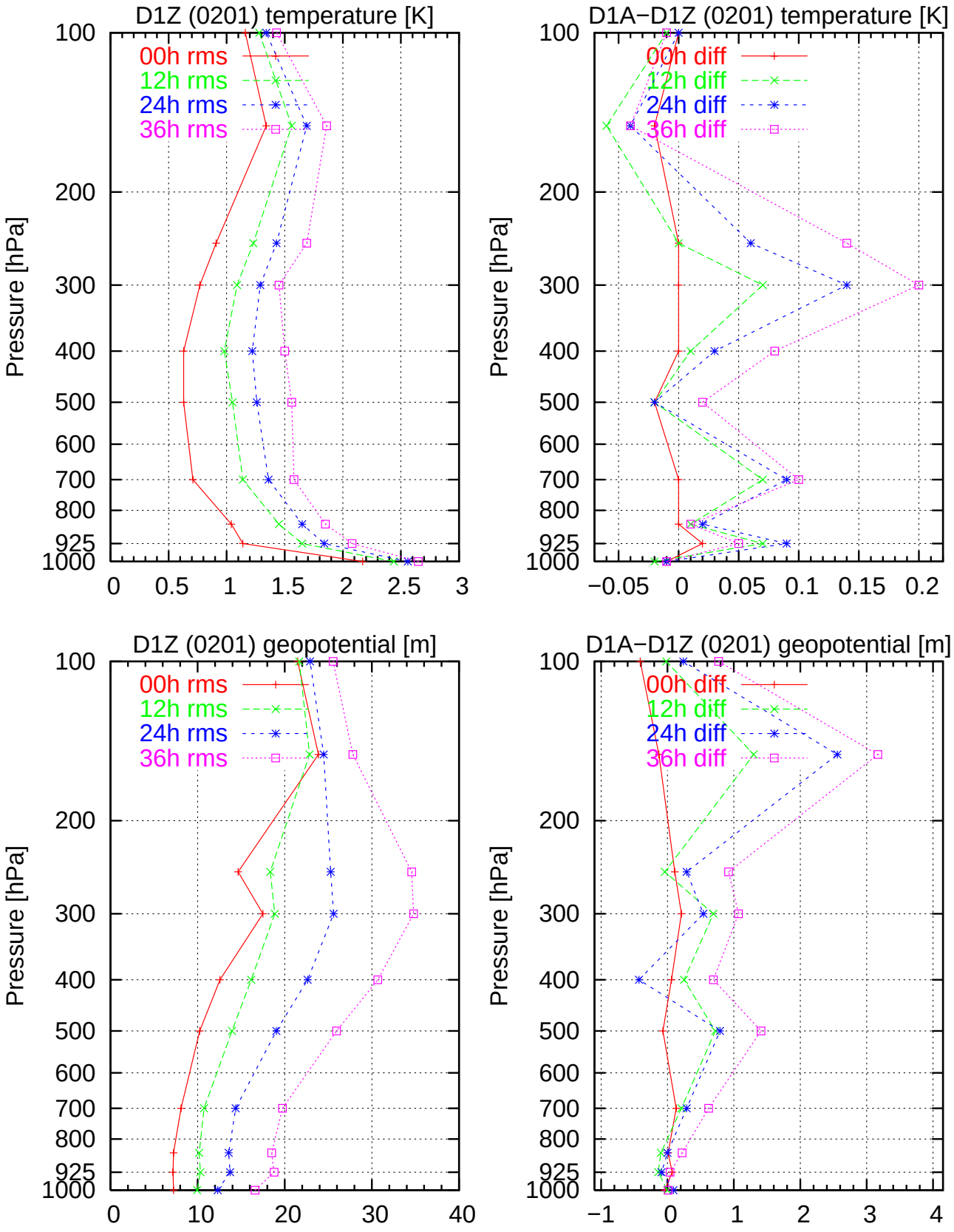

Figure 32: Rms scores for D1Z (left) and differences in rms scores between D1A and D1Z (right) at analysis time and for the 12, 24 and 36 hour forecasts as a function of pressure in January 2002. Top row is for temperature and bottom row is geopotential. Positive values in the difference plots where D1Z has better rms scores.

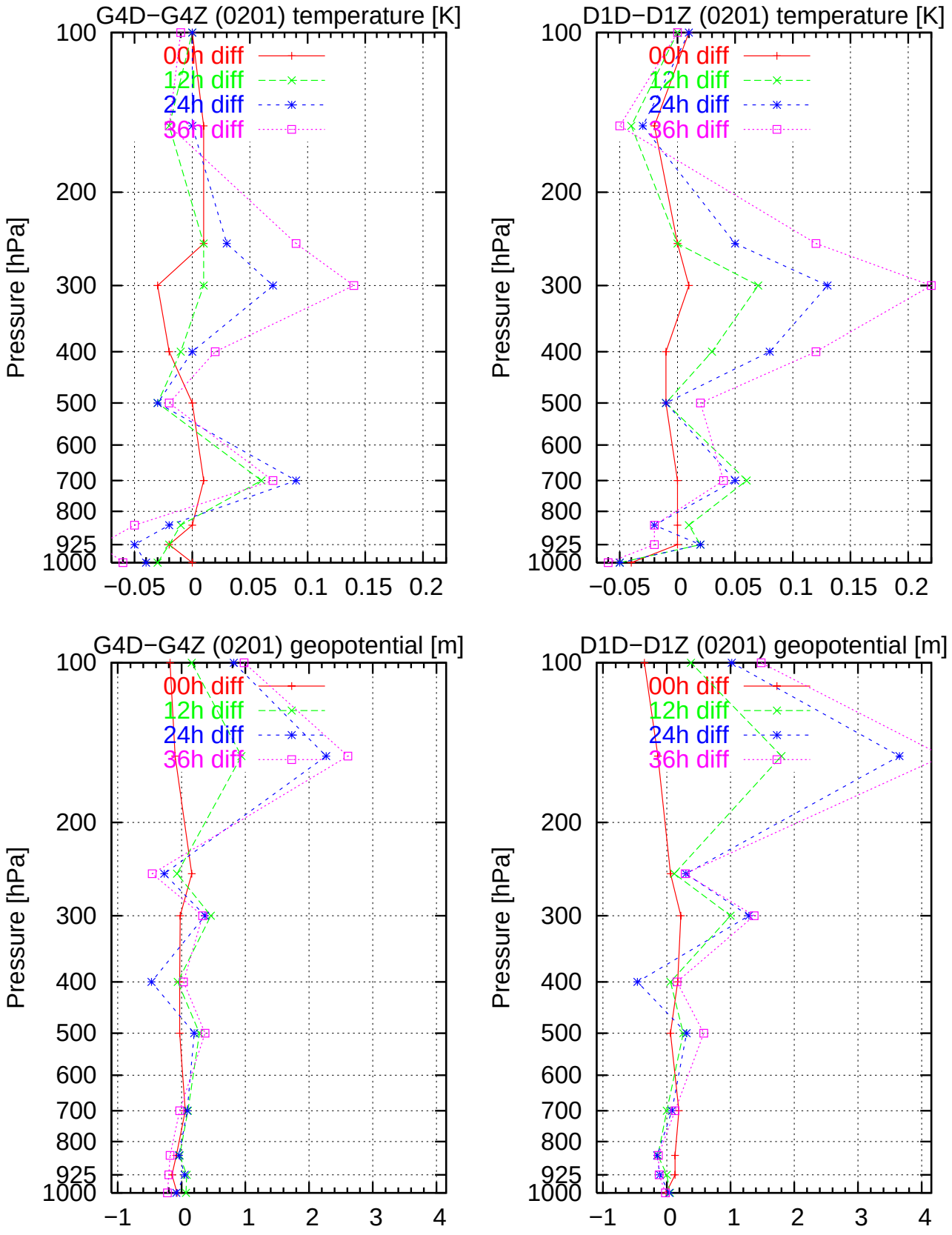

Figure 33: Differences in rms scores between G4D and G4Z (left) and between D1D and D1Z (right) at analysis time and for the 12, 24 and 36 hour forecasts as a function of pressure in January 2002. Top row is for temperature and bottom row is geopotential. Positive values where G4Z/D1Z has better rms scores.

DANISH METEOROLOGICAL INSTITUTE

Scientific Reports

Scientific reports from the Danish Meteorological Institute cover a variety of geophysical fields, i.e. meteorology (including climatology), oceanography, subjects on air and sea pollution, geomagnetism, solar-terrestrial physics, and physics of the middle and upper atmosphere.

Reports in the series within the last five years:

No. 97-1
E. Friis Christensen og C. Skøtt: Contributions from the International Science Team. The Ørsted Mission - a pre-launch compendium

No. 97-2
Alix Rasmussen, Sissi Kiilsholm, Jens Havskov Sørensen, Ib Steen Mikkelsen: Analysis of tropospheric ozone measurements in Greenland: Contract No. EV5V-CT93-0318 (DG 12 DTEE):
DMI's contribution to CEC Final Report Arctic Trophospheric Ozone Chemistry ARCTOC

No. 97-3
Peter Thejll: A search for effects of external events on terrestrial atmospheric pressure: cosmic rays

No. 97-4
Peter Thejll: A search for effects of external events on terrestrial atmospheric pressure: sector boundary crossings

No. 97-5
Knud Lassen: Twentieth century retreat of sea-ice in the Greenland Sea

No. 98-1
Niels Woetman Nielsen, Bjarne Amstrup, Jess U. Jørgensen: HIRLAM 2.5 parallel tests at DMI: sensitivity to type of schemes for turbulence, moist processes and advection

No. 98-2
Per Høeg, Georg Bergeton Larsen, Hans-Henrik Benzon, Stig Syndergaard, Mette Dahl Mortensen: The GPSOS project
Algorithm functional design and analysis of ionosphere, stratosphere and troposphere observations

No. 98-3
Mette Dahl Mortensen, Per Høeg: Satellite atmosphere profiling retrieval in a nonlinear troposphere
Previously entitled: Limitations induced by Multipath

No. 98-4
Mette Dahl Mortensen, Per Høeg: Resolution properties in atmospheric profiling with GPS

No. 98-5
R.S. Gill and M. K. Rosengren: Evaluation of the Radarsat imagery for the operational mapping of sea ice around Greenland in 1997

No. 98-6
R.S. Gill, H.H. Valeur, P. Nielsen and K.Q. Hansen: Using ERS SAR images in the operational mapping of sea ice in the Greenland waters: final report for ESA-ESRIN's: pilot projekt no. PP2.PP2.DK2 and 2nd announcement of opportunity for the exploitation of ERS data projekt No. AO2..DK 102

No. 98-7
Per Høeg et al.: GPS Atmosphere profiling methods and error assessments

No. 98-8
H. Svensmark, N. Woetmann Nielsen and A.M. Sempreviva: Large scale soft and hard turbulent states of the atmosphere

No. 98-9
Philippe Lopez, Eigil Kaas and Annette Guldberg: The full particle-in-cell advection scheme in spherical geometry

No. 98-10
H. Svensmark: Influence of cosmic rays on earth's climate

No. 98-11
Peter Thejll and Henrik Svensmark: Notes on the method of normalized multivariate regression

No. 98-12
K. Lassen: Extent of sea ice in the Greenland Sea 1877-1997: an extension of DMI Scientific Report 97-5

No. 98-13
Niels Larsen, Alberto Adriani and Guido DiDonfrancesco: Microphysical analysis of polar stratospheric clouds observed by lidar at McMurdo, Antarctica

No.98-14
Mette Dahl Mortensen: The back-propagation method for inversion of radio occultation data

No. 98-15
Xiang-Yu Huang: Variational analysis using spatial filters

No. 99-1
Henrik Feddersen: Project on prediction of climate variations on seasonel to interannual timescales (PROVOST) EU contract ENVA4-CT95-0109: DMI contribution to the final report: Statistical analysis and post-processing of uncoupled PROVOST simulations

No. 99-2
Wilhelm May: A time-slice experiment with the ECHAM4 A-GCM at high resolution: the experimental design and the assessment of climate change as compared to a greenhouse gas experiment with ECHAM4/OPYC at low resolution

No. 99-3
Niels Larsen et al.: European stratospheric monitoring stations in the Artic II: CEC Environment and Climate Programme Contract ENV4-CT95-0136. DMI Contributions to the project

No. 99-4
Alexander Baklanov: Parameterisation of the deposition processes and radioactive decay: a review and some preliminary results with the DERMA model

No. 99-5
Mette Dahl Mortensen: Non-linear high resolution inversion of radio occultation data

No. 99-6
Stig Syndergaard: Retrieval analysis and methodologies in atmospheric limb sounding using the GNSS radio occultation technique

No. 99-7
Jun She, Jacob Woge Nielsen: Operational wave forecasts over the Baltic and North Sea

No. 99-8
Henrik Feddersen: Monthly temperature forecasts for Denmark - statistical or dynamical?

No. 99-9
P. Thejll, K. Lassen: Solar forcing of the Northern hemisphere air temperature: new data

No. 99-10
Torben Stockflet Jørgensen, Aksel Walløe Hansen: Comment on "Variation of cosmic ray flux and global coverage - a missing link in solar-climate relationships" by Henrik Svensmark and Eigil Friis-Christensen

No. 99-11
Mette Dahl Meincke: Inversion methods for atmospheric profiling with GPS occultations

No. 99-12
Hans-Henrik Benzon; Laust Olsen; Per Høeg: Simulations of current density measurements with a Faraday Current Meter and a magnetometer

No. 00-01
Per Høeg; G. Leppelmeier: ACE - Atmosphere Climate Experiment

No. 00-02
Per Høeg: FACE-IT: Field-Aligned Current Experiment in the Ionosphere and Thermosphere

No. 00-03
Allan Gross: Surface ozone and tropospheric chemistry with applications to regional air quality modeling. PhD thesis

No. 00-04
Henrik Vedel: Conversion of WGS84 geometric heights to NWP model HIRLAM geopotential heights

No. 00-05
Jérôme Chenevez: Advection experiments with DMI-Hirlam-Tracer

No. 00-06
Niels Larsen: Polar stratospheric clouds microphysical and optical models

No. 00-07
Alix Rasmussen: "Uncertainty of meteorological parameters from DMI-HIRLAM"

No. 00-08
A.L. Morozova: Solar activity and Earth's weather. Effect of the forced atmospheric transparency changes on the troposphere temperature profile studied with atmospheric models

No. 00-09
Niels Larsen, Bjørn M. Knudsen, Michael Gauss, Giovanni Pitari: Effects from high-speed civil traffic aircraft emissions on polar stratospheric clouds

No. 00-10
Søren Andersen: Evaluation of SSM/I sea ice algorithms for use in the SAF on ocean and sea ice, July 2000

No. 00-11
Claus Petersen, Niels Woetmann Nielsen: Diagnosis of visibility in DMI-HIRLAM

No. 00-12
Erik Buch: A monograph on the physical oceanography of the Greenland waters

No. 00-13
M. Steffensen: Stability indices as indicators of lightning and thunder

No. 00-14
Bjarne Amstrup, Kristian S. Mogensen, Xiang-Yu Huang: Use of GPS observations in an optimum interpolation based data assimilation system

No. 00-15
Mads Hvid Nielsen: Dynamisk beskrivelse og hydrografisk klassifikation af den jyske kyststrøm

No. 00-16
Kristian S. Mogensen, Jess U. Jørgensen, Bjarne Amstrup, Xiaohua Yang and Xiang-Yu Huang: Towards an operational implementation of HIRLAM 3D-VAR at DMI

No. 00-17
Sattler, Kai; Huang, Xiang-Yu: Structure function characteristics for 2 meter temperature and relative humidity in different horizontal resolutions

No. 00-18
Niels Larsen, Ib Steen Mikkelsen, Bjørn M. Knudsen m.fl.: In-situ analysis of aerosols and gases in the polar stratosphere. A contribution to THESEO. Environment and climate research programme. Contract no. ENV4-CT97-0523. Final report

No. 00-19
Amstrup, Bjarne: EUCOS observing system experiments with the DMI HIRLAM optimum interpolation analysis and forecasting system

No. 01-01
V.O. Papitashvili, L.I. Gromova, V.A. Popov and O. Rasmussen: Northern polar cap magnetic activity index PCN: Effective area, universal time, seasonal, and solar cycle variations

No. 01-02
M.E. Gorbunov: Radioholographic methods for processing radio occultation data in multipath regions

No. 01-03
Niels Woetmann Nielsen; Claus Petersen: Calculation of wind gusts in DMI-HIRLAM

No. 01-04
Vladimir Penenko; Alexander Baklanov: Methods of sensitivity theory and inverse modeling for estimation of source parameter and risk/vulnerability areas

No. 01-05
Sergej Zilitinkevich; Alexander Baklanov; Jutta Rost; Ann-Sofi Smedman, Vasiliy Lykosov and Pierluigi Calanca: Diagnostic and prognostic equations for the depth of the stably stratified Ekman boundary layer

No. 01-06
Bjarne Amstrup: Impact of ATOVS AMSU-A radiance data in the DMI-HIRLAM 3D-Var analysis and forecasting system

No. 01-07
Sergej Zilitinkevich; Alexander Baklanov: Calculation of the height of stable boundary layers in operational models

No. 01-08
Vibeke Huess: Sea level variations in the North Sea – from tide gauges, altimetry and modelling

No. 01-09
Alexander Baklanov and Alexander Mahura: Atmospheric transport pathways, vulnerability and possible accidental consequences from nuclear risk sites: methodology for probabilistic atmospheric studies

No. 02-01
Bent Hansen Sass and Claus Petersen: Short range atmospheric forecasts using a nudging procedure to combine analyses of cloud and precipitation with a numerical forecast model

No. 02-02
Erik Buch: Present oceanographic conditions in Greenland waters

No. 02-03
Bjørn M. Knudsen, Signe B. Andersen and Allan Gross: Contribution of the Danish Meteorological Institute to the final report of SAMMOA. CEC contract EVK2-1999-00315: Spring-to.-autumn measurements and modelling of ozone and active species

No. 02-04
Nicolai Kliem: Numerical ocean and sea ice modelling: the area around Cape Farewell (Ph.D. thesis)

No. 02-05
Niels Woetmann Nielsen: The structure and dynamics of the atmospheric boundary layer

No. 02-06
Arne Skov Jensen, Hans-Henrik Benzon and Martin S. Lohmann: A new high resolution method for processing radio occultation data

No. 02-07
Per Høeg and Gottfried Kirchengast: ACE+: Atmosphere and Climate Explorer

No. 02-08
Rashpal Gill: SAR surface cover classification using distribution matching

No. 02-09
Kai Sattler, Jun She, Bent Hansen Sass, Leif Laursen, Lars Landberg, Morten Nielsen og Henning S. Christensen: Enhanced description of the wind climate in Denmark for determination of wind resources: final report for 1363/00-0020: Supported by the Danish Energy Authority

No. 02-10
Michael E. Gorbunov and Kent B. Lauritsen: Canonical transform methods for radio occultation data

No. 02-11
Kent B. Lauritsen and Martin S. Lohmann: Unfolding of radio occultation multipath behavior using phase models

No. 02-12
Rashpal Gill: SAR ice classification using fuzzy screening method

No. 02-13
Kai Sattler: Precipitation hindcasts of historical flood events

No. 02-14
Tina Christensen: Energetic electron precipitation studied by atmospheric x-rays

No. 02-15
Alexander Mahura and Alexander Baklanov: Probablistic analysis of atmospheric transport patterns from nuclear risk sites in Euro-Arctic Region

No. 02-16
A. Baklanov, A. Mahura, J.H. Sørensen, O. Rigina, R. Bergman: Methodology for risk analysis based on atmospheric dispersion modelling from nuclear risk sites

No. 02-17
A. Mahura, A. Baklanov, J.H. Sørensen, F. Parker, F. Novikov K. Brown, K. Compton: Probabilistic analysis of atmospheric transport and deposition patterns from nuclear risk sites in russian far east

No. 03-01
Hans-Henrik Benzon, Alan Steen Nielsen, Laust Olsen: An atmospheric wave optics propagator, theory and applications

No. 03-02
A.S. Jensen, M.S. Lohmann, H.-H. Benzon and A..S. Nielsen: Geometrical optics phase matching of radio occultation signals